Stony Brook University

OFFICIAL COPY

The official electronic file of this thesis or dissertation is maintained by the University Libraries on behalf of The Graduate School at Stony Brook University.

© All Rights Reserved by Author.

Coupled Ra and Mn Cycling in Long Island Sound

A Thesis Presented

by

John Wallace Roland Daniel

to

The Graduate School

in Partial Fulfillment of the

Requirements

for the Degree of

Master of Science

in

Marine and Atmospheric Science

Stony Brook University

May 2011

Stony Brook University

The Graduate School

John Wallace Roland Daniel

We, the thesis committee for the above candidate for the

Master of Science degree, hereby recommend

acceptance of this thesis.

J. Kirk Cochran – Thesis Advisor
Professor
School of Marine and Atmospheric Sciences

Henry Bokuniewicz – Second Reader
Professor
School of Marine and Atmospheric Sciences

Robert C. Aller – Third Reader
Distinguished Professor
School of Marine and Atmospheric Sciences

This thesis is accepted by the Graduate School

Lawrence Martin
Dean of the Graduate School

Abstract of the Thesis

Coupled Ra and Mn Cycling in Long Island Sound

by

John Wallace Roland Daniel

Master of Science

in

Marine and Atmospheric Science

Stony Brook University

2011

The four naturally occurring Ra isotopes serve as tools to quantify submarine groundwater discharge (SGD) in coastal areas. In constructing the Ra mass balance for a given system, Ra sources and sinks must be accurately determined, then measured or eliminated as negligible. SGD – a Ra source – is commonly determined by difference. In Long Island Sound (LIS), a significant Ra source is diffusive flux from muddy sediments. This study investigates the seasonality of ^{223,224}Ra diffusive fluxes linked to seasonal Mn redox cycling correlated with hypoxia (dissolved oxygen $\leq$ 3.0 mg l^{-1}) in LIS. The three components of this study – water column and shore concentrations and laboratory flux core incubations – demonstrate a coupling of Ra and Mn cycling in LIS, both temporally and spatially. The overall relationship between Mn and Ra in LIS suggests that seasonal redox cycling of Mn is an important factor controlling Ra distributions in the Sound. Solid phase Mn^{4+} (under oxic conditions) appears to restrict the diffusion of Ra from muddy sediment, whereas dissolved phase Mn^{2+}(under hypoxic conditions) is associated with higher Ra concentrations in LIS and 'pulses' of Ra in laboratory flux core incubations. Therefore, the diffusive flux of Ra to a given coastal sea should be evaluated seasonally to more accurately quantify SGD.

Table of Contents

List of Figures

List of Tables

Acknowledgments

This project was funded by New York Sea Grant.

Kirk Cochran – my advisor – provided invaluable guidance and insight throughout all aspects of this thesis.

Christina Heilbrun, a wealth of relevant knowledge regarding laboratory methods, was my radiochemistry guru.

Shaily Rahman imparted her extensive knowledge of graphite furnace atomic absorption spectrometry (GFAAS) to me. I appreciate her patience and willingness to assist me.

Bob Aller facilitated coherent interpretation of the Mn data in this thesis.

My parents and sister provided constant moral support and part-time therapy. Cheers, Momma, Daddy-O, and Narnia!

1. Introduction

The four naturally occurring Ra isotopes serve as tools for both quantifying submarine groundwater discharge (SGD) fluxes in coastal sediments and indicating sources (as reviewed by Moore 1999; Moore 2003; Charette *et al*. 2003; Moore and Wilson 2005; Beck *et al*. 2008). Ra remains mostly particle-bound in fresh water but desorbs upon contact with saline water (Moore 2003). The short-lived isotopes, ^{223}Ra ($t_{1/2}$ = 11.3 days) and ^{224}Ra ($t_{1/2}$ = 3.66 days), experience continual regeneration via decay of their particle-bound thorium (Th) parents and have been used to determine residence times and mixing rates of coastal waters (e.g. Moore 2010).

The differences in regeneration rates can be used to determine flushing frequency – or exposure to saline water. For example, fresh water contained in an aquifer for thousands of years will exhibit a ^{228}Ra/^{226}Ra activity ratio (AR) (^{228}Ra $t_{1/2}$ = 5.75 years; ^{226}Ra $t_{1/2}$ = 1,600 years) similar to the particle-bound ^{232}Th/^{230}Th AR (usually 0.5 – 1.5); an aquifer with a high flushing frequency will exhibit a high ^{228}Ra /^{226}Ra AR consistent with the more rapid regeneration of ^{228}Ra.

Assuming steady state, the Ra mass balance can be used to determine the magnitude of submarine groundwater discharge (SGD) in a coastal system (Moore 2003; Beck *et al*. 2007, 2008). In constructing the Ra balance all Ra sources and sinks must be accurately determined, then measured or eliminated as negligible (Fig. 1). Sources of Ra to coastal waters include the following: fluvial/riverine inputs, fringe marsh inputs, diffusive flux from sediments, SGD, and tidal/ocean exchange; sinks include decay and exchange with the ocean. SGD is commonly determined by difference (Beck *et al*. 2007, 2008).

In Long Island Sound (LIS), one of the most significant Ra sources is the diffusive flux from fine-grained sediments (Cochran 1984, Torgersen *et al*. 1996), because Ra is high in fine-grained sediments and because fine-grained sediments make up approximately two-thirds of the total surficial sediment distribution (Fig. 2). Ra is initially released to sediment pore water by means of recoil during its production from the alpha decay of its particle-bound Th parent. In the case of muddy sediments, Ra in its dissolved form, Ra^{2+}(aq), diffuses or is irrigated by the benthic fauna from sediments into the water column. Estimates of SGD often use a diffusive flux term derived from sediment core incubations during a discrete (usually summer) season. We hypothesize that the diffusive flux of Ra from the muddy sediments of LIS varies seasonally, driven in part by variations in the Mn redox cycle, for MnO_2(s) adsorbs Ra.

Manganese (Mn) plays an important role in estuarine sediments. In the absence of oxygen, early diagenesis proceeds such that Mn^{4+} in the solid form, MnO_2(s), is utilized by anaerobes as a primary electron acceptor in the decomposition of organic matter (C_{org}); thus, it is reduced to the dissolved form, Mn^{2+}(aq). The vertical position of the suboxic boundary in the sediments (or water column) and reprecipitation rates in the surface oxic layer dictate seasonal variations in net benthic fluxes of Mn^{2+}(aq) (Aller 1994). Particulate Mn^{4+}(s) dominates oxic marine environments whereas dissolved Mn^{2+}(aq) is found in anoxic environments. Thus, under oxic sediment conditions, zones of Mn oxides in muddy sediments may scavenge Ra, thus acting as a control on the Ra diffusive flux (Torgersen *et al*. 1996). Conversely, in the absence of oxygen, Mn^{4+}(s) is

reduced – as described above – to Mn^{2+}(aq), potentially releasing associated Ra into sediment pore water and diminishing its effect on Ra diffusion into the overlying water.

Historically, bottom water dissolved oxygen (DO) decreases during summer in Long Island Sound (LIS), such that hypoxia (DO $\leq$ 3.0 mg l^{-1}) persists in the East River and western Narrows (Parker and O'Reilly 1991). This seasonal hypoxia is attributed to the combined effects of phytoplankton and bacteria on biochemical oxygen demand (BOD), coupled with maximum density stratification of the water column (Jensen *et al*. 1991, Lee and Lwiza 2008). As a result, net benthic Mn^{2+}(aq) fluxes vary seasonally in LIS (see Fig. 3). For example, Aller (1994) observed that high net benthic Mn fluxes occurred in the western Sound during spring as phytoplankton bloom debris is deposited, and expanded eastward during summer, in accordance with the east-west gradient of decreasing bottom DO. The fall is characterized by a decrease in benthic Mn^{2+}(aq) fluxes (Aller 1994) and a recovery of bottom DO due to reduced microbial activity or mixing with high DO waters (Lee and Lwiza 2008). Additionally, any increase in reductant C_{org} flux from overlying waters (e.g. bloom deposition) will alter the position of the suboxic boundary, thereby potentially increasing the net benthic Mn^{2+} flux.

This study seeks to elucidate the magnitude of seasonal Ra diffusive fluxes from LIS sediments and their coupling to the redox cycling of Mn. The adsorption of Ra^{2+} by MnO_2 is well known (Moore and Reid 1973, Reid *et al*. 1979, Crespo *et al*. 1993) and presumably oxic conditions would attenuate benthic Ra^{2+} fluxes due to the presence of Mn oxides as adsorptive compounds in the sediments. Conversely, as the suboxic boundary migrates into the water column during summer hypoxia, Ra^{2+} is presumably released due to the reduction of particulate MnO_2 to dissolved-phase Mn^{2+}. We expect to see variations in net benthic fluxes of Ra^{2+}(aq) (especially the short-lived ^{224}Ra and ^{223}Ra) and Mn^{2+}(aq) at the sediment-water interface based on seasonal changes in sediment redox conditions (see Fig. 4). Mn cycling is linked to seasonal hypoxia, although, migration of the oxic-anoxic boundary in the sediments may occur either through seasonal or local variations in bottom water DO or in reductant C_{org} flux to the bottom. Thus, variations in Ra and Mn fluxes may not be solely dependent upon hypoxia, for oxygen at the sediment-water interface is not the exclusive control on net fluxes (Aller 1994). Elucidating seasonality in Ra fluxes from the muddy sediments of LIS will facilitate more accurate SGD estimates using ^{223}Ra and ^{224}Ra mass balances. Past annual SGD estimates – using the Ra-tracer method – may be inaccurate if Ra fluxes exhibit seasonal variability in estuarine environments due to seasonal Mn cycling correlated with hypoxia.

2. Study Site and Previous Work

LIS is is the sixth largest estuary in the United States. It is approximately 150 km long, 20 km wide, and averages 20 m deep. North-south oriented shoals separate LIS into discrete basins: The Narrows, Western, Central and Eastern (Fig. 5). Cable and Anchor Reef separates the Narrows from the Western Basin. A deep channel extends from the eastern Narrows through the Western Basin (Vieira 2000). Stratford Shoal and Mattituck Sill bound the Central basin. This basin exhibits an asymmetrical V-shaped cross section with a 40 m deep channel on the southern side and a gradual slope on the

northern (Lee and Lwiza 2008). Between Mattituck Sill and the Race lies the Eastern Basin, which forms a deep, narrow channel.

Tidal ranges in LIS differ from west to east. In the western Sound the range is 2 – 3.5 m, whereas the range is small along the eastern Shores (0 – 1 m). The volume of nearshore SGD may be affected by tidal fluctuations along the sandy shores of LIS based on the findings of Urish and McKenna (2004) in a Cape Cod embayment (Fig. 6). A hydraulic gradient is imposed by the tide on the beach during flood and high tides. Salt water infiltrates the beach, overlying and mixing with fresh ground water, and ground water flow is landward. The hydraulic gradient reverses during ebb tide; thus, ground water flow moves seaward. Tide-influenced SGD reaches a maximum at low tide before the hydraulic gradient is reversed during flood tide (Urish and McKenna 2004).

Tidal currents are strong in LIS, exceeding 1 m s^{-1} in the East River – a tidal strait connecting western LIS to the lower Hudson River – and ranging from about 0.5 m s^{-1} in the central basin to 1 m s^{-1} at the eastern end (Blumberg and Pritchard 1997, Vieira 1990). However, mean circulation is fairly weak, approximately 0.1 m s^{-1} or less (Vieira 2000).

LIS circulation follows a traditional two-layered estuarine flow, but the saline layer flow does not always stay exclusively underneath (Lee and Lwiza 2005). Oceanic water enters LIS through the Race underneath outgoing less saline water. Traveling west, oceanic flow occupies the southern side of the Eastern Basin channel from top to bottom; outgoing water is restricted to the channel along the Connecticut shore. In the Central Basin, westward flow occupies the main channel; thus, lighter water to flows out above it at a lower speed (Lee and Lwiza 2005). Classical estuarine circulation is fully developed in the Western Basin (Vieira 2000). Three major rivers – Thames, Housatonic, and Connecticut – contribute 90% of the freshwater input into LIS; the Connecticut River contributes the most (mean annual flow = 475 m^3 s^{-1}) – more than 70% of the total LIS freshwater influx (Lee and Lwiza 2005). Precipitation in LIS (110 cm yr^{-1}) slightly exceeds annual evaporation (93 cm yr^{-1}) and is evenly distributed throughout the year (Thomas et al. 2000).

DO varies both annually and seasonally in LIS, illustrated by this and previous studies (Figs. A1 – A4; Parker and O'Reilly 1991). Parker and O'Reilly (1991) confirmed a general west-to-east gradient of increasing DO throughout LIS in all examined historical data, also in agreement with the results of the present study. The emergence of hypoxia (DO $\leq$ 3.0 mg l^{-1}) in the western Sound occurred as early as the 1970s and has been a reoccurring event during the summer season (Parker and O'Reilly 1991, Anderson and Taylor 2001). Lee and Lwiza (2008) found that summer hypoxia occurred every year from 1995 to 2004 in the Narrows and less frequently in the Western and Central Basins.

Many studies have elucidated the mechanisms that control summer seasonal hypoxia in the western Sound. During non-summer, temperature controls LIS DO concentrations; i.e., colder temperatures increase the solubility of O_2(g) in seawater. During summer, density stratification due to weak winds controls DO in shallow regions and western LIS; biological processes are the main control in other regions, and DO in the Eastern Basin is most affected by solubility year-round (O'Shea and Brosnan 2000,

Lee and Lwiza 2008). Welsh and Eller (1991) found LIS DO most affected by both physical stratification and biological production and respiration. Lee and Lwiza (2008) concluded that the variability of the hypoxic volume is dependent upon primary production in the spring (i.e., the quantity of source C_{org}).

Hypoxic conditions in overlying waters lead to elevated benthic fluxes of reduced metals involved in sedimentary diagenetic processes (e.g., Mn, Fe; Kristiansen *et al*. 2002). Mn remains oxidized in sediments throughout most of the year particularly in the form of solid-phase manganese oxides – Mn(III) and Mn(IV) – due to well-mixed overlying water with a low biochemical oxygen demand (BOD). Thus, the suboxic boundary remains below the sediment-water interface. As summer hypoxia develops, the suboxic boundary migrates upward toward the sediment-water interface and may move into the bottom water. In the absence of O_2(aq), Mn(III) and Mn(IV) are reduced to the dissolved phase (Mn^{2+}) and an increase in benthic Mn flux occurs (Aller 1994).

Submarine groundwater discharge (SGD) can play a significant role in enhancing fluxes out of estuarine sediments (Moore 2010). Moore *et al*. (2008) estimated a total SGD flux to the Atlantic Ocean of 2 – 4 x 10^{13} m^3 yr^{-1}, a value comparable to the riverine flux of water. Additionally, SGD often contains nutrients in higher concentrations than river water thus confirming its ecological significance (Moore 2010). For example, in Port Royal Sound, South Carolina (SC), Crotwell and Moore (2003) found higher concentrations of ammonium (NH_4^+) and phosphate (PO_4^{3-}) in groundwater compared to the local riverine source (Savannah River). Subsequent fluxes of these nutrients due to SGD were estimated to be greater than local atmospheric and riverine inputs combined. Similarly, Oberdorfer *et al*. (1990) found that, during summer, the nutrient load contributed by SGD to Tomales Bay, California was comparable to that of river runoff. Krest *et al*. (2000) observed nutrient concentrations in North Inlet, SC groundwater more than ten times greater than surface water concentrations. They concluded that SGD is the major source of dissolved inorganic nitrogen (DIN) and dissolved reactive phosphorus (DRP) to this system effectively driving primary production. Furthermore, data from both Johannes' (1980) study in Western Australia and Capone and Bautista's (1985) research in Great South Bay, NY indicate significant nitrate (NO_3^-) fluxes via SGD. Other studies further document the role of SGD in nutrient fluxes to coastal oceans (Charette and Buessler 2004; Kim *et al*. 2005; Hwang *et al*. 2005), thus confirming its ecological significance.

Moore (2003) describes three components of SGD: (1) freshwater flow from an aquifer to the ocean, (2) recirculated seawater, and (3) mixtures of fresh- and seawater from "deeper semi-confined aquifers." Assuming that the Upper Glacial Aquifer – which facilitates SGD in Great South Bay, NY (Perlmutter and Crandell 1959; as cited by Bokuniewicz 1980) – is the hydraulic head driving SGD through permeable/sandy sediments of LIS, SGD may account for as much as two-thirds of total freshwater inflow (Bokuniewicz 1980). Additionally, groundwater flow rates decrease rapidly offshore, with typical rates ranging from 40 l m^{-2} d^{-1} within 30 m of shore to less than 10 l m^{-2} d^{-1} 100 m from shore (Bokuniewicz 1980). Therefore, a substantial flux of pore water through permeable sediments occurs close to shore.

As mentioned in section 1, the four naturally occurring Ra isotopes serve as tools

to quantify SGD in coastal areas. Previous LIS studies have employed Ra radioisotopes to better understand circulation and transport. The findings of the studies below provide an understanding of the Ra budget in LIS such that Ra may be used to quantify LIS SGD. Using ^{228}Ra as a tracer, Turekian *et al*. (1996) estimated the rate of water transfer from the East River to LIS to be between 0.40×10^{14} l yr^{-1} and 1.1×10^{14} l yr^{-1} during summer. The residence time of ^{228}Ra in the western Sound ranged between 63 and 166 days depending on flux estimates of ^{228}Ra from sediments. Torgersen *et al*. (1996) used ^{224}Ra to identify differences in transport between surface and bottom waters of LIS. They determined that nearshore fine-grained sediments and salt marshes are sources of ^{224}Ra to LIS surface waters (i.e. above the thermocline). During summer, central LIS surface waters are isolated from bottom sediments by the thermocline; thus, Torgersen *et al*. (1996) concluded that shore-derived ^{224}Ra is redistributed by horizontal eddy dispersion (5 – 50 m^2 s^{-1}). However, they identified "an apparent mid-LIS source…greater than the periphery source" below the established summer pycnocline. They proposed two explanations: (1) an inhomogeneous distribution of sediments (i.e., preferential accumulation of ^{228}Th-rich fine-grained sediments in the central Sound) or (2) a homogenous distribution of sediments with increased ^{224}Ra flux due to summer hypoxic conditions and the associated lack of Mn^{2+}(aq) oxidation. Thus, this study examines the latter hypothesis.

3. Methods

3.1. Field Sampling – Long Island Sound water samples

Water samples were obtained from stations in Long Island Sound (LIS) aboard the R/V Seawolf during spring (24 – 30 April) and summer (29 July – 04 August) 2009, and summer (03 – 12 August) 2010. Stations were oriented along 4 transects: one axial extending from the Narrows to the Race and three longitudinal transects in the western, central and eastern Sound (Fig. 7). A CTD was deployed at each station to determine profiles of temperature, salinity, and dissolved oxygen (DO).

3.1.1. Large volume sampling

Samples comprising 60 liters of seawater were acquired at two depths – surface and deep – for every station. Surface samples were obtained with a 115-volt submersible sump pump lowered over the side of the ship to a depth of approximately 0.5 m; deep samples were taken with Niskin bottles attached to the ship's CTD rosette tripped ~1 m from the bottom. These water samples were stored in triple-rinsed plastic carboys. The 60 l water samples were subsequently filtered on-board through cartridges containing ~15 g Ra-adsorptive MnO_2-impregnated acrylic fiber (Mn-fiber). Glass fiber was placed at both ends of the cartridge during filtration to ensure adequate removal of suspended particles and to prevent Mn-fiber loss. In the lab, the same evening or the following day (because ^{224}Ra $t_{1/2}$ = 3.66 days), Mn-fiber was analyzed for ^{223}Ra and ^{224}Ra by employing delayed-coincidence counting methods (Moore and Arnold 1996, Beck *et al*. 2007).

3.1.2. Small volume sampling

A second set of surface and deep samples was also obtained for additional analyses. Surface samples were taken with a Rubbermaid® HDPE 14-liter bucket lowered over the side of the ship; deep samples were taken according to the same method described in section 3.1.1.

***a. Chlorophyll* a**. 60 ml each, surface and deep, was filtered through a Gelman® 25mm glass fiber filter using a 60-ml plastic syringe. Filters were stored in Falcon® Blue Max™ 15-ml polystyrene conical tubes on ice in the dark aboard the ship and frozen upon return to the lab. Samples were later extracted in a 7 ml solution comprising 90% HPLC grade acetone, 10% deionized water for 24 hours at –20ºC. Samples were removed, allowed to reach room temperature, and analyzed with a Turner Designs 10–AU flourometer.

b. Nutrients. 10 – 15 ml of filtered seawater from chlorophyll *a* (Chl-*a*) samples were collected in Falcon® Blue Max™ 15-ml polystyrene conical tubes for nutrient analyses. These nutrient samples were acidified with one drop of 12 N HCl, stored on ice in the dark on the ship, and frozen upon returning to the lab. Samples were later analyzed for ammonia (NH_4), total nitrate (NO_3+NO_2), and orthophosphate (PO_x) with a flow injection type Lachat Instruments FIA-5000 automated colorimetric analyzer using standard methods.

c. POC. 100 ml of each sample was filtered with a rubber-free syringe through a filter housing containing a combusted Gelman® 25mm glass fiber filter. Filters were stored in petri dishes on ice in the dark aboard ship and frozen upon returning to the lab. Filters were later cut in half and treated with HCl fumes overnight to evolve off inorganic C. POC and PON were then analyzed with a Carlo-Erba CHNS 1200 analyzer.

d. Mn(aq). 30 ml of each sample was filtered through a Whatman® Puradisc™ 0.2 μm PES filter (Cat. No. 6780-2502), acidified to 1.2 N with TMG concentrated HCl, and stored in acid-washed Nalgene® 30-ml HDPE bottles.

e. Suspended particulate matter (SPM), Mn(s) and Al(s). 500 ml of each sample was transferred to an acid-washed Nalgene® 500-ml LDPE bottle and stored in the dark. In the lab samples were vacuum-filtered through pre-weighed Whatman® Nuclepore membrane filters. Filters were dried in Rubbermaid® plastic tubs over a bed of Drierite™ anhydrous calcium carbonate and re-weighed. Filters were then transferred to acid-washed Falcon® Blue Max™ 15-ml polystyrene conical tubes. 10 ml 6 N trace metal grade (TMG) HCl was added, the samples were vortexed, and leached for ~12 hours. Samples were then centrifuged at 3,500 – 4,000 rpm for ~20 min and supernatant transferred to acid-washed Wheaton® 8-ml HDPE bottles. *All* Mn and Al analyses were done on a Perkin-Elmer AAnalyst 800 atomic absorption spectrometer equipped with graphite furnace (GFAAS), employing Zeeman background correction. Acidified Mn(aq)

seawater samples and supernatant Mn(s) and Al(s) samples were diluted with de-ionized water and triplicate concentration (in μg l^{-1}, or ppb) values obtained.

3.2. Field Sampling – Shore samples

Water samples were also obtained from stations along the north and south shores of Long Island Sound (CT and LI respectively) during the summers of 2009 and 2010 (Fig. 8, Appendix Table A1). Surface (overlying) water samples were obtained during ebb tide, between mid- and low tide. At each station, a Rubbermaid® HDPE 14-liter bucket was employed to collect 40 liters of surface water at a water depth of ~10 cm. The surface water was stored in 20-liter plastic carboys. For all 2010 LI stations and four CT stations, pore water samples (5 – 10 L) were also obtained. Pore water samples were taken *at least* 1 hour after surface water samples – and closest to low tide – in the same location (after the overlying water had retreated). A standard spade-headed shovel (wooden handle) was used to excavate a hole 15 – 30 cm deep to collect pore water. The water that accumulated within the hole was mostly pore water with a minor beach surface flow component. A 1-liter HDPE Nalgene® bottle was used to transfer water to a 20-liter plastic carboy. In all cases three or four initial dips of the Nalgene® bottle were discarded, and close attention was paid such that skin was never submerged in the collected pore water. Temperature, salinity and DO measurements were recorded for samples using a YSI 556 Multiple Probe System (MPS).

a. Ra. ^{224}Ra and ^{223}Ra were extracted from the samples and analyzed as described in Section 3.1.

b. Nutrients. An additional 10 – 15 mL sample was collected during each sampling event using a 60-mL syringe and attached Whatman® Puradisc™ 1.0 μm GMF-150 filter media (Cat. No. 6783-2510) for nutrient analyses. These nutrient samples were kept cold and in the dark in the field and frozen upon returning to the lab. Samples were later analyzed for NH_4 and NO_3+NO_2 (see Section 3.1.2*b*).

3.3. Sediment sampling and flux measurements

Subcores were taken from the ship using a Soutar box corer (25 cm × 25 cm) according to the methods described in Sun *et al*. (1991) and Aller (1994). Cores were obtained from Stations 8, 13, 16, and 120E (sta8, sta13, sta16 and sta120E, see Fig. 7) aboard the R/V Seawolf. Sta13 and sta120E cores were taken on 29 July 2009 and sta8 and sta16 cores were taken on 09 August 2010 and 12 August 2010 respectively. A core was also collected by hand from a shallow muddy sand station in Smithtown Bay (West Meadow Beach) on 24 July 2009. In 2010, two box cores were taken at each station. From one box-core, a subcore (9.5 cm diameter) was taken by pushing a butyrate acetate tube into the sediment, two subcores (7.5 cm diameter) were taken in the same manner, and a rectangular subcore was taken for x-radiography. From the other box core, one large subcore (20 cm diameter) was taken. All subcores were 10 – 20 cm in length.

a. Ra flux. Ra-flux incubations were carried out using the 20 cm-diameter subcores (Nalgene® polycarbonate multipurpose jars). The cores were covered with between 2.6 and 2.9 liters of overlying Ra-free water from the bottom water taken at each site. For all cores (2009 and 2010) Ra fluxes were determined under oxic conditions by aerating the overlying water and circulating it continuously *via* a peristaltic pump connected to an in-line cartridge filled wih 15 g of Mn-fiber (see Fig. 9). At intervals ranging from 0.5 – 3 days, the cartridge was removed and the fiber was analyzed for ^{223}Ra and ^{224}Ra by delayed-coincidence counting methods ('RaDeCC,' Moore and Arnold 1996, Beck *et al*. 2007). Ra concentrations were determined five times over the first ~250 hours after core collection under these aerated conditions. For cores collected in 2010, fluxes under hypoxic conditions were determined by covering the cores with hypoxic seawater achieved by bubbling nitrogen gas – N_2(g) – through LIS bottom water of the respective station. The cores were sealed, and the overlying water was continuously circulated with a magnetically coupled stirrer modified from the methods of Mackin and Swider (1989) and Aller (1994) (Fig. 9). The overlying water was removed – and immediately replaced with the same Ra-free water mentioned above – at intervals ranging from 1 – 3 days, filtered through Mn-fiber, and analyzed for ^{223}Ra and ^{224}Ra by RaDeCC. Ra concentrations were determined three times from hours 250 to 420 under hypoxic conditions.

b. Mn(aq) flux. Incubations to determine the Mn-flux were carried out in the 9.5 cm-diameter cores, adding as overlying water ~700 ml of unfiltered LIS bottom water (collected in a Niskin bottle) from the respective station. Two flux cores from each station were incubated in the dark at an *in situ, s*ummer temperature of 21ºC. The overlying water in one subcore was continuously circulated to ensure aeration; the other was sealed and continuously circulated with a magnetically coupled stirrer according to the methods of Mackin and Swider (1989) and Aller (1994) (see Fig. 10). These subsequently will be referred to as "summer oxic" and "summer hypoxic" Mn flux cores respectively. At the close of these initial incubations the summer hypoxic Mn flux cores from each station were moved to a dark coldroom set to an *in situ* winter temperature of 2.5ºC and allowed to acclimate for 24 hours. After acclimation the seal was broken in order to allow gradual re-oxygenation. These are referred to as "winter oxic" Mn flux cores accordingly.

For all Mn flux core incubations a time series of multiple overlying water samples were extracted into syringes at 6-hour intervals during, at least, the first 24 hours then at various intervals thereafter based on observed DO. At each sampling time approximately 10 ml of overlying water was removed and simultaneously replaced with the aforementioned bottom water. Samples were passed through a Whatman® Puradisc™ 0.2 μm PES filter (Cat. No. 6780-2502), and DO concentrations were determined via a modified Winkler titration method (Mackin *et al.* 1991). One hour later (after the modified Winkler titration was performed) another 9 ml was extracted and replaced. These samples were also filtered, acidified to 1.09 N with TMG concentrated HCl, and analyzed for dissolved Mn(aq).

All Mn analyses were done on a GFAAS (see section 3.1.2*e*). Acidified seawater samples were diluted with de-ionized water and analyzed in triplicate to determine Mn(aq) concentrations (in μg l^{-1}, or ppb).

c. Sediment core solid phase analyses. The 7.5 cm-diameter subcores were sampled to obtain profiles of water content, organic matter content, and total leachable Mn. Cores were sectioned at 0.5 cm intervals to a depth of 3 cm, and at 1 cm intervals from 3 cm to a depth of 6 cm. Sections were dried at 60ºC for 24 h to determine water content. The core sections were then pulverized to a powder with an agate mortar and pestle for the analyses. Sediment (~1.5 g) from each core section was combusted in a muffle furnace at 450ºC for 6 h and organic matter content determined by loss-on-ignition. Approximately 150 to 200 mg of dry sediment from each core section was leached with 10 ml 6 N trace metal grade (TMG) HCl for 24 hours in acid-washed Falcon® Blue Max™ 15-ml polystyrene conical tubes. Samples were then centrifuged at 3,500 – 4,000 RPM for ~20 min and the supernatant was transferred to acid-washed Wheaton® 8-ml HDPE bottles. Total leachable Mn and Al were determined via GFAAS (see section 2.1.2*e*).

d. X-radiographs. Rectangular subcores were stored in LIS water and aerated. Images were taken in the days immediately following coring with a digital x-ray setup.

4. Results

4.1. Long Island Sound water column

During summer 2010 the water column was well-mixed in western LIS, and stratified in the central and eastern Sound (Appendix Figs. A5 – A7). Both a strong pycnocline and oxycline were apparent between 8 and 10 m depth at sta8 in the central Sound where density increased from 1018.5 kg m^{-3} to 1019.5 kg m^{-3} and DO decreased from 6.3 to 5.0 mg l^{-1} (Appendix Fig. A6). At station 3 (sta3) in the eastern Sound a strong pycnocline was apparent between 3 and 10 m depth where density increased from 1018.6 kg m^{-3} to 1020.5 kg m^{-3} (Appendix Fig. A7). The oxycline was apparent at about 5 m depth, yet the difference in DO values immediately above and below the oxycline was approximately 0.5 mg l^{-1} (Appendix Fig. A7).

DO was nearly constant throughout LIS during spring 2009. The average concentration was 9.8 mg l^{-1} in the bottom waters with surface values of 10.2 mg l^{-1}. Stations 16 and 13 (sta16, sta13) in the western Sound were the only stations that exhibited notable differences in surface and deep DO concentrations during spring 2009 (sta16: 10.7 mg l^{-1} surface, 9.4 mg l^{-1} deep; sta13 11.4 mg l^{-1} surface, 9.4 mg l^{-1} deep). Summer 2009 and especially summer 2010 DO data showed overall depleted DO throughout the Sound compared with spring, especially in the western Sound and in bottom waters relative to surface waters (Appendix Figs. A1 – A4). Summer surface and deep average DO concentrations were, respectively, 4.6 mg l^{-1} and 7.6 mg l^{-1} in 2009 and 4.4 mg l^{-1} and 6.3 mg l^{-1} in 2010.

4.1.1. *Ra*. ^{223}Ra and ^{224}Ra activities were strongly correlated (Fig. 11); therefore, subsequent discussion will focus on ^{224}Ra. The average spring 2009 ^{224}Ra concentration in western Sound deep samples was 6.7 dpm 100 l^{-1}, more than 2-fold higher than an average concentration of 3.2 dpm 100 l^{-1} in western LIS surface samples (Figs. 12 – 13, Appendix Table A2; stations 16, 13, 120W and 120E), perhaps indicating a bottom source. Summer 2009 and summer 2010 data showed markedly higher ^{224}Ra concentrations than spring with a general pattern of higher ^{224}Ra in the western sound and greater concentrations in deep samples (Table 1, Figs. 12 – 13), with the exception of the extreme western Sound where surface and deep concentrations were not substantially different (Figs. 12 – 13). Furthermore, the summer 2010 data more clearly exhibited the pattern of higher ^{224}Ra concentrations in deep samples throughout the Sound (Figs. 12 – 13). This pattern is consistent with a release of Ra with reduced Mn^{2+}(aq) under hypoxic conditions. Summer 2010 ^{224}Ra also decreased from west to east except along the Sound margins (Appendix Table A2).

4.1.2. *Chl-a, dissolved nutrients, and POC*. Spring 2009 Chl-*a* concentrations were highest in the western Sound (Appendix Table A3, stations 16, 13, 120W). Additionally, western stations followed a trend of higher concentrations in surface waters than at depth. Summer 2009 Chl-*a* concentrations in both the western and eastern Sound were higher than spring 2009 and followed a similar pattern where surface values were greater than deep values (Appendix Table A3). LIS summer 2010 sampling was characterized by elevated surface relative to deep concentrations extending from the western Sound well into the central basin (Appendix Table A3). Furthermore, compared with spring 2009, Chl-*a* concentrations were higher throughout LIS, most notably in surface waters.

The spring and summer nutrient concentrations in 2009 were either insignificant or erratic respectively. More than a year transpired before analyses were conducted on the frozen 2009 samples, so perhaps the results are not indicative of the true nutrient regimes of LIS for the given sampling seasons. In contrast, 2010 nutrient concentrations revealed patterns for the individual analytes. NH_4 was confined to the extreme western Sound and deep samples of the central Sound, whereas NO_3+NO_2 concentrations were highest in the western and eastern Sound with lower values in the central Sound (Appendix Table A3). PO_x was constant throughout LIS during summer 2010 (Appendix Table A3).

Summer 2010 POC concentrations were highest in the western Sound. Within the Narrows, deep concentrations exceeded surface concentrations, whereas the remaining LIS stations displayed higher surface POC relative to deep (Appendix Table A4). Deep POC concentrations were lowest in the central Sound.

4.1.3. *Dissolved and particulate Mn and Al, and SPM*.

Spring 2009 Mn(aq) concentrations were similar throughout LIS with lower concentrations by about 32% in the central Sound and lowest concentrations at the Race (Table 2). Additionally, surface Mn(aq) values were higher by about 23% than deep values in the western Sound (Table 2 and Appendix Table A4). Summer 2009

Mn(aq) were highest in deep samples throughout the Sound with the exception of station 16 in the Narrows (Table 2 and Appendix Table A4). Compared with spring 2009, summer 2009 deep Mn(aq) concentrations within the western Sound were higher, and surface concentrations throughout LIS were lower, with the exception of station 16 (Appendix Table A4). Summer 2010 Mn(aq) concentrations followed the pattern of summer 2009, but showed higher concentrations: western LIS values were 168% higher than spring 2009 values and deep sample concentrations in the central and eastern Sound were 158% higher than surface Mn(aq) (Table 2). Overall, the 2010 data shows a general pattern of elevated deep Mn(aq) concentrations compared with surface and highest values in the western Sound and along the Sound margins (Table 2 and Appendix Table A4).

SPM concentrations were generally higher in deep than in surface samples, and higher concentrations occurred in summer compared with spring (Appendix Table A4). Mn(s) concentrations in spring and summer 2009 showed no trends, and many samples displayed unrealistic values attributed to sampling errors. Summer 2010 data showed a clear pattern of elevated surface Mn(s) concentrations relative to deep with highest values occurring in the central Sound (Appendix Fig. A8 and Table A4). When normalized to Al(s), this pattern was more apparent (Fig. 14). Overall, Summer 2010 LIS Mn(s) concentrations were higher in surface waters of the central Sound than in bottom waters (Fig. 14, Appendix Table A4).

4.2. Long Island Sound shore samples

Temperature varied between surface water and the adjacent nearshore beach pore water samples, and no apparent patterns were observed (Appendix Table A5). However, salinity was generally higher in the nearshore surface waters as was DO (Appendix Table A5).

a. Ra. In all cases pore water Ra concentrations were, on average, nearly 9-fold (774%) higher than surface waters (Appendix Figs. A9 – A10, Appendix Table A6). Furthermore, CT and LI displayed similar ^{224}Ra concentration values from west to east with the exception of stations along the edge of Smithtown Bay on Long Island (Crab Meadow beach – CRM, Sunken Meadow – SKN, West Meadow Beach – WMB; Appendix Figs. A9 – A10, Appendix Table A6).

b. Nutrients. NH_4 was absent at all stations except in pore waters at West Neck Road (WNR) and Crab Meadow Beach (CRM) on Long Island (Appendix Table A7). NO_3+NO_2 concentrations followed a general pattern of higher values in pore waters relative to surface waters. In many cases pore water concentrations were an order of magnitude higher than surface concentrations (Appendix Table A7).

4.3. Sediment Cores

4.3.1*. Ra fluxes*. ^{223}Ra and ^{224}Ra fluxes under oxic conditions were estimated in two ways: (1) by plotting Ra concentrations (dpm l^{-1}) with time (Appendix Fig. B1) and (2)

using equation 1 (below) to calculate the flux for each incubation time (Fig. 15). The slopes of the respective trendlines were multiplied by the overlying water volume and divided by the surface area of the polycarbonate containers. ^{223}Ra and ^{224}Ra fluxes, $\boldsymbol{J_{Ra}}$ (dpm m^{-2} d^{-1}), under hypoxic conditions were calculated for each time point according to the following equation:

$$\boldsymbol{J_{Ra}} = [C_{Ra}(t) - C_{Ra}(t_0)]\,V(t) / [A * (\Delta t)] \quad (1)$$

where $C_{Ra}(t)$ = Ra concentration at time t (dpm l^{-1}),
$C_{Ra}(t_0)$ = initial Ra concentration in the added overlying water, $C_{Ra}(t_0)$ = 0 dpm l^{-1},
$V(t)$ = volume of the core overlying water (l),
A = surface area of the core (m^2),
Δt = change in time since replacement of Ra-free overlying water (d).

Under oxic, well-mixed conditions the ^{224}Ra flux at sta13 was 312 dpm m^{-2} d^{-1}, about 84% greater than sta120E in 2009 (Appendix Table B1), and ^{224}Ra flux at sta8 was 135 dpm m^{-2} d^{-2}, approximately 26% greater than sta16 in 2010 (Fig. 15, Appendix Fig. B1A and Table B1). The ^{223}Ra fluxes for sta8 and sta16 were virtually the same in 2010 (Appendix Fig. B1B and Table B1). Furthermore, a linear correlation between ^{224}Ra and ^{223}Ra concentrations was observed for both stations in 2010 (sta8 r^2 = 0.85; sta 16 r^2 = 0.98; Appendix Fig. B2). In summary, ^{224}Ra fluxes – under aerated, summer conditions – among the four stations sampled in 2009 and 2010 displayed the following relationship: $\boldsymbol{J_{Ra}^{sta13} > J_{Ra}^{sta120E} > J_{Ra}^{sta8} > J_{Ra}^{sta16}}$.

In the hypoxic phase of the experiment (carried out on the 2010 cores), the two cores displayed differences in Ra flux values, yet similar variations in flux with time (Fig. 15). DO remained less than 1.5 mg l^{-1} for all incubations. At sta8, ^{224}Ra fluxes decreased from the final oxic phase flux (139 dpm m^{-2} d^{-1}) to 38 DPM m^{-2} d^{-1} for the first 3-day hypoxic incubation (Fig. 15A). ^{224}Ra flux then increased for the following two incubation periods, first peaking at 126 dpm m^{-2} d^{-1} for the 1-day incubation then decreasing to 59 dpm m^{-2} d^{-1} for the final 2-day incubation.

A similar pattern was observed at sta16, although the fluxes were higher (Fig. 15B, Appendix Table B1). The initial 3-day sta16 ^{224}Ra hypoxic flux showed no virtually no change from the final oxic phase flux (97 dpm m^{-2} d^{-1} to 100 dpm m^{-2} d^{-1}). Thereafter, fluxes increased to values 82% and 31% higher than the average oxic phase flux for the following two incubation periods. The ^{224}Ra flux reached a maximum of 195 dpm m^{-2} d^{-1} during the following 1-day incubation period and decreased moderately to 140 dpm m^{-2} d^{-1} during the final 2-day incubation (Fig. 15B).

4.3.2*. Mn fluxes*. Dissolved Mn concentrations in the overlying water of the flux cores were corrected for dilution due to replacement of seawater taken for DO measurements (dilution factors were variable in the different cores due to differences in core overlying water volumes). Because samples were passed through a 0.2 μm filter (thus excluding sediment), a correction for particulate Mn contribution to the "dissolved" Mn was not necessary. Net dissolved Mn fluxes, $\boldsymbol{J_{Mn}}$ (mmol m^{-2} d^{-1}), were estimated according to the following equation modified from Aller (1994):

$$\boldsymbol{J_{Mn}} = [C_{Mn}(t) - C_{Mn}(t - \Delta t)]\,V(t) / [A * (\Delta t)] \quad (2)$$

Where $C_{Mn}(t)$ = Mn(aq) concentration at time t (mmol l^{-1})

$C_{Mn}(t - \Delta t)$ = Mn(aq) concentration in the previous sample (mmol l^{-1}),
$V(t)$ = volume of the core overlying water (l),
A = surface area of the core (m^2),
Δt = change in time since the previous sample (d).

Mn fluxes at sta8 displayed varying values depending on DO. For example, the summer oxic Mn flux core maintained saturated concentrations of DO and Mn(aq) fluxes were small, less than 0.50 mmol m^{-2} d^{-1}, after an initial pulse (1.59 mmol m^{-2} d^{-1}, Fig. 16A, Appendix Table B2). The summer hypoxic Mn flux core showed negative fluxes (i.e. Mn removal from the overlying water) until DO reached a value near 3.0 mg L^{-1} (Fig. 17A, Appendix Table B2) after which the flux increased significantly over ~29 hours and then decreased slightly for the final two sampling times (Appendix Table B2).

Mn fluxes at sta16 were also very low under oxic conditions (Fig 16B, Appendix Table B2). The summer hypoxic Mn flux core from this station went hypoxic within the first 6 hours – more rapidly than sta8 (48 hours) – and displayed an immediate high Mn flux of 2.91 mmol m^{-2} d^{-1}, decreasing gradually thereafter (Fig. 17B, Appendix Table B2).

The winter oxic flux cores displayed essentially similar patterns for both stations. Both reached DO saturation within 9 hours after the start of aeration (Fig. 17A, B). At sta8, however, a relatively high initial positive Mn flux (3.22 mmol m^{-2} d^{-1}) was followed by high negative fluxes (-8.87 mmol m^{-2} d^{-1}, -9.11 mmol m^{-2} d^{-1}, etc.), while sta16 showed an initial, minor negative flux (-0.48mmol m^{-2} d^{-1}) followed by Mn removal at a lesser magnitude than seen at sta8 (-2.66 mmol m^{-2} d^{-1}, -1.29 mmol m^{-2} d^{-1}, etc.; Fig. 17, Appendix Table B2).

4.3.3*. Sediment core physical analyses and Mn(s)*. Water content was almost identical between sta8 and sta16 and indicative of the muddy nature of the sediments (Appendix Table A8). Sta16 had a slightly greater percentage of organic matter in the top 0.5 cm of sediments than sta8; the same pattern emerged at sediment depths below 3.0 cm (Appendix Table A8). Mn(s) concentrations were more than two-fold higher in the top 0.5 cm at sta8 than sta16. Below 1 cm both subcores exhibited similar Mn(s) concentrations, although concentrations decreased gradually with depth at sta8 and increased gradually with depth at sta16 (Appendix Table A8).

4.3.4*. X-radiographs*. Benthic infaunal organism abundances were higher at station 16 than station 8 due to the greater number of burrows and remnant shell (Figs. A11 – A12). However, structure and actual abundances may differ because the former can integrate over time.

5. Discussion

5.1 *LIS water column*. DO in LIS during spring 2009 was uniform in surface and deep samples except in the Narrows where surface DO concentrations were 14% and 21% higher compared with bottom waters at sta16 and sta13 respectively. This was most likely due to the elevated concentrations of Chl-*a* contributing to a higher biochemical

oxygen demand (BOD) at depth than stations in the central Sound. However, the spring phytoplankton bloom occurred in early March of 2009 (Connecticut Department of Environmental Protection (CTDEP) data). Thus, increases in water column BOD and sediment oxygen demand (SOD) most likely occurred in the weeks immediately following the bloom. However, we observed no evidence of such increases during our late-April cruise, for Chl-*a* concentrations were less than at the height of the bloom (e.g., 41.8 μg l^{-1} in surface waters during early-March compared with 3.1 μg l^{-1} during our cruise in late-April) and SPM values (related to POC) were, on average, about one half of summer values (Appendix Table A3). Furthermore, early-April CTDEP BOD data for stations analogous to our lateral transect show greater BOD in the western and eastern Sound with little variation between surface and bottom waters, except in the Western Narrows (Appendix Fig. A13). During summer 2009 and summer 2010, DO values were not only lower overall compared with spring, but lower in deep samples than in surface samples (Appendix Figs. A1 – A4). For both summer sampling seasons, total average Chl-*a* concentrations were two- to three-fold higher than spring concentrations, indicative of increased surface productivity (Table A3). We attribute the disparity between surface and deep DO values during summer to stratification of the water column, which occurred in the central Sound (see Appendix Figs. A5 – A7), coupled with an increase in SOD. Although we have no estimate of either BOD of SOD for the summer sampling periods, we observed both elevated Chl-*a* and POC values for the summer 2010 sampling period compared with spring. This is indicative of an increased reductant C_{org} flux to the benthos in central LIS. Due to stratification, DO-depletion was localized below the pycnocline. During summer 2010, the extreme western Narrows showed little to no stratification and uniformly hypoxic or near-hypoxic conditions. Chl-*a*, nutrient, and POC values were all elevated in the western Sound during summer 2010, indicative of increased SOD (Appendix Tables A3 and A4). The absence of stratification there provided for DO-depletion throughout the water column (Appendix Fig. A5).

Both deep Mn(aq) and deep ^{224}Ra were strongly correlated with DO concentrations in LIS summer 2010 (Figs. 18 – 19). Again, ^{223}Ra and ^{224}Ra concentrations were strongly correlated for all stations sampled in LIS, so we focus on the ^{224}Ra data (referred to as simply 'Ra') for this discussion (see Fig. 11). Ra concentrations were highest during summer sampling periods in regions of the Sound with low DO concentrations. In hypoxic regions of LIS – excluding stations near the margins – Ra showed a general pattern of higher deep concentrations than surface concentrations, especially in the central and eastern Sound (Figs. 13 and 20, Appendix Table A2). Stations experiencing marginal input of Ra showed less difference in surface and deep concentrations presumably due to SGD or marginal salt marsh or sediment Ra inputs (Torgersen *et al.* 1996; Figs. 21 – 22; Appendix Table A2). In addition to marginal Ra input, stations 18 and 16 in the western Narrows exhibited little or no stratification; thus, Ra concentrations were high in both surface and deep water (see Fig. 20). Similarly Mn(aq) concentrations were highest during summer sampling periods in the western Sound (Fig. 23). Furthermore, a pattern of higher deep Mn(aq) concentrations in the central Sound was evident during summer 2009 and was observed again during summer 2010. This is in agreement with seasonal Mn redox

cycling (Aller 1994). Mn(aq) concentrations in the western Sound were more uniform throughout the water column presumably due to a greater reductant C_{org} flux and low DO. The Chl-*a*, nutrient, and POC data from all years and all sampling periods further corroborate this supposition.

5.2 *LIS nearshore Ra activities*. Elevated Ra concentrations in pore waters compared with surface (overlying) waters along the LIS shore illustrates the process of Ra input from nearshore sandy sediments (Boehm *et al*. 2006). As seawater percolates through the beach face between tidal cycles Ra accumulates in pore waters and is transported to surface waters (Urish and McKenna 2004). Subsequent dilution occurs due to wave action and mixing over the course of the tidal cycle. However, Ra concentrations in surface waters of LIS marginal/shore stations were somewhat comparable to LIS water column stations in close proximity. For example, the concentration of ^{224}Ra in surface waters at the Peck Avenue (PCK) shore station (on the CT shore) was 37.1 dpm 100 l^{-1}. PCK is closest to LIS water column station 9 (sta9), which had surface and deep ^{224}Ra concentrations of 20.4 and 27.6 dpm 100 l^{-1}, respectively. Table 3 displays all other analogous LIS shore and water column station comparisons. All the LIS water column stations under comparison were along the Sound margin and were characterized by higher Ra concentrations than other stations in the respective transect (Table 3; Figs 21 – 22). Deep water column samples were closest in value to shore overlying water samples. Thus, the LIS nearshore data reveals a marginal input of Ra to LIS, especially in areas comprising sandy sediments. Torgersen *et al.* (1996) found that the distribution of surface ^{224}Ra along the same western longitudinal transect sampled in this study is a function of cross-LIS (N – S) distance and eddy dispersive mixing; i.e., the "major source for ^{224}Ra to the surface water at stations along [the western longitudinal transect] could only arise from sources more shoreward than the transect endpoints (with minimal water column production)" (Torgersen *et al*. 1996). Based on our observed data, we suggest that SGD along LIS margins in the form of re-circulated seawater is a major contributor of Ra to LIS along the shore.

5.3 *Mn fluxes*. The Mn flux core results support the summer LIS Mn cycling regime described by Aller (1994). Under oxic conditions, Mn fluxes are low for both sta8 and sta16 (Fig. 16) because Mn was effectively retained in the sediments presumably as MnO_2 or Mn_2O_3 – Mn(IV) or Mn(III) – due to an oxic/anoxic boundary *within* in the sediments (i.e., below the sediment-water interface, see Fig. 3). We attribute the initial positive fluxes in the sta8 core to handling artifacts. Briefly, DO was 4.8 mg l^{-1} in the overlying water at sta8 when we retrieved the core. DO most likely decreased further during transport to the lab initiating an increase in Mn(aq) in the overlying water (Aller, pers. comm.), for – as discussed below – the Mn(s) inventory was more than two-fold higher in the surficial sta8 sediments.

In the hypoxic incubations, DO at sta8 decreased gradually and Mn(aq) fluxes increased once DO fell below 3.0 mg l^{-1} (Fig. 17A). In contrast, DO at sta16 decreased rapidly and Mn flux showed an immediate increase (Fig. 17B). Mn(aq) fluxes from both stations increased to ~3 mmol m^{-2} d^{-1} once DO fell below a "critical" value (~3.0 mg l^{-1})

and then decreased thereafter to values less than 2.0 mmol m^{-2} d^{-1}. The maximum Mn(aq) flux was more delayed at sta8 compared with sta16, such that the Mn(aq) flux reached 3.0 mmol m^{-2} d^{-1} within 24 h of the critical DO concentration. Whereas at sta16 the Mn(aq) flux reached its maximum within 6 h of the critical DO concentration.

These differences may be attributed partly to the benthic communities at the two stations and the abundance of Mn oxides in surficial sediments – namely Mn oxides. The x-radiographs taken for each station show well-defined burrows and remnant epi- and infaunal calcareous shells of opportunistic bivalves at sta16 and a lesser-defined benthic community structure at sta8 (Appendix Figs. A11 – A12). However, it is difficult to determine whether the burrows at sta16 are active or relic, and we assume that both systems are equally bioturbated (Aller, pers. comm.). We also assume SOD was higher at sta16 as indicated by the higher organic matter content of the sediment at sta16 (Appendix Table A8) as well as greater concentrations of Chl-*a* (surface: 4.68 μg l^{-1}; mid: 1.63 μg l^{-1}; deep: 1.04 μg l^{-1}) and POC (surface: 0.371 mg l^{-1}; mid: 0.369 mg l^{-1}; deep: 0.643 mg l^{-1}) in the water column compared with the values at sta8 – Chl-*a* (surface: 1.06 μg l^{-1}; deep: 0.18 μg l^{-1}) and POC (surface: 0.385 mg l^{-1}; deep: 0.184 mg l^{-1}). Enhanced SOD at sta16 also could explain the more rapid DO decrease in the flux core from this station. Additionally, observed surface and deep *in situ* DO values at time-of-sampling were, respectively, 7.2 mg l^{-1} and 4.8 mg l^{-1} at sta 8 and 4.2 mg l^{-1} and 2.6 mg l^{-1} at sta 16 further supporting greater SOD at sta16 (or DO consumption in the bottom water). Particulate, or total leachable, Mn – presumably MnO_2 – was more than two-fold higher in the top 0.5 cm of sediments at sta8 (Appendix Table A8). The presence of Mn oxides effectively buffers the release of Mn(aq) thus altering the timing of increased Mn(aq) flux in the sta8 core (Aller, pers. comm.). In summary, sta8 has a less reactive C_{org} pool and lower SOD to drive the release of Mn(aq) and more Mn(IV) and Mn(III) in surficial sediments which buffer Mn(aq) flux; therefore, sta8 DO is depleted more slowly and the increased Mn(aq) flux under hypoxic conditions is delayed.

The differences in total leachable Mn in the surficial sediments at these stations may also explain the differences in observed Mn(aq) fluxes after DO reached the critical value (Appendix Table A8; see Fig. 17). Sta8 Mn(aq) fluxes decreased slightly following the aforementioned pulse yet remained more constant for the final two time points (1.60 and 2.07 mmol m^{-2} d^{-1}, respectively), whereas sta16 decreased sequentially following the pulse toward zero (in order, 1.71, 0.99, 1.14, 0.33 mmol m^{-2} d^{-1}). As already stated, the Mn(s) inventory was greater in the surface sediments at sta8; therefore, more Mn was available to be mobilized at sta8. Furthermore, Aller (pers. comm.) affirms that roughly 80% of the particulate Mn in LIS is diagenetically reactive – or reducible – explaining the continued flux of Mn post-flux in the sta8 core.

The winter temperature hypoxic-to-oxic phase further elucidates the differences between the two cores. We changed boundary conditions in this manner to simulate a rapid change from summer to fall/winter conditions in order to observe associated changes in Mn(aq) fluxes. Sta8 exhibited an initial positive flux as DO increased followed by subsequent negative fluxes 3- and 4-fold greater than the constant negative flux values observed in the sta16 core (Fig. 17, Appendix Table B2); Mn removal was

~3-fold greater at sta8. This is in agreement with the constant sta8 Mn(aq) flux observed post-pulse during the hypoxic phase and a greater Mn(s) inventory in sta8 surficial sediments. More Mn was mobilized into the water column in the sta8 core under hypoxic conditions due to a greater Mn inventory; therefore, when oxic conditions are re-established – at higher concentrations due to increased solubility associated with a winter temperature – Mn(aq) fluxes are proportional to the initial Mn mobilized from surficial sediments.

5.4 *^{224,223}Ra fluxes*. The measured ^{224}Ra and ^{223}Ra fluxes were strongly correlated (Appendix Fig. B2); thus, we refer to only ^{224}Ra fluxes in this discussion. One check on the Ra fluxes from the incubation cores is to compare them with values determined from pore water Ra gradients. Pore water Ra was measured on the 2009 cores after the oxic incubation was completed (Fig. 24). We modeled expected ^{224}Ra fluxes (J_{Ra}) due to both molecular diffusion alone (D_M) and molecular diffusion plus bioirrigation ($D_M + D_I = D_E$, where "E" denotes "effective") according to Fick's first law. Using the pore water ^{224}Ra data from the 2009 cores (see Fig. 24) and taking $D_M = 4.7 \times 10^{-10}$ m^2 s^{-1} and $D_E = 1.0 \times 10^{-9}$ m^2 s^{-1} (Cochran 1979) yields a ^{224}Ra flux of 58 dpm m^{-2} d^{-1} in the absence of bioirrigation. At steady state reversible adsorption can be ignored. In contrast, the flux including bioirrigation (J_E^{Ra}) is 124 dpm m^{-2} d^{-1}. However, the uncertainty associated with these predicted values is large because of uncertainties in the Ra gradient at the sediment-water interface.

The measured Ra fluxes among the four cores incubated under aerated conditions followed a spatial pattern such that the highest J_{Ra} was observed in the sta13 core from western LIS, and fluxes decreased moving eastward (from sta120E to sta8; Appendix Table B1). This mirrors *in situ* DO data and associated Mn redox cycling. Western LIS bottom waters were hypoxic whereas central LIS bottom waters were not, suggesting that surficial sediment Mn(s) inventories had been depleted at sta13 and remained well established in the central Sound as observed at sta8 (Appendix Table A8). Assuming that the presence of Mn oxides in the sediment act as a trap for Ra we would expect to see decreases in flux from cores in more oxic settings where more adsorptive metal oxides are present in the surficial sediments. The results of the oxic Ra flux core incubations are in agreement with this expectation.

The measured Ra fluxes were all close to that predicted from pore water data except at sta13, which was more than two-fold higher (312 dpm m^{-2} d^{-1}). We speculate that irrigation was increased in this core during the incubation due to saturated oxic conditions in the overlying water, which rarely occur at this station during summer temperatures. Thus, the benthic fauna became hyperactive, leading to greater bioirrigation. The lowest Ra flux of the four cores occurred at sta16 in the Western Narrows, perhaps due to a lower rate of irrigation at this station. Although the x-radiograph of this station does show evidence of bioturbation, we cannot ascertain whether the burrows are active or relic (see Appendix Fig. A12). The remnant shell of opportunistic bivalves and historical DO data showing well-developed annual hypoxia at sta16 suggest that the benthic community may be more transient or ephemeral there. In the case of late-summer hypoxic conditions, benthic fauna were likely dead or subdued

at the time of core collection. Therefore, upon re-oxygenating the sta16 core D_I was most likely lower than the other cores due to the absence of bioirrigating infaunal organisms.

Further evidence that the differences in Ra fluxes between sta8 and sta16 are most likely attributed to differences in benthic faunal activity comes from the solid phase radionuclide data (Appendix Table B3). The source of ^{224}Ra and ^{223}Ra is alpha decay from their Th parents (^{228}Th and ^{227}Th). Since ^{228}Th activities were nearly the same in upper 7 cm of both cores (Appendix Table B3), the differences in Ra flux were not due to contrasting source activities. The oxic ^{224}Ra flux is slightly greater for sta8 than sta16 (135 dpm m^{-2} d^{-1} and 107 dpm m^{-2} d^{-1} respectively), yet, as discussed previously, the Mn(s) inventory is greater in surficial sediments at sta8. This Mn(s) acts as a potential sorptive zone for Ra. However, the benthic community at sta8 is more established and thriving, this likely diminished the effect of the Mn(s) sorptive zone and contributed to a greater observed J_{Ra} than at sta16. Sta16 surely exhibited less of a J_{Ra}-controlling Mn(s) zone compared with sta8, yet D_I was presumably much lower as discussed above.

During the hypoxic phase of the 2010 flux core incubations, the Ra fluxes mirror the anoxic Mn(aq) fluxes. The sta16 and sta8 cores were aerated for 10 and 13 days respectively prior to the hypoxic phase. This is sufficient time for the re-establishment of particulate adsorptive Mn(IV) and Mn(III) in the surficial sediments of these cores. The first hypoxic incubation was a 3-day incubation in which sta8 J_{Ra} decreased to 38 dpm m^{-2} d^{-1}, a value in agreement with the Ra flux predicted from the pore water gradient based on molecular diffusive transport (58 dpm m^{-2} d^{-1}). This suggests that bioirrigation was diminished under hypoxic settings at sta8 (i.e. D_I was negligible). Sta16, however, showed no decrease in J_{Ra} during the first incubation period under hypoxic conditions, which is in agreement with our assumption that sta16 harbors an ephemeral benthic community that was mostly absent over the course of these experiments. Both cores exhibited a Ra “pulse” during the following 1-day incubation analogous to the Mn(aq) pulse observed under hypoxic conditions for these stations (compare Figs. 15 and 17). J_{Ra} decreased during the final 2-day incubation in both cores, and at sta16 were still greater than J_{Ra} during the 3-day hypoxic incubation. Sta8 hypoxic J_{Ra} values were less than or approximately equal to the respective oxic J_{Ra} value, suggesting that bioirrigation plays a greater role in modulating J_{Ra} in muddy sediments of LIS with sufficient DO. Mn mobilization does produce an increased Ra flux, however it appears that a thriving benthic community plays a greater role in this setting. Conversely, sta16 hypoxic values were *greater* than or equal to its respective oxic J_{Ra} value. In muddy sediments of LIS experiencing severe annual hypoxia, the benthic community is presumably more ephemeral. Therefore, the particulate Mn(s) adsorptive zone appears to be a more significant control on J_{Ra} as indicated by the sustained increases in J_{Ra} at sta16 under hypoxic conditions (see Fig. 4).

6. Conclusions

This study provides strong evidence for the role of Mn in the seasonal variations in observed Ra concentrations in LIS (Fig. 25). Our results from the three components of this study demonstrate a coupling of Ra and Mn cycling in LIS, both temporally and

spatially. During spring, when Sound waters are well-oxygenated and well-mixed, Mn(aq) is mostly restricted to pore waters beneath the sediment-water interface and low concentrations were observed in this study. In summer, under hypoxic conditions, Ra adsorbed to Mn(III, IV) is released to overlying waters upon Mn reduction. Thus, solid phase Mn appears to restrict the diffusion of Ra from muddy sediments, and the diffusive flux of Ra to a given coastal sea should be evaluated seasonally.

The laboratory results show significant ^{224,223}Ra fluxes out of the incubated cores, but the difference between oxic and hypoxic conditions is not large. At stations 8 and 16 the average ^{224}Ra flux is 120 dpm m^{-2} d^{-1} under oxic conditions and 94 dpm m^{-2} d^{-1} under hypoxic conditions. Several factors, likely related to the experimental set up, contribute to this difference. First, the fluxes under warm oxic conditions reflect an active benthic community, with effective bioirrigation. During our hypoxic incubation, this community was inactive. Second, the overlying water was maintained near 0 dpm ^{224,223}Ra l^{-1} in the oxic re-circulated incubations. Thus, the Ra fluxes were in near steady state during the oxic incubations but in a non-steady state during hypoxic (Fig. 9) making detailed comparisons difficult. In the hypoxic incubations, Ra was allowed to increase in the overlying water, decreasing the concentration gradient at the sediment-water interface and the diffusive flux.

Nevertheless, the overall relationship between Mn and Ra in LIS (Fig. 25) suggests that seasonal redox cycling of Mn is an important factor controlling Ra distributions in the Sound. Further laboratory experiments are needed to characterize adequately the controls on the flux of Ra from the muddy sediments of LIS.

Figures

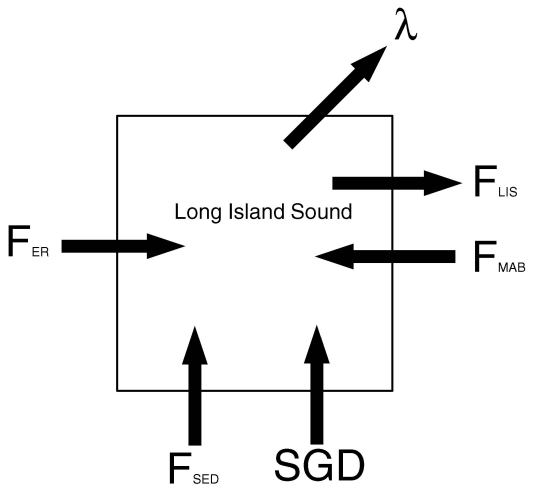

Figure 1. Schematic representation of fluxes of Ra isotopes in Long Island Sound (LIS). ER represents the East River, MAB is the Mid-Atlantic Bight (i.e. Block Island Sound), SED refers to diffusion from sediments; prepared by A. Beck.

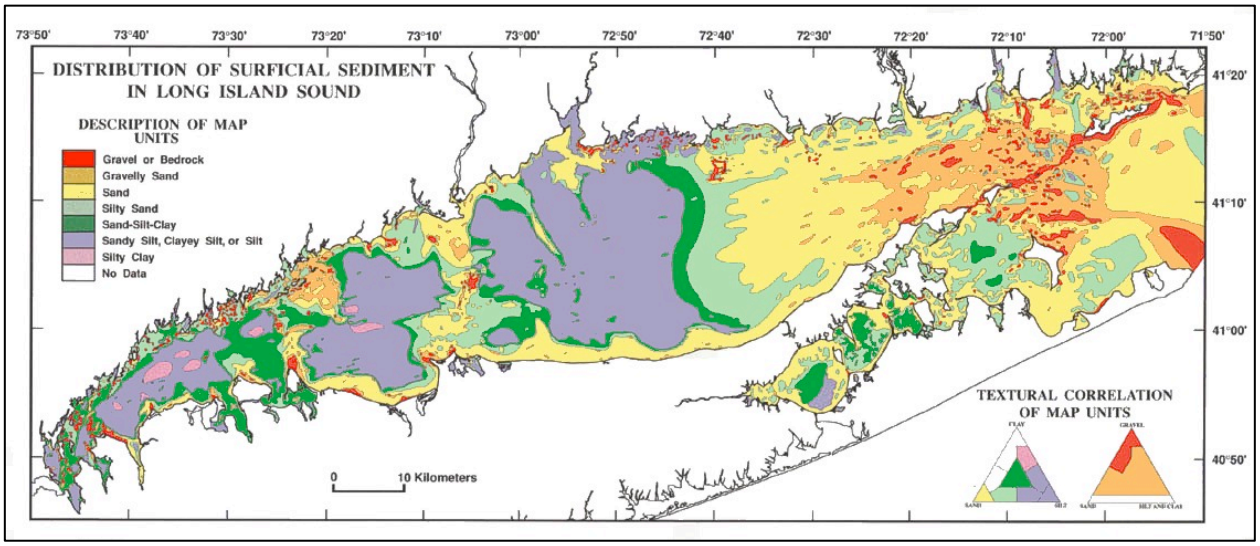

Figure 2. Map of Long Island Sound (LIS) showing the distribution of surficial sediments (from Poppe *et al*. 2000). Triangular and block diagrams explain the map units. Fine-grained sediments predominate the western and central sound. Therefore, diffusive flux from fine-grained sediments is a significant component in the Ra balance for LIS.

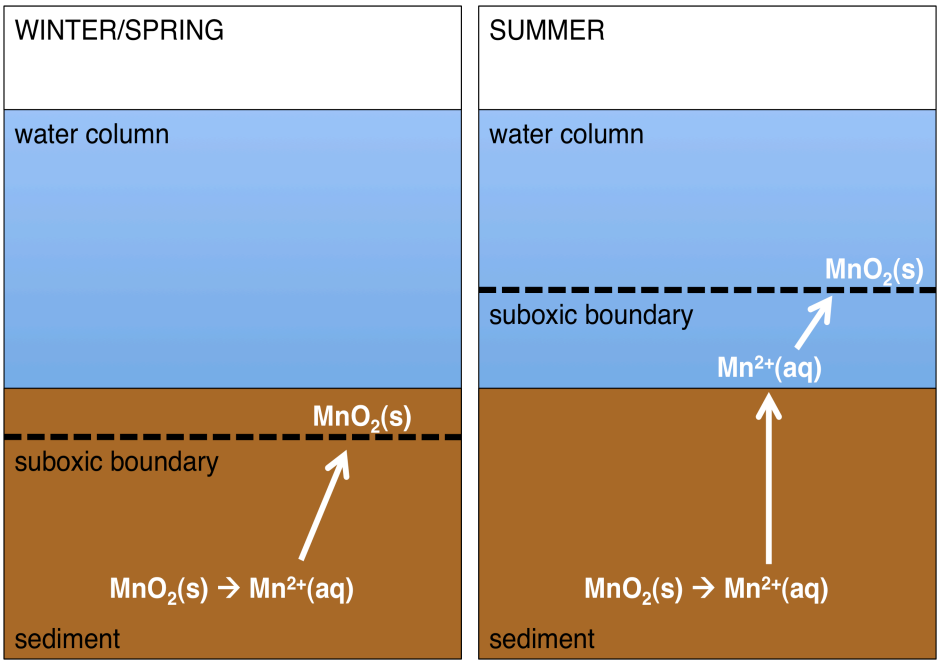

Figure 3. Schematic of benthic Mn flux winter/spring vs. summer in Long Island Sound (LIS). During **winter/spring**, oxic conditions restrict dissolved Mn^{2+}(aq) to pore waters of the sediment. Mn^{2+}(aq) is "re-oxidized" upon contact with oxygen; thus, net Mn^{2+}(aq) flux from sediment to overlying water is low. In **summer**, bottom DO decreases such that the suboxic boundary may exist above the sediment-water interface within the water column. Mn^{2+}(aq) remains reduced and net flux to the bottom water is high. A rapid pulse of organic matter, such as occurs during the spring bloom, can also result in the reduction of MnO_2 and the "uncapping" of the seabed Mn trap.

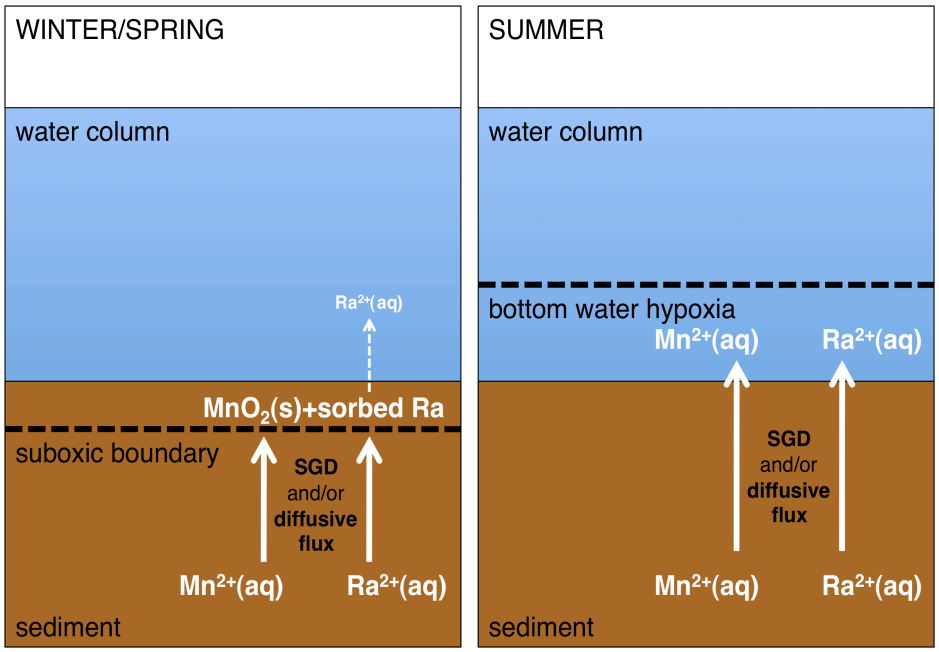

Figure 4. Schematic of Mn and Ra fluxes including submarine groundwater discharge, diffusive and bioirrigation fluxes in Long Island Sound (LIS). **Winter/spring** conditions, characterized by sufficient bottom DO, restrict Mn and Ra to particulate forms in the sediments. Since Mn^{2+}(aq) within pore waters is oxidized to Mn^{4+} and precipitates as MnO_2(s), which adsorbs Ra^{2+}(aq), the fluxes of both elements out of the sediments due to advection and/or diffusion should be low. During **summer**, bottom DO is depleted and flux of Mn^{2+}(aq) and Ra^{2+}(aq) dissolved in pore waters should be high.

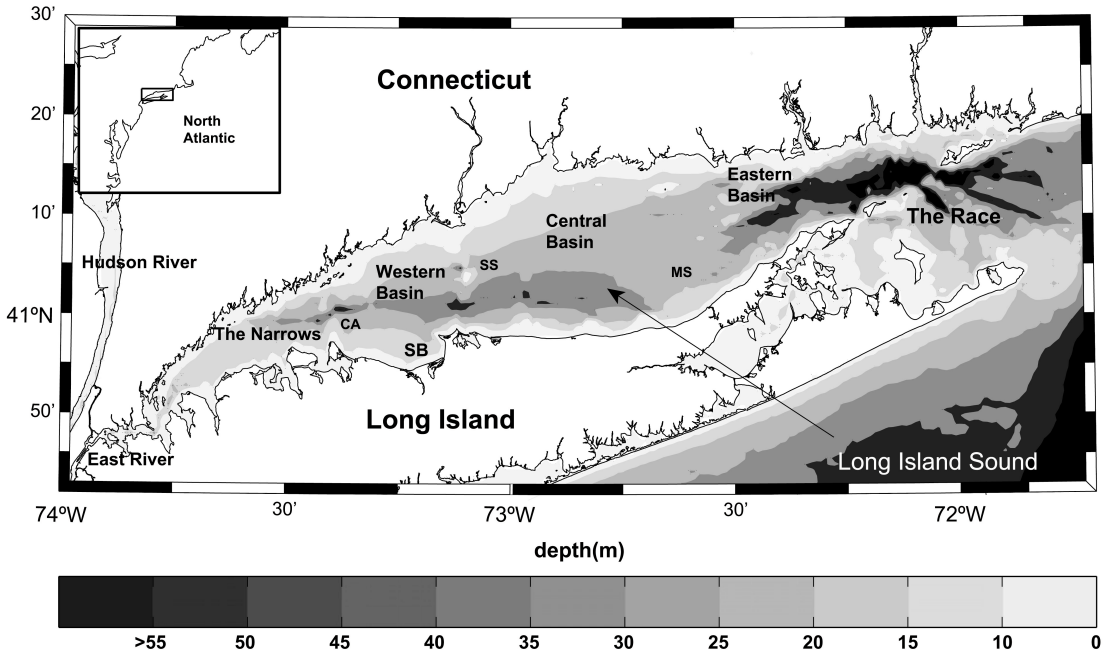

Fig. 5. Bathymetry of Long Island Sound (CA, Cable and Anchor Reef; SB, Smithtown Bay; SS, Stratford Shoal; MS, Mattituck Sill). From Lee and Lwiza (2008).

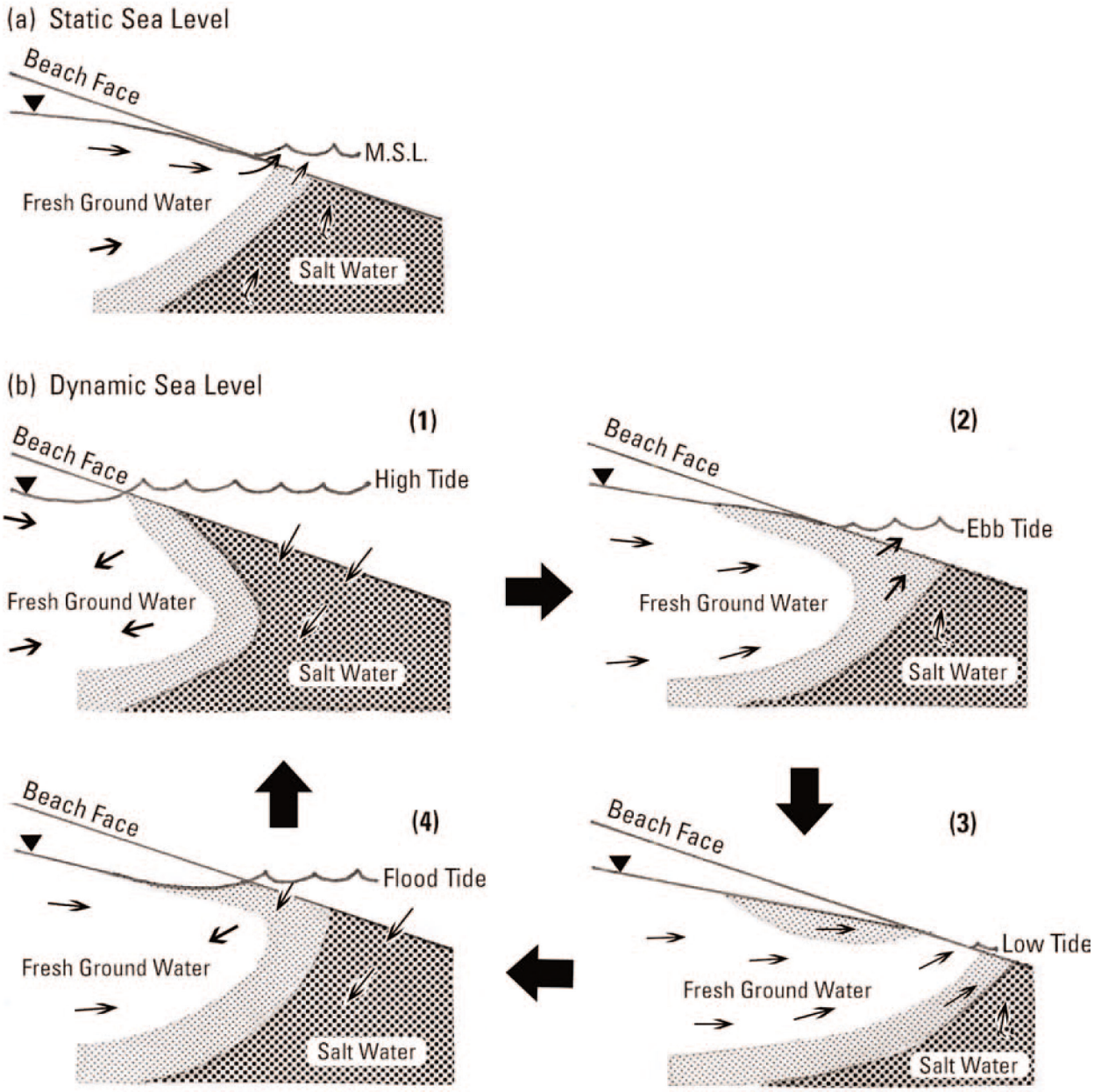

Figure 6. Beach ground water discharge and infiltration concept: (a) is the discharge for a static sea level and (b) is the discharge and infiltration for a dynamic tidal cycle during (1) high tide, (2) ebb tide, (3) low tide, and (4) flood tide. The arrows indicate the general direction and pattern of flow. The stippled pattern between fresh water and salt water indicates a zone of mixing between the two water. Figure and accompanying text from Urish and McKenna (2004).

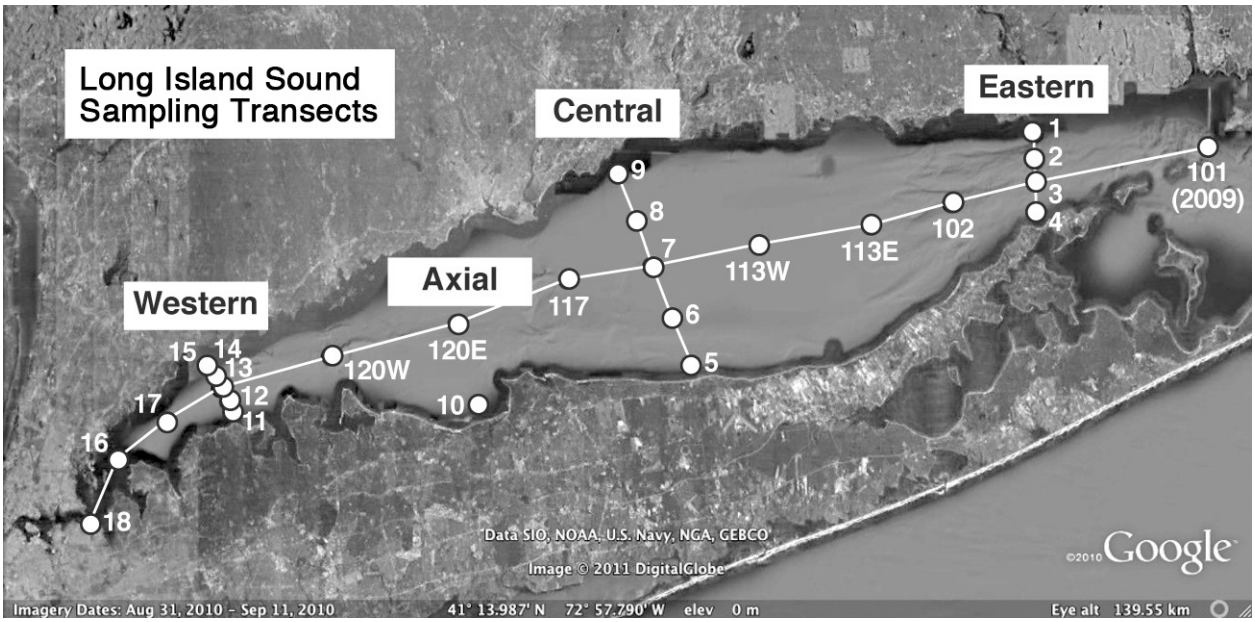

Figure 7. Long Island Sound transects and associated sampling stations. Spring 2009 sampling excluded stations 17, 18 and 113E. Summer 2009 sampling included only the axial transect extending from the Narrows to the Race, excluding station 101. Summer 2010 sampling included all stations except station 101.

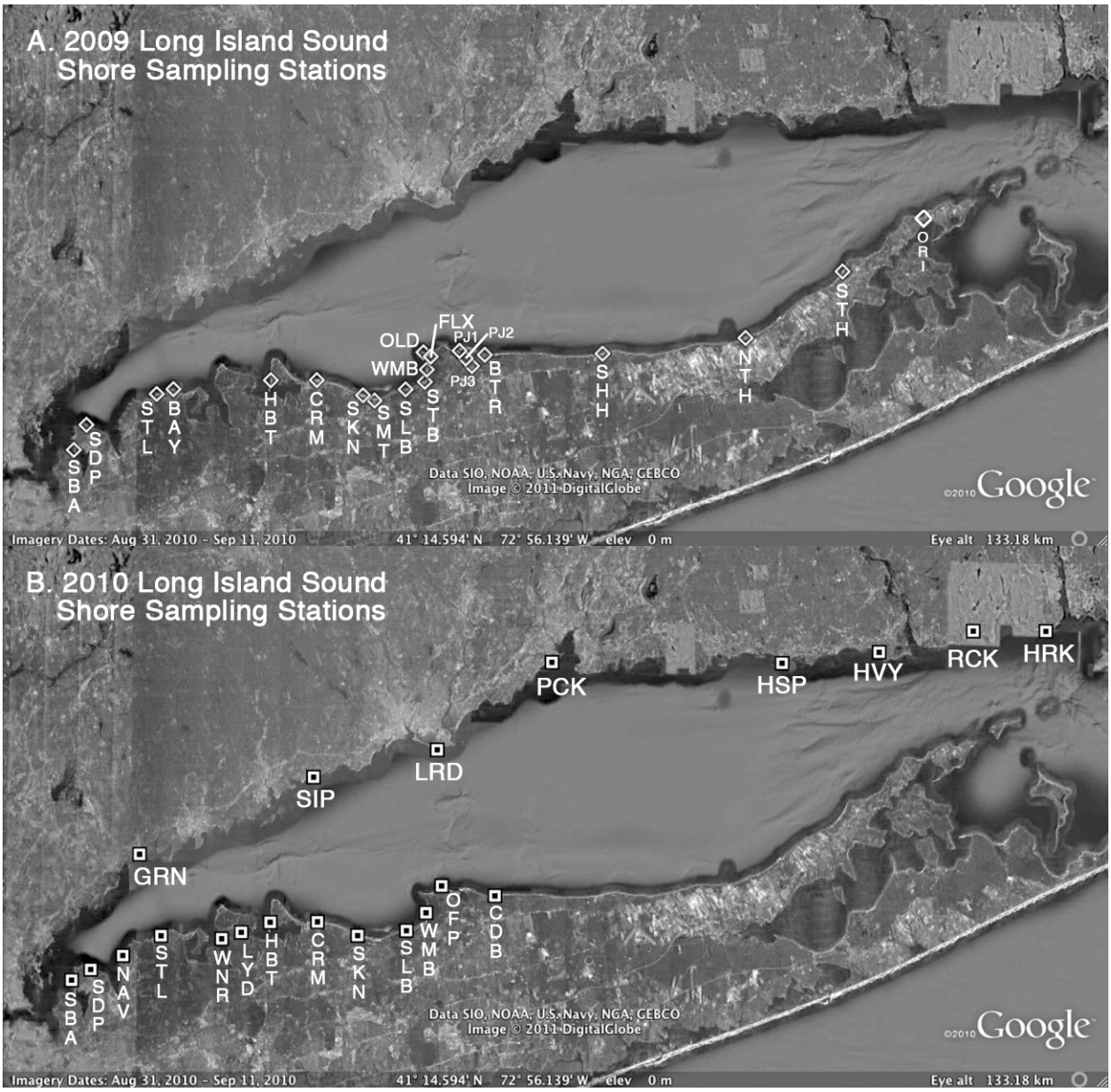

Figure 8. **A**. 2009 Ra shore stations along the shore of Long Island Sound (LIS): New York; **B**. 2010 Ra shore stations along the shore of Long Island Sound: Connecticut and Western Long Island, New York.

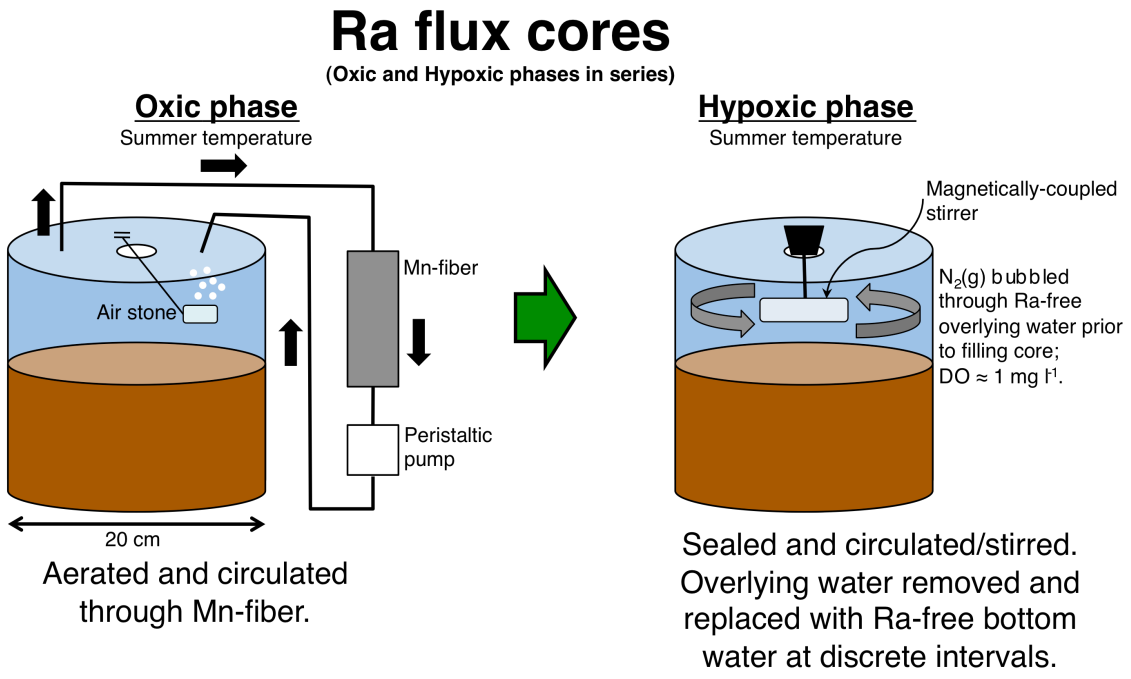

Figure 9. Schematic representation of Ra flux core laboratory methods. In the **oxic phase** of the experiment the cores were aerated and the overlying water was continuously circulated through a cartridge filled with ~15 g MnO_2-impregnated acrylic fiber (Mn-fiber) thus removing Ra from the water. The Mn-fiber was removed at specific time intervals and analyzed for ^{224}Ra and ^{223}Ra to determine concentrations. Diffusive flux was calculated from the slope of the trendline of Ra concentrations plotted with respective incubation times. The **hypoxic phase** was initiated after approximately 200 h of oxic conditions. The cores were covered with Ra-free, de-oxygenated bottom water from the respective station, sealed, and circulated continuously via a magnetically-coupled stirring rod. The overlying water was removed at discrete time intervals and analyzed for ^{224}Ra and ^{223}Ra to determine concentrations. Diffusive flux was calculated from these concentration values and the respective incubation time (time since overlying water was replaced with Ra-free water).

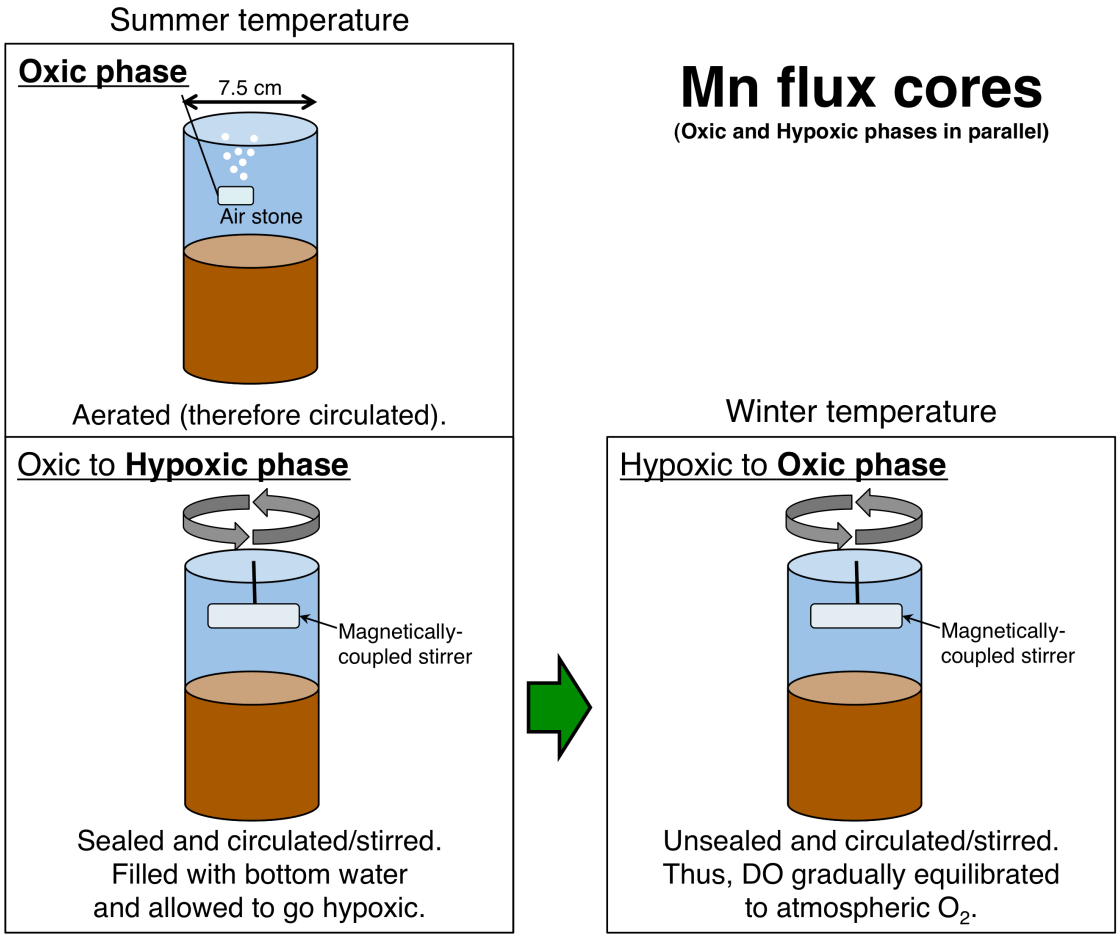

Figure 10. Schematic representation of Mn flux core laboratory methods. Two cores from each station were set up in parallel: the **oxic phase** cores were aerated; the oxic to **hypoxic phase** cores were sealed, circulated, and allowed to go hypoxic. Small volume water samples were taken (and replaced) at fixed internals to determine dissolved oxygen (DO) and Mn(aq) in the overlying water. The cores were incubated until the overlying water in the hypoxic phase cores displayed DO concentrations less than 3.0 mg l^{-1} for multiple time intervals. The hypoxic cores were then transferred to a winter temperature coldroom and unsealed. Water samples were taken in the same manner as above. Mn(aq) fluxes were calculated from the change in Mn(aq) concentrations over time in the overlying water of the cores.

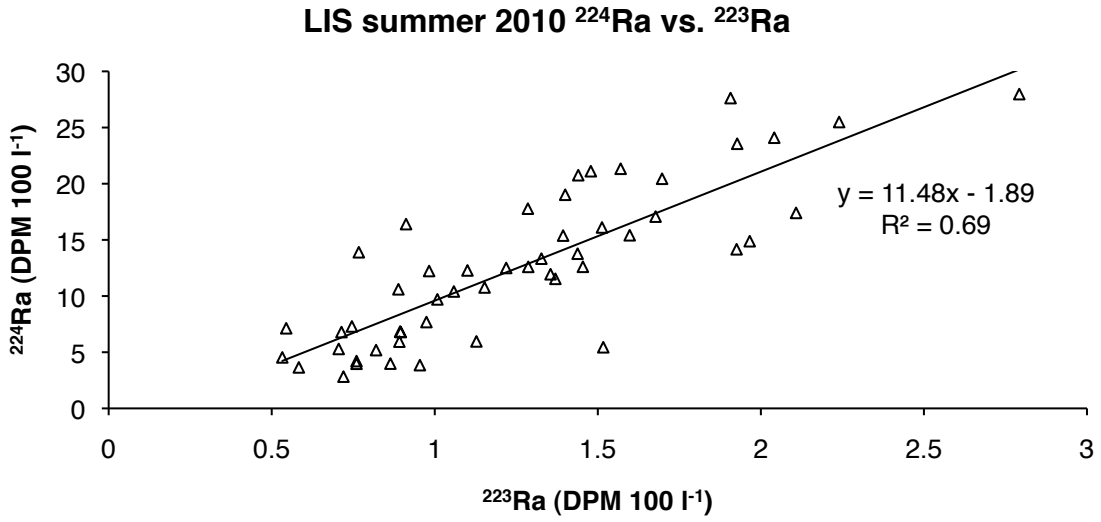

Figure 11. ^{224}Ra concentration values plotted against corresponding ^{223}Ra values for all samples obtained summer 2010, Long Island Sound (n = 51).

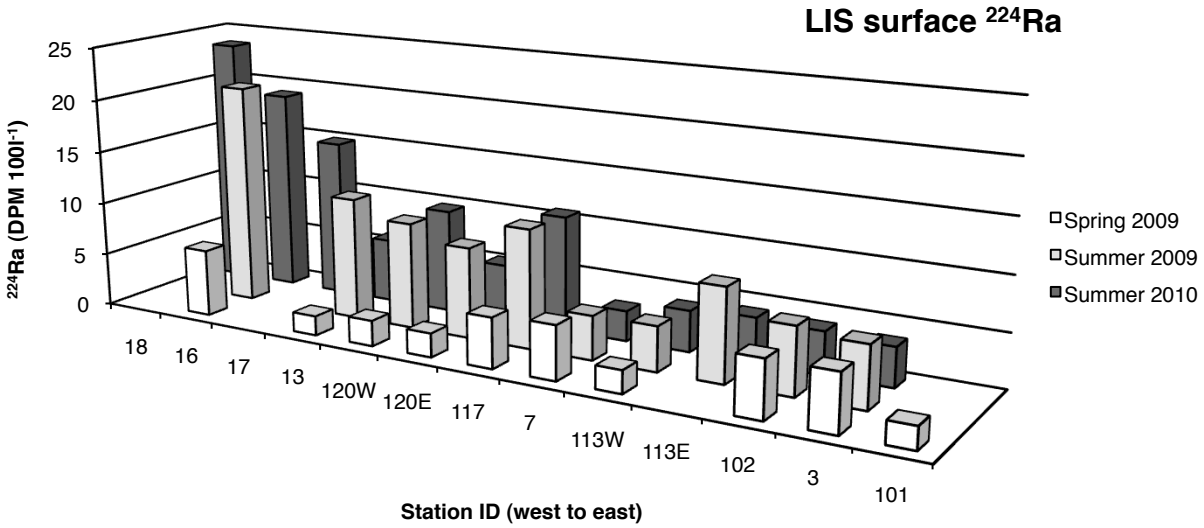

Figure 12. Long Island Sound (LIS) **surface ^{224}Ra concentrations** along the axial transect, from the Narrows to the Race.

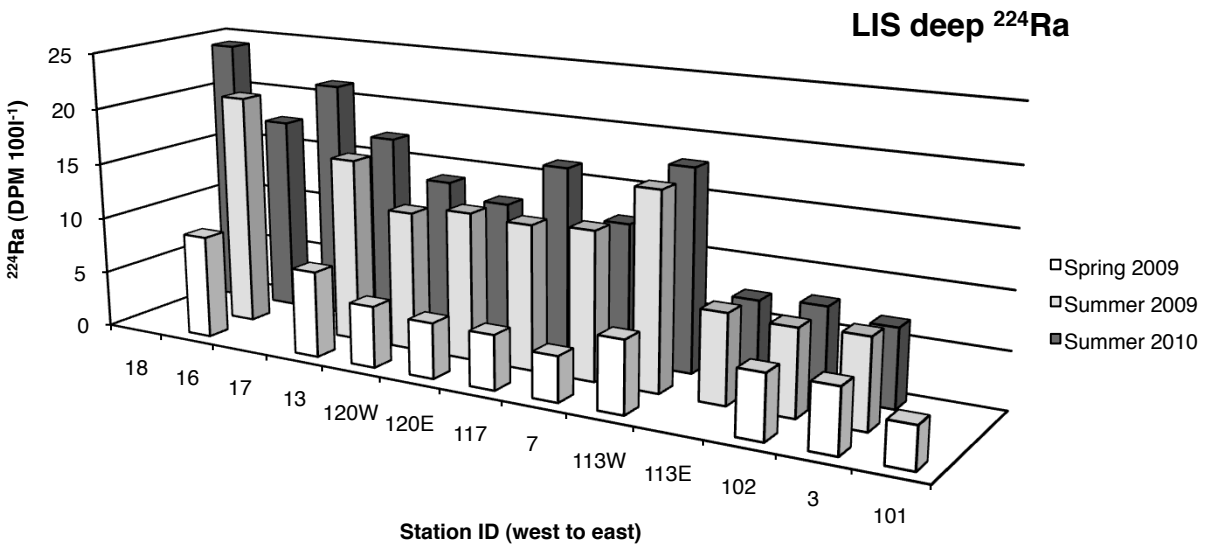

Figure 13. Long Island Sound (LIS) **deep ^{224}Ra concentrations** along the axial transect, from the Narrows to the Race.

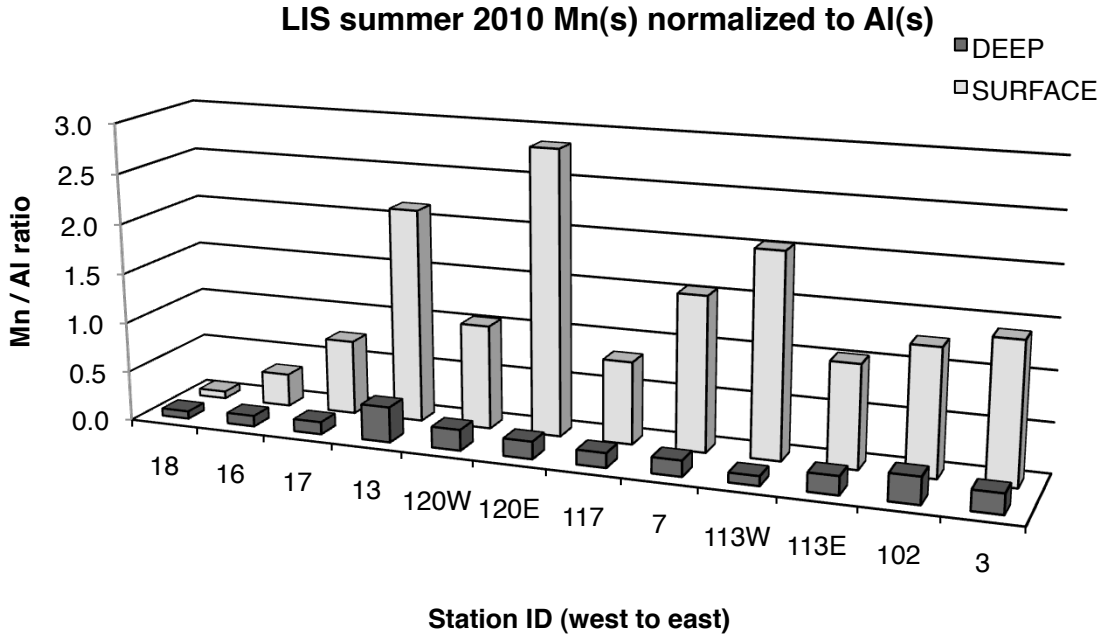

Figure 14. Long Island Sound (LIS) summer 2010 water column Mn(s) normalized to Al(s).

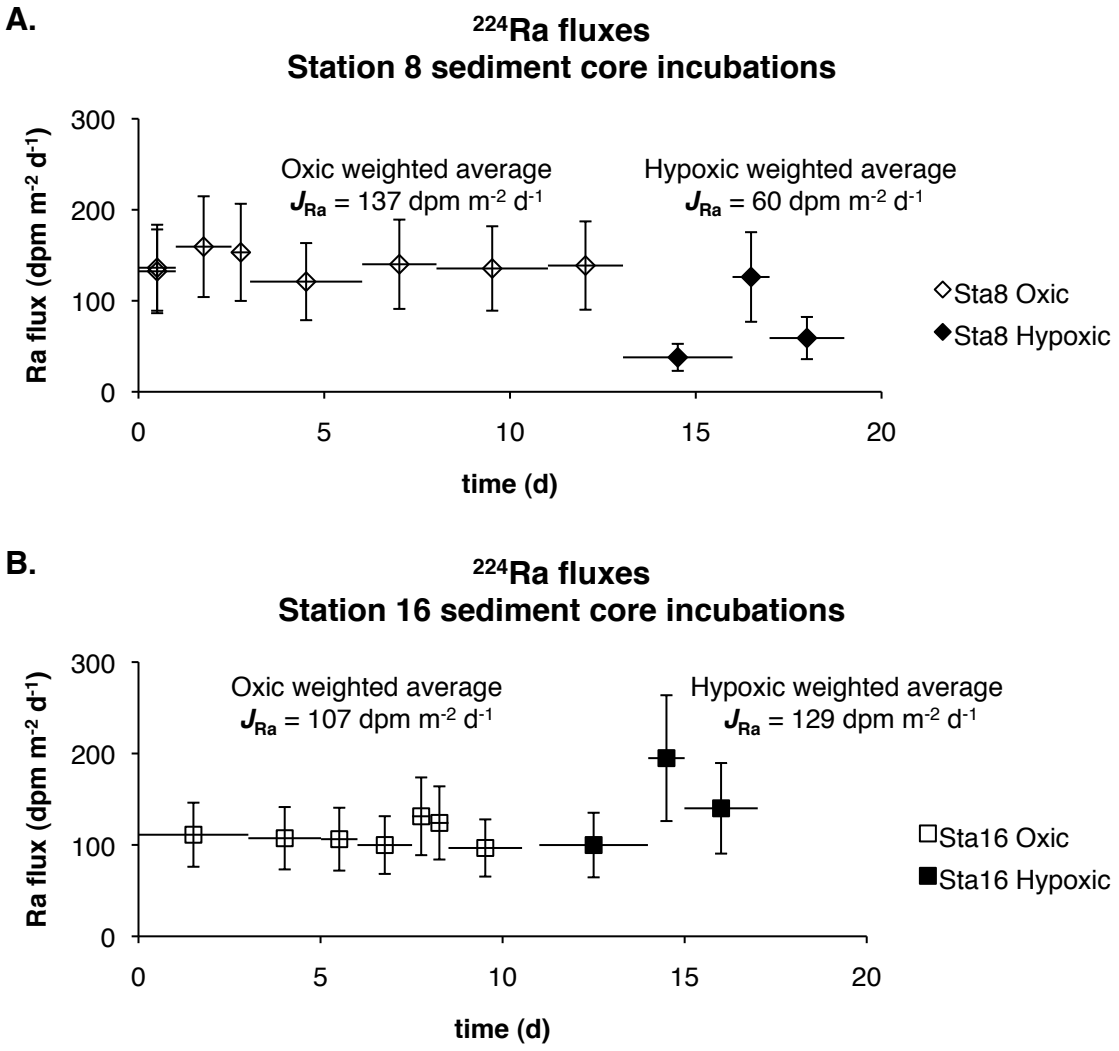

Figure 15. **A**. ^{224}Ra fluxes over time for the station 8 flux core; **B**. ^{224}Ra fluxes over time for the station 16 flux core.

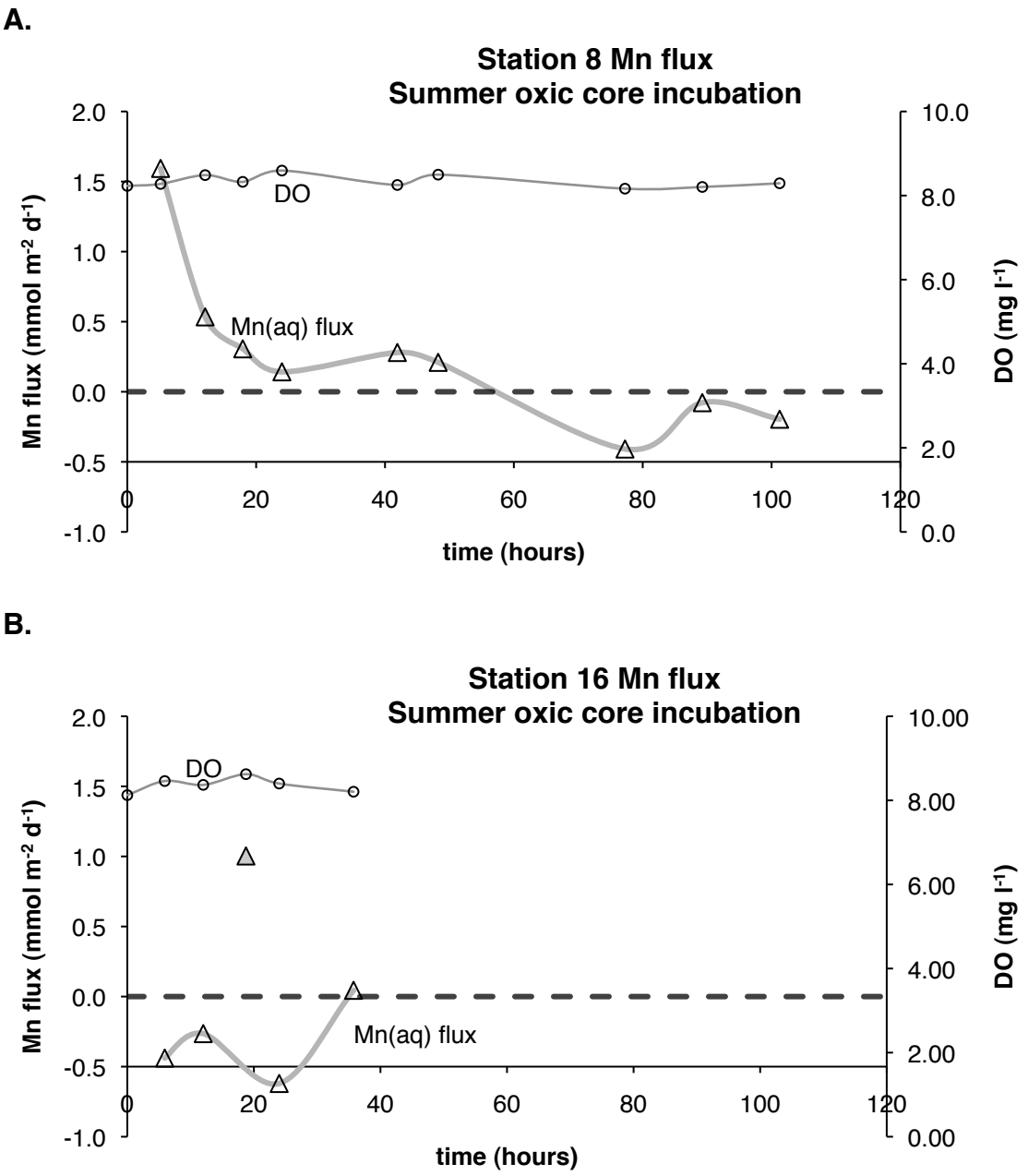

Figure 16. Mn(aq) fluxes and accompanying DO concentrations over time for summer oxic Mn flux cores: **A**. Station 8; **B**. Station 16. Dashed lines represent Mn flux = 0 mmol m^{-2} d^{-1}.

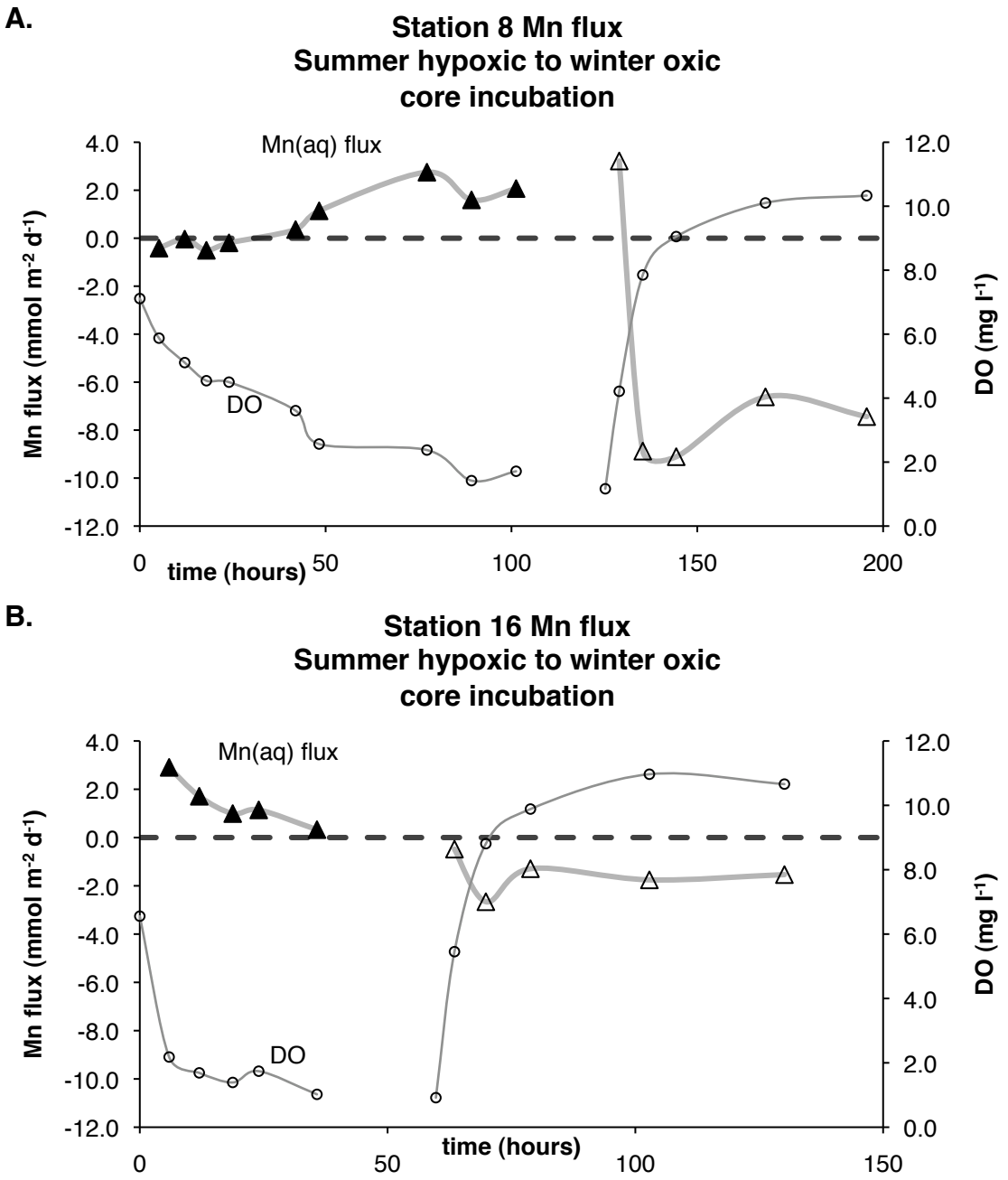

Figure 17. Mn(aq) fluxes and accompanying DO concentrations over time for summer anoxic to winter oxic Mn flux cores: **A**. station 8; **B**. station 16. Core temperatures for summer and winter phases were 21ºC and 2.5ºC respectively. Dashed lines represent Mn flux = 0 mmol m^{-2} d^{-1}.

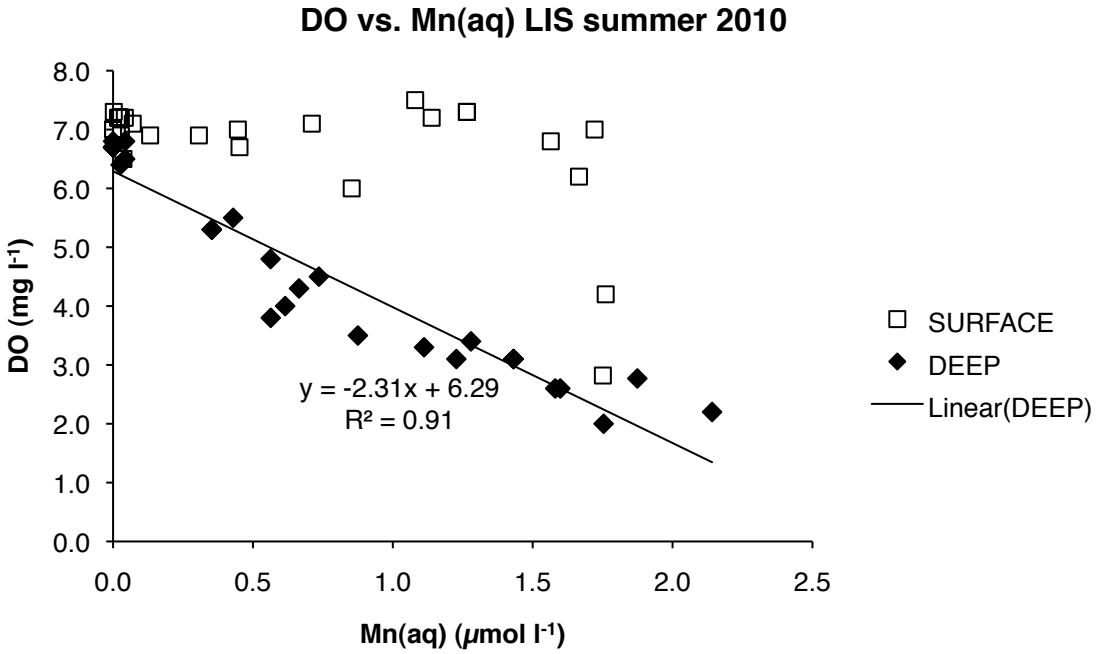

Figure 18. LIS Summer 2010 surface and deep Mn(a) concentrations plotted against corresponding DO concentrations. A strong correlation between deep Mn(aq) and DO values was observed.

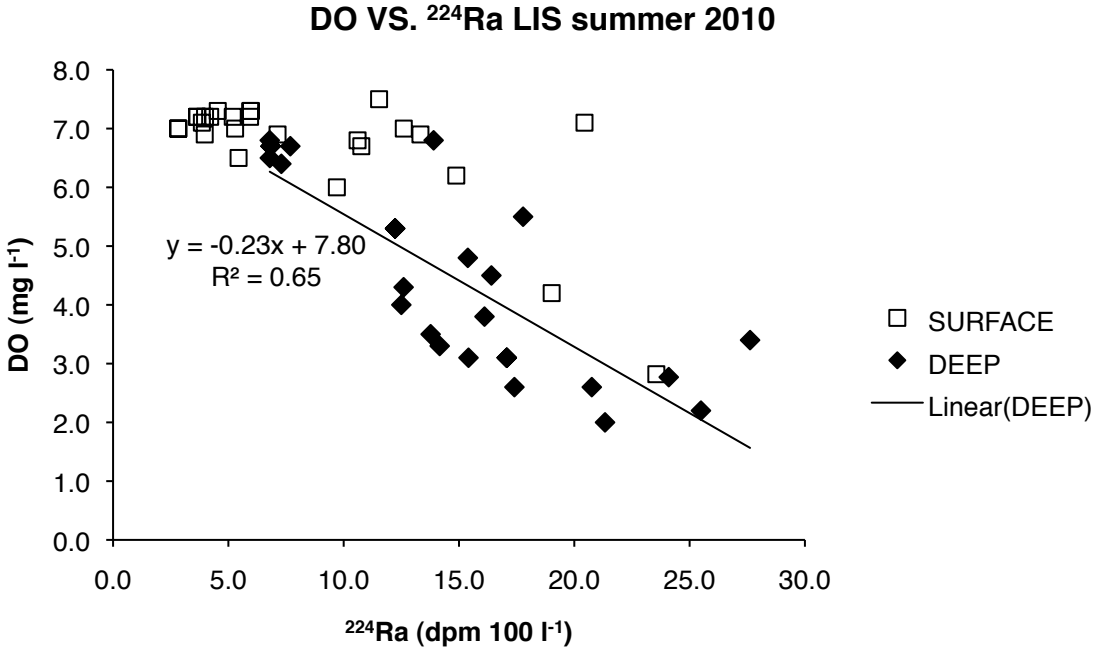

Figure 19. LIS summer 2010 surface and deep ^{224}Ra concentrations plotted against corresponding DO concentrations. A correlation between deep ^{224}Ra and DO values was observed.

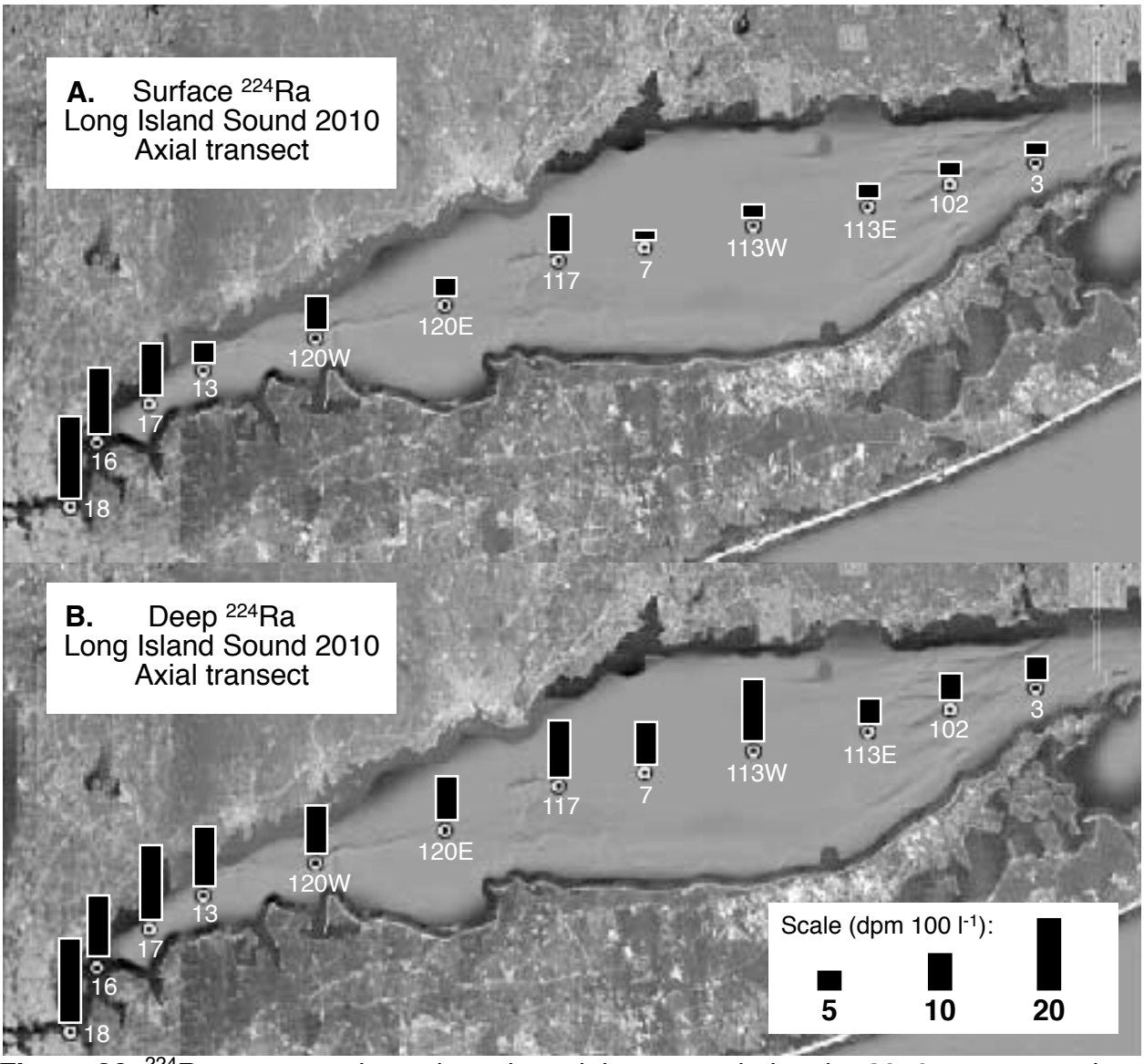

Figure 20. ^{224}Ra concentrations along the axial transect during the 2010 summer cruise in Long Island Sound: **A**. Surface; **B**. deep. Heights of the black bars above each station are proportional to the ^{224}Ra concentration in dpm 100 l^{-1} observed for the given station.

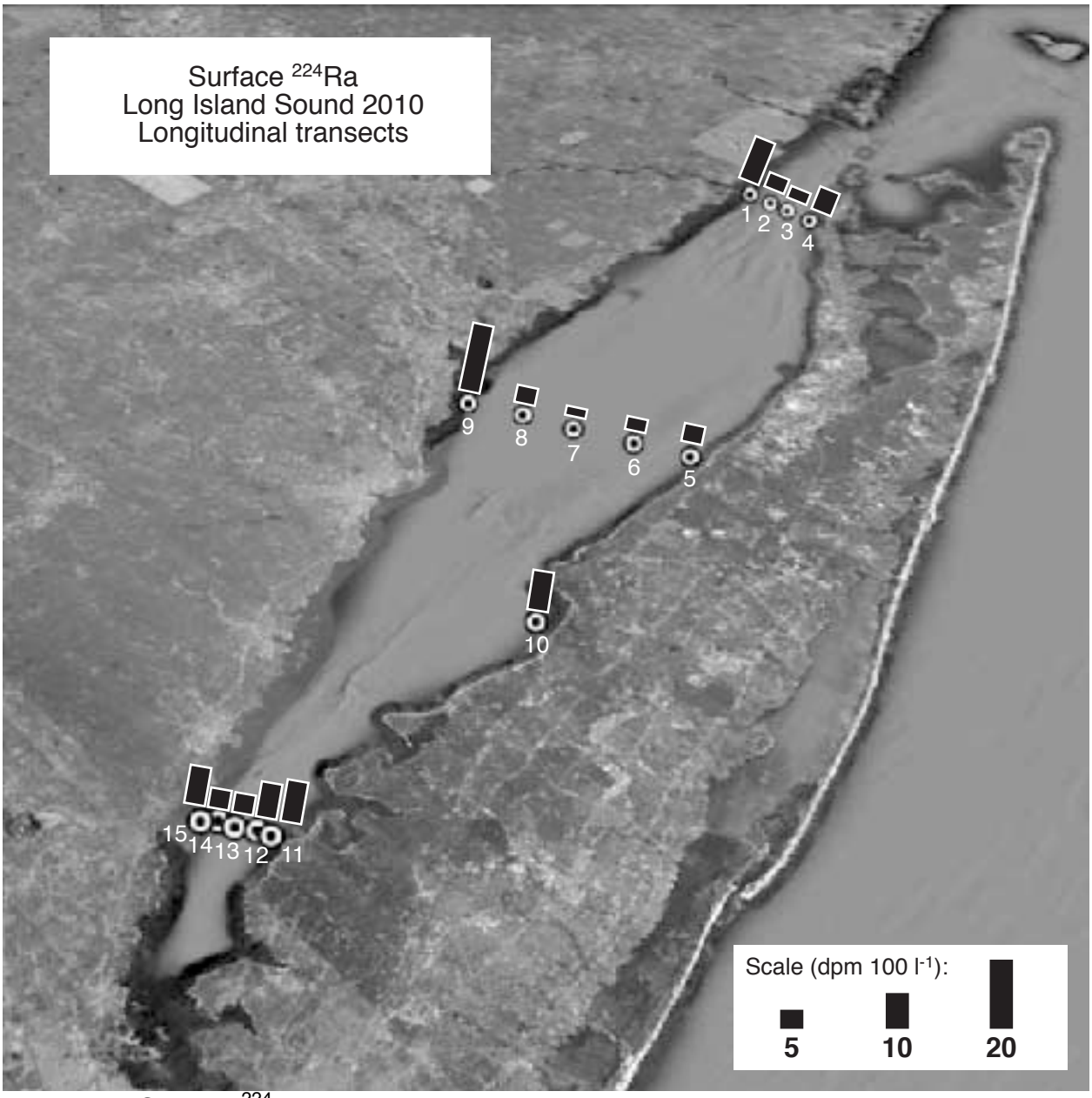

Figure 21. Surface ^{224}Ra concentrations along the longitudinal transects showing the marginal input of Ra to Long Island Sound. Heights of the red bars above each station are proportional to the ^{224}Ra concentration in DPM 100l^{-1} observed for the given station during the 2010 summer cruise in Long Island Sound.

Figure 22. Deep ^{224}Ra concentrations along the longitudinal transects showing the marginal input of Ra to Long Island Sound. Heights of the red bars above each station are proportional to the ^{224}Ra concentration in DPM 100l^{-1} observed for the given station during the 2010 summer cruise in Long Island Sound.

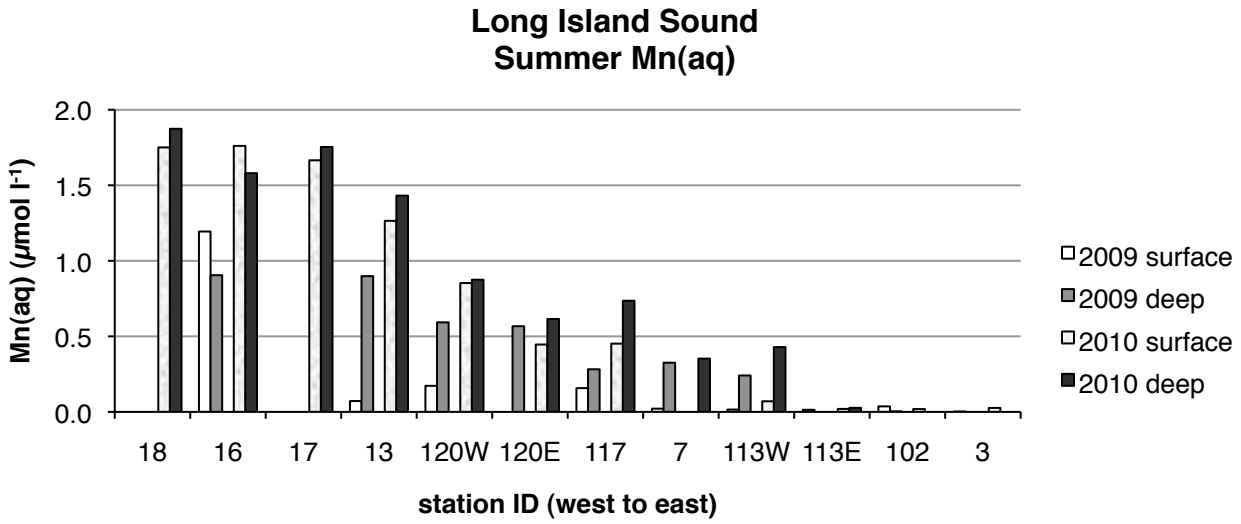

Figure 23. Water column Mn(aq) during summer in Long Island Sound, 2009 and 2010.

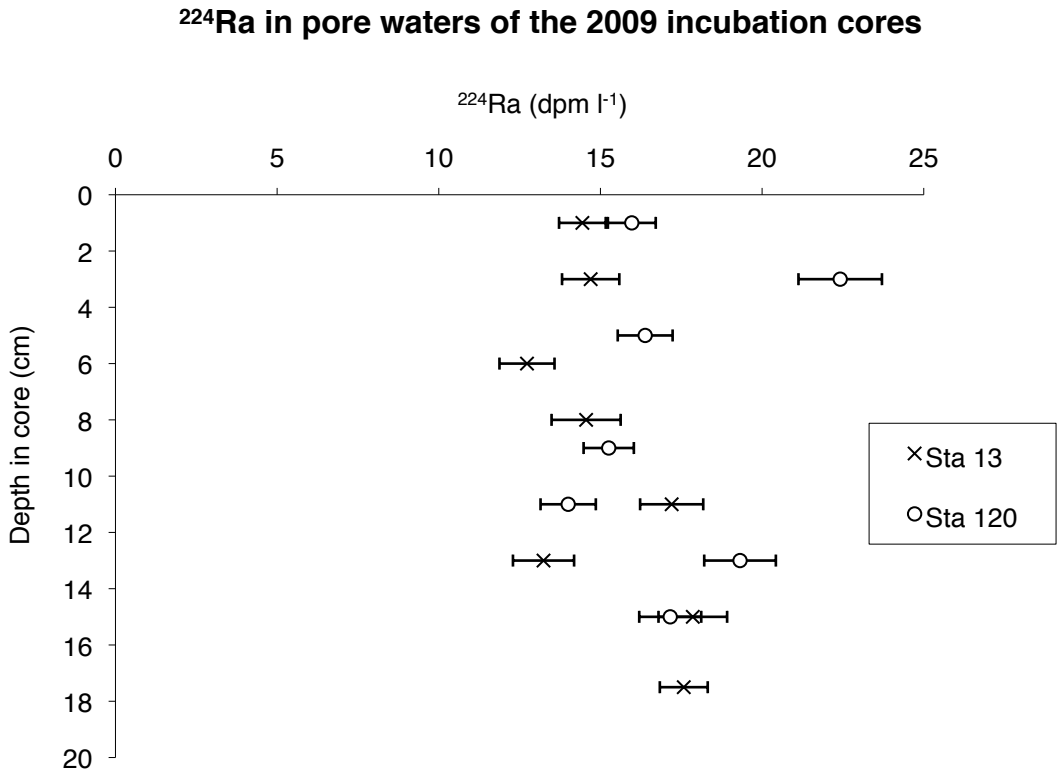

Figure 24. Pore water ^{224}Ra values in the two 2009 Ra flux cores. A $\Delta C\ \Delta x^{-1}$ value of 14.4 dpm l^{-1} 1 cm^{-1} was used to model expected fluxes using Fick's first law, where $J = D\ (\Delta C / \Delta x)$.

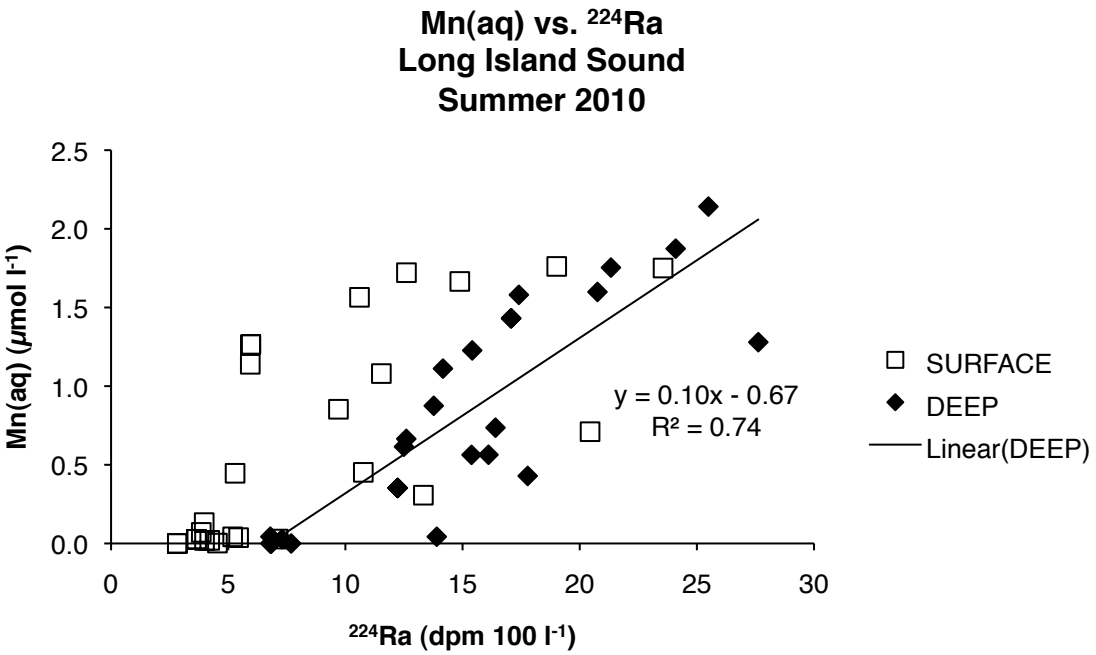

Figure 25. Plotted Mn(aq) and corresponding ^{224}Ra concentrations for all stations sampled, Long Island Sound (LIS) summer 2010. A strong correlation exists between dissolved Mn and Ra in bottom waters supporting our hypothesis of the coupling of seasonal Mn redox cycling and Ra diffusion from sediments.

Tables

Table 1. Average **^{224}Ra concentrations** (dpm 100 l^{-1}) in Long Island Sound (LIS). Values are given in dpm 100 l^{-1}.

		2009	2010
SPRING	**total**	**5.1 ± 2.0** (n = 47)	-
	surface	4.5 ± 1.9 (n = 22)	-
	deep	6.0 ± 1.9 (n = 22)	-
SUMMER	**total**	**10.6 ± 4.8** (n = 23)	**12.6 ± 6.8** (n = 51)
	surface	9.0 ± 4.6 (n = 11)	9.2 ± 5.8 (n = 24)
	deep	12.2 ± 4.6 (n = 11)	15.7 ± 6.4 (n = 24)

Table 2. Average **dissolved phase Mn** concentrations in Western, Central, and Eastern Long Island Sound (LIS). Values are given in μmol l^{-1}.

		2009			2010		
		Western	Central	Eastern	Western	Central	Eastern
SPRING	**total**	**0.53 ± 0.10** (n = 6)	**0.36 ± 0.08** (n = 8)	**0.04 ± 0.02** (n = 4)	**-**	**-**	**-**
	surface	0.59 ± 0.02 (n = 3)	0.31 ± 0.08 (n = 4)	0.04 ± 0.01 (n = 2)	-	-	-
	deep	0.48 ± 0.11 (n= 3)	0.34 ± 0.08 (n = 4)	0.04 ± 0.02 (n = 2)	-	-	-
SUMMER	**total**	**0.55 ± 0.44** (n = 6)	**0.20 ± 0.20** (n = 8)	**0.01 ± 0.01** (n = 6)	**1.42 ± 0.38** (n = 23)	**0.44 ± 0.30** (n =16)	**0.04 ± 0.08** (n = 12)
	surface	0.48 ± 0.62 (n = 3)	0.05 ± 0.07 (n = 4)	0.02 ± 0.02 (n = 3)	1.33 ± 0.43 (n = 10)	0.24 ± 0.30 (n = 8)	0.07 ± 0.12 (n = 6)
	deep	0.80 ± 0.18 (n = 3)	0.35 ± 0.15 (n = 4)	0 (n = 3)	1.51 ± 0.37 (n = 10)	0.78 ± 0.30 (n = 8)	0.02 ± 0.02 (n = 6)

Table 3. Comparison of Long Island Sound (LIS) shore station ^{224}Ra concentrations in surface waters with corresponding LIS water column ^{224}Ra concentrations. The criterion for "corresponding stations" is simply water column station in closest proximity to shore station. Stations are in ascending order from west to east.

	LIS shore	^{224}Ra pore H_2O (dpm 100 l^{-1})	^{224}Ra surface (dpm 100 l^{-1})	^{224}Ra deep (dpm 100 l^{-1})	^{224}Ra surface (dpm 100 l^{-1})	**LIS H_20 column**	
CT	Greenwich (**GRN**)	–	38.5	14.2	11.5	station 15	**CT**
	Peck Avenue (**PCK**)	378.0	37.1	27.6	20.4	station 9	
	Harvey's Beach (**HVY**)	–	40.1	13.9	13.3	station 1	
LI	Stehli Beach (**STL**)	260.0	36.0	25.5	12.6	station 11	**LI**
	Sunken Meadow (**SKN**)	430.4	210.6	28.0	11.9	station 10	
	Cedar Beach (**CDB**)	160.6	34.5	16.1	5.4	station 5	

Works Cited

Aller, RC. 1994. The sedimentary Mn cycle in Long Island Sound: Its role as intermediate oxidant and the influence of bioturbation, O_2, and C_{org} flux on diagenetic reaction balances. J. Mar. Res. 52: 259–295.

Anderson, TH and GT Taylor. 2001. Nutrient pulses, plankton blooms, and seasonal hypoxia in western Long Island Sound. Estuaries 24: 228–243.

Beck, AJ, JP Rapaglia, JK Cochran, HJ Bokuniewicz. 2007. Radium mass-balance in Jamaica Bay, NY: Evidence for a substantial flux of submarine groundwater. Marine Chemistry 106: 419–441.

Beck, AJ, JP Rapaglia, JK Cochran, HJ Bokuniewicz, S Yang. 2008. Submarine groundwater discharge to Great South Bay, NY, estimated using Ra isotopes. Marine Chemistry 109: 279–291.

Blumberg, AF and DW Pritchard. 1997. Estimates of the transport through the East River, New York. J. of Geophys. Res. 102: 5685–5703.

Boehm, AB, A Paytan, GG Shellenbarger, KA Davis. 2006. Composition and flux of groundwater from a California beach aquifer: Implications for nutrient supply to the surf zone. Continental Shelf Research 26: 269–282.

Bokuniewicz, H. 1980. Groundwater seepage into Great South Bay, New York. Estuarine and Coastal Marine Science 10: 437–444.

Burnett, WC, R Peterson, WS Moore, J de Oliveira. 2008. Radon and radium isotopes as tracers of submarine groundwater discharge – Results from the Ubatuba, Brazil SGD assessment intercomparison. Estuarine, Coastal and Shelf Science 76: 501–511

Capone, DG and MF Bautista. 1985. A groundwater source of nitrate in nearshore marine sediments. Nature 313: 214–216.

Charette, MA and KO Buessler. 2004. Submarine groundwater discharge of nutrients and copper to an urban subestuary of Chesapeake Bay (Elizabeth River). Limnology and Oceanography 49: 376–385.

Charette, MA, R Splivallo, C Herbold, MS Bollinger, WS Moore. 2003. Salt marsh submarine groundwater discharge as traced by radium isotopes. Marine Chemistry 84: 113–121.

Cochran JK. 1979. The Geochemistry of ^{226}Ra and ^{228}Ra in Marine Deposits, Ph.D. Thesis, Yale University, New Haven, CT.

Cochran, JK. 1984. The fates of uranium and thorium decay series nuclides in the estuarine environment. *In* The Estuary as a Filter. Ed. VS Kennedy. Academic Press, New York. pp 179–220.

Crespo, MT, JL Gascón, ML Aceña. 1993. Techniques and analytical methods in the determination of uranium, thorium, plutonium, americium and radium by adsorption on manganese dioxide. Sci. Tot. Environ. 130: 383–391.

Crotwell, AM and WS Moore. 2003. Nutrient and radium fluxes from submarine groundwater discharge to Port Royal Sound, South Carolina. Aquatic Geochemistry 9: 191–208.

Hwang, D-W, G Kim, Y-W Lee, H-S Yang. 2005. Estimating submarine inputs of

groundwater and nutrients to a coastal bay using radium isotopes. Marine Chemistry 96: 61–71.
Jensen, LM, K Sand-Jensen, S Marcher, M Hansen. 1990. Plankton community respiration along a nutrient gradient in a shallow Danish estuary. Marine Ecology Progress Series 61: 75–85.
Johannes, RE 1980. The ecological significance of the submarine discharge of groundwater. Marine Ecology Progress Series 3: 365–373.
Kim, G, J-W Ryu, H-S Yang, S-T Yun. 2005. Submarine groundwater discharge (SGD) into the Yellow Sea revealed by ^{228}Ra and ^{226}Ra isotopes: Implications for global silicate fluxes. Earth and Planetary Science Letters 237: 156–166.
Krest, JM., WS Moore, LR Gardner, JT Morris. 2000. Marsh nutrient export supplied by groundwater discharge: Evidence from radium measurements. Global Biogeochemical Cycles 14: 167–176.
Kristiansen, KD, E Kristensen, EMH Jensen. 2002. The influence of bottom water hypoxia on the behavior of manganese and iron in sandy coastal marine sediment. Estuarine, Coastal and Shelf Science 55: 645–654.
Lee, YJ and KMM Lwiza. 2005. Interannual variability of temperature and salinity in shallow water: Long Island Sound, New York. J. of Geophys. Res. 110: C09022, 12 pp.
Lee, YJ and KMM Lwiza. 2008. Characteristics of bottom dissolved oxygen in Long Island Sound, New York. Estuarine, Coastal and Shelf Science 76: 187–200.
Mackin, J, R Aller, H Vigil, P Rude. 1991. Nutrient and dissolved oxygen fluxes across the sediment-water interface. *In* Long Island Sound Study Final Report, Sediment Geochemistry and Biology, US-EPA Contract CE 002870026. Section IV: 1–252.
Mackin, JE and KT Swider. 1989. Organic matter decomposition pathways and oxygen consumption in coastal marine sediments. J. of Marine Research 47: 681–716.
Moore, WS and R Arnold. 1996. Measurement of ^{223}Ra and ^{224}Ra in coastal waters using a delayed coincidence counter. J. of Geophys. Res. 101: 1321–1329.
Moore, WS 1976. Sampling ^{228}Ra in the deep ocean. Deep Sea Research and Oceanographic Abstracts 23: 647–651.
Moore, WS 1999. The subterranean estuary: A reaction zone of ground water and sea water. Marine Chemistry 65: 111–126.
Moore, WS 2003. Sources and fluxes of submarine groundwater discharge delineated by radium isotopes. Biogeochemistry 66: 75–93.
Moore, WS 2010. The effect of submarine groundwater discharge on the ocean. Annu. Rev. Mar. Sci. 2: 59–88.
Moore, WS and R Arnold. 1996. Measurement of ^{223}Ra and ^{224}Ra in coastal waters using a delayed coincidence counter. J. Geophys. Res. 101: 1321–1329.
Moore, WS and DF Reid. 1973. Extraction of radium from natural waters using manganese-impregnated acrylic fibers. J. of Geophys. Res. 78: 8880–8886.
Moore, WS and AM Wilson. 2005. Advective flow through the upper continental shelf driven by storms, buoyancy, and submarine groundwater discharge. Earth and Planetary Science Letters 235: 564–576.
Moore, WS., JL Sarmiento, RM Key. 2008. Submarine groundwater discharge

revealed by ^{228}Ra distribution in the upper Atlantic Ocean. Nature Geoscience 1: 309–311.
Oberdorfer, JA, MA Valentino, SV Smith. 1990. Groundwater contributions to the nutrient budgets of Tomales Bay, California. Biogeochemistry 12: 199–216.
O'Shea, ML and TM Brosnan. 2000. Trends in indicators of eutrophication in western Long Island Sound and the Hudson-Raritan Estuary. Estuaries 23: 877–901.
Parker, CA and JE O'Reilly. 1991. Oxygen depletion in Long Island Sound: a historical perspective. Estuaries 14: 248–264
Perlmutter, NM and HC Crandell. 1959. Geology and ground-water supplies of the south shore beaches of Long Island , NY. New York Academy of Sciences Annals 50: 1060–1076.
Poppe, LJ, HJ Knebel, BA Seekins, ME Hastings. 2000. Map showing the distribution of surficial sediments in Long Island Sound. *In* Georeferenced sea floor mapping and bottom photography in Long Island Sound. Eds. VF Paskevich and LJ Poppe. U.S. Geological Survey open-file report 00-304 (http://pubs.usgs.gov/of/2000/of00-304/htmldocs/toc.htm).
Reid, DF, RM Key, DR. Schink. 1979. Radium, thorium, and actinium extraction from seawater using an improved manganese-oxide-coated fiber. Earth and Planetary Science Letters 43: 223–226.
Sun, M, RC Aller, C Lee. 1991. Early diagenesis of chlorophyll-*a* in Long Island Sound sediments: A measure of carbon flux and particle reworking. J. of Marine Research 49: 379–401.
Sun, M-Y, RC Aller, C Lee. 1994. Spatial and temporal distributions of sedimentary chloropigments as indicators of benthic processes in Long Island Sound. J. of Mar. Res. 52: 149–176.
Thomas, E, T Gapotchenko, JC Varekamp, EL Mecray, and MR Buchholtz ten Brink. 2000. Benthic foraminifera and environmental changes in Long Island Sound. J. Coastal Res. 16: 641–655.
Torgersen, T, KK Turekian, VC Turekian, N Tanaka, E DeAngelo, J O'Donnell. 1996. ^{224}Ra distribution in surface and deep water of Long Island Sound: sources and horizontal transport rates. Continental Shelf Research 16: 1545–1559.
Turekian, KK, N Tanaka, VC Turekian, T Torgersen, EC DeAngelo. 1996. Transfer rates of dissolved tracers through estuaries based on ^{228}Ra: A study of Long Island Sound. Continental Shelf Research 16: 863–873.
Urish, DW and TE McKenna. 2004. Tidal effects on ground water discharge through a sandy marine beach. Ground Water – Oceans 42: 971–982.
Vieira, MEC. 1990. Observations of Currents, Temperature and Salinity in Long Island Sound, 1988. A Data Report. Special Data Report #6, Marine Sciences Research Center, State University of New York. Stony Brook, New York, USA.
Vieira, MEC. 2000. The long-term residual circulation in Long Island Sound. Estuaries 23: 199–207.
Welsh, BR and FC Eller. 1991. Mechanisms controlling summertime hypoxia in western Long Island Sound. Estuaries and Coasts 14: 265–278.

Appendix A: Long Island Sound field data

Figures

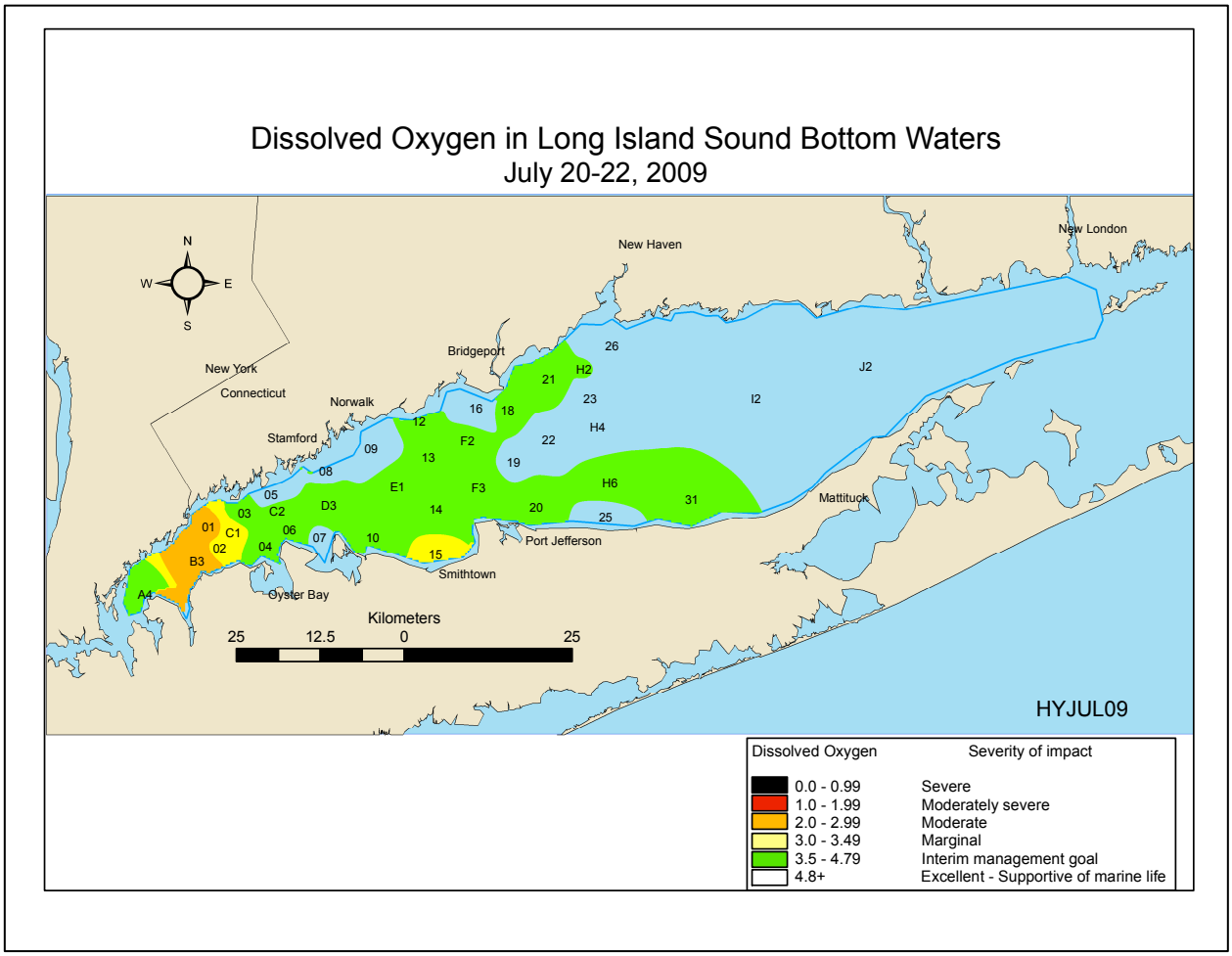

Figure A1. Connecticut Department of Environmental Protection Long Island Sound (LIS) bottom water dissolved oxygen concentrations, summer 2009 pre-cruise.

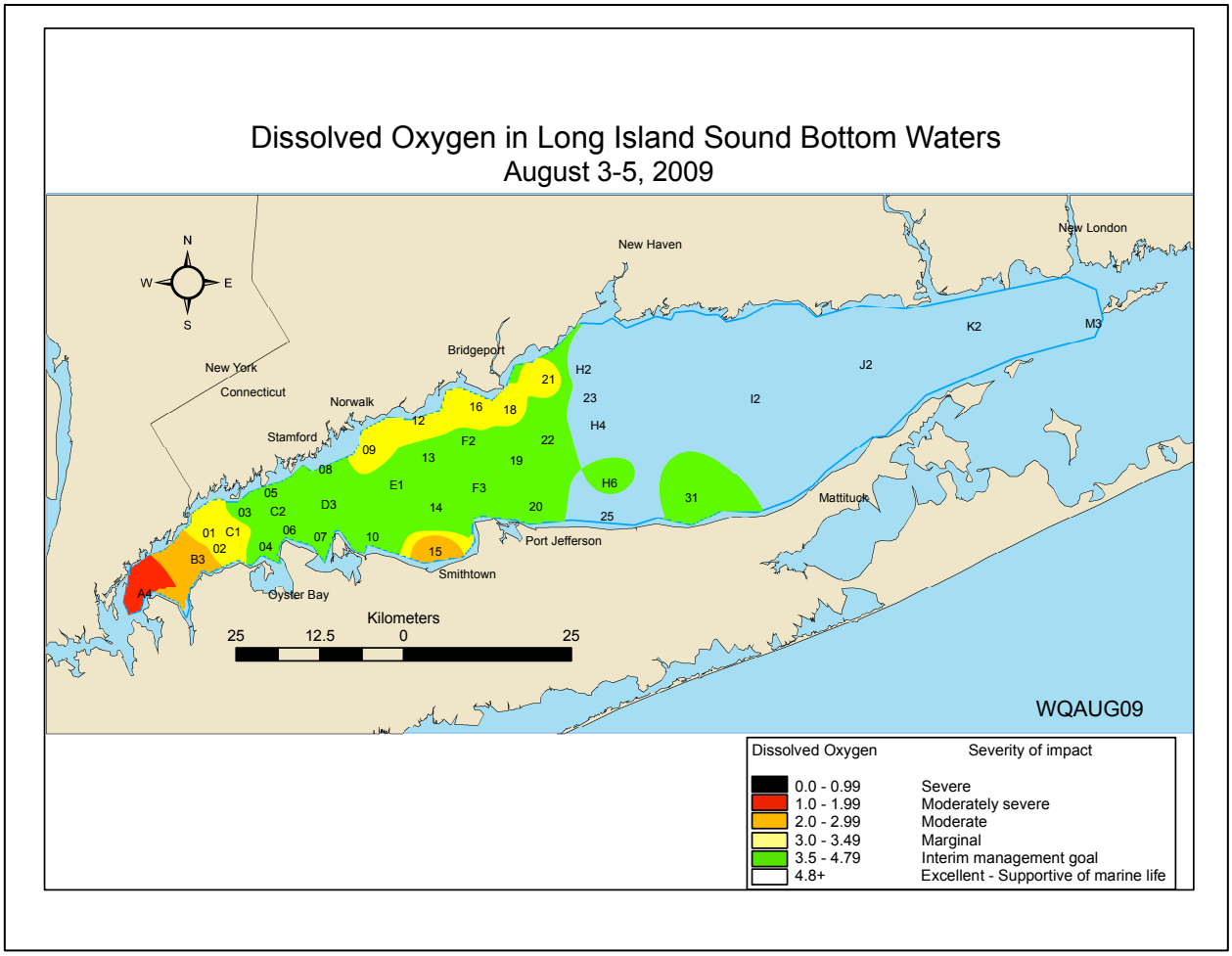

Figure A2. Connecticut Department of Environmental Protection Long Island Sound (LIS) bottom water dissolved oxygen concentrations, summer 2009. This survey was completed shortly after the 2009 Ra sampling described herein.

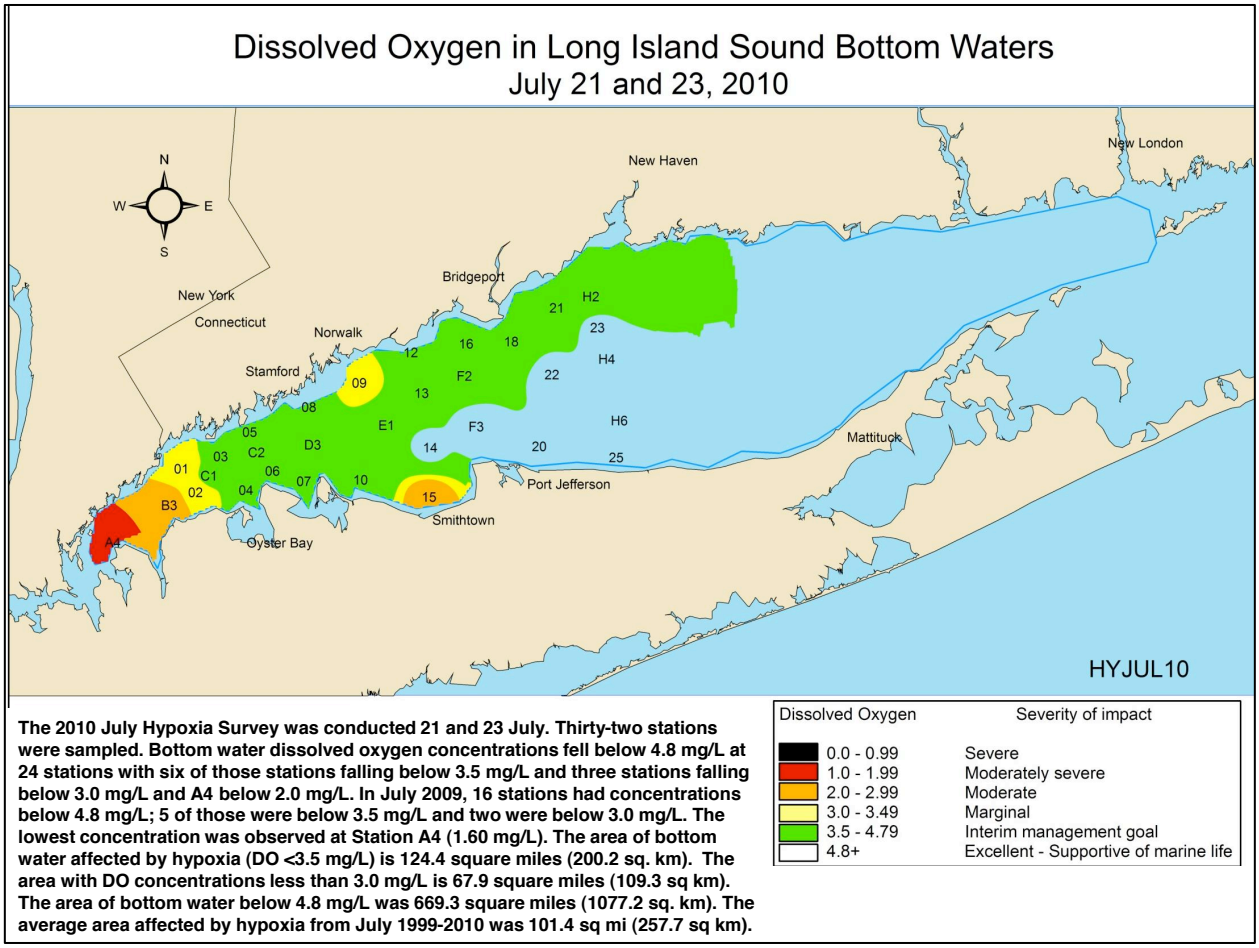

Figure A3. Connecticut Department of Environmental Protection Long Island Sound (LIS) bottom water dissolved oxygen concentrations, summer 2010. This survey was completed before the 2010 Ra sampling described herein.

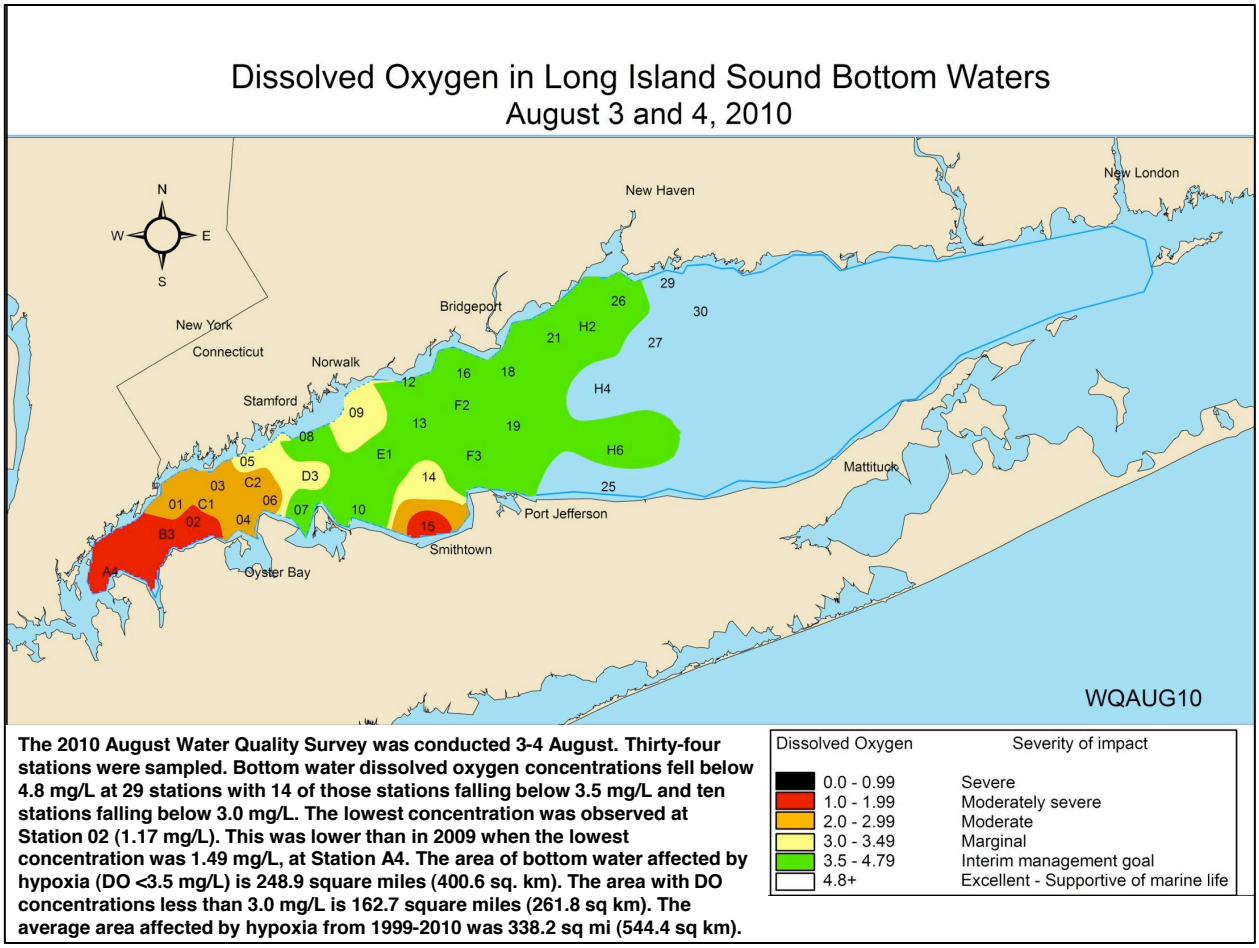

Figure A4. Connecticut Department of Environmental Protection Long Island Sound bottom water dissolved oxygen concentrations, summer 2010. This survey was completed at the start of the 2010 Ra sampling described herein.

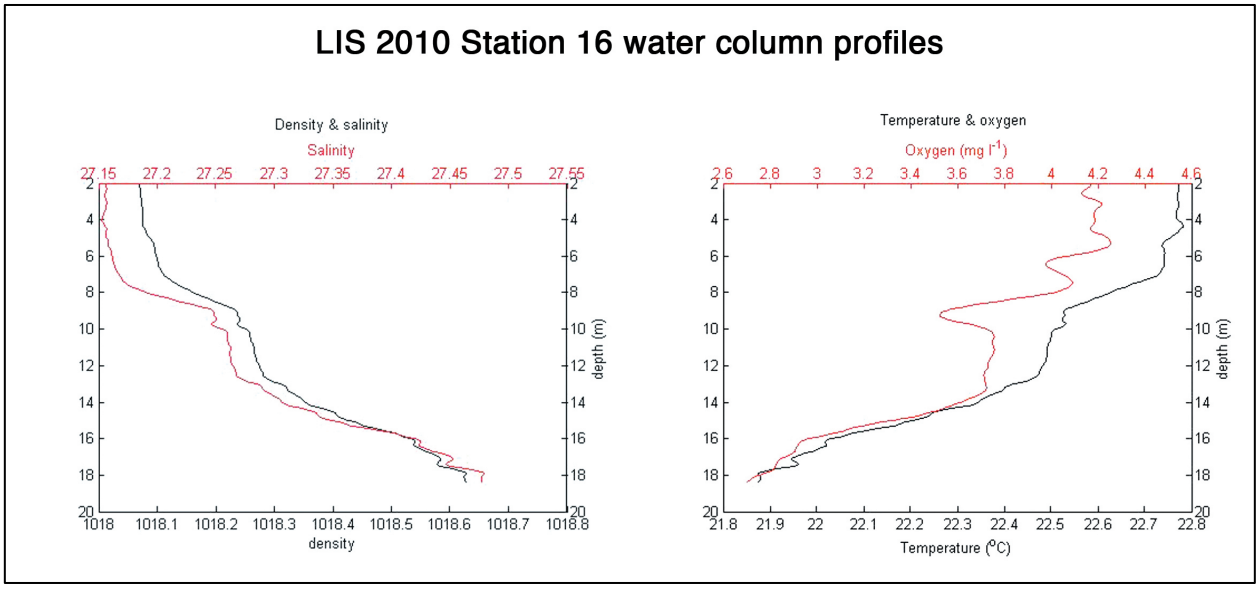

Figure A5. Water column profiles of density, salinity, temperature and dissolved oxygen at station 16, Long Island Sound summer 2010. Density and salinity are given in the units kg m^{-3} and psu, respectively.

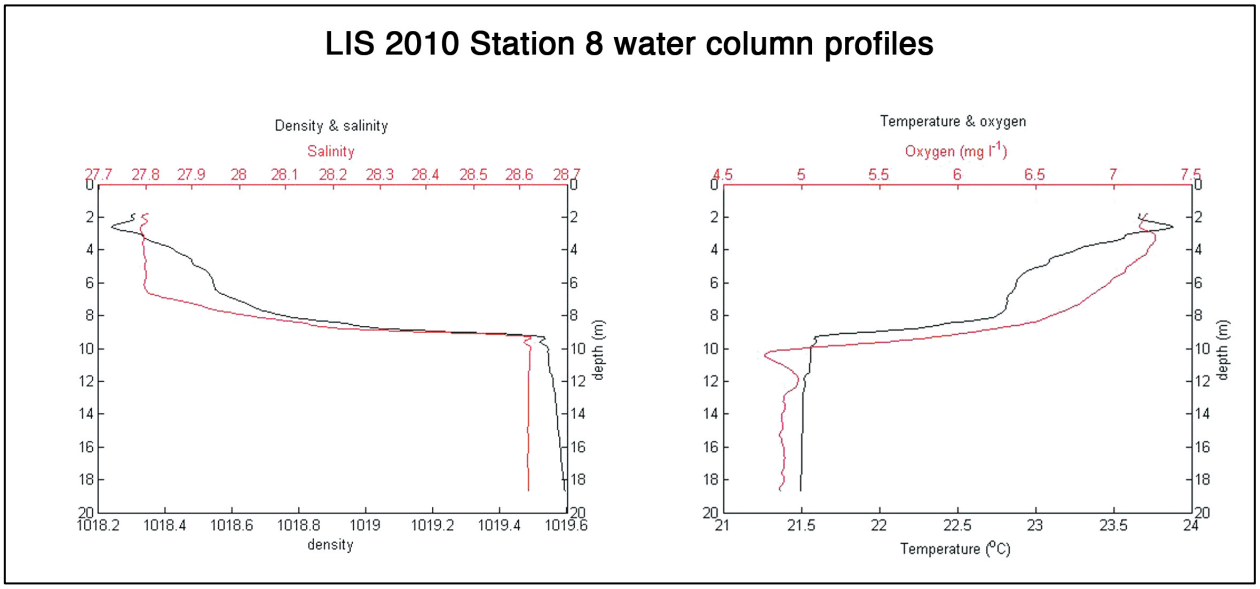

Figure A6. Water column profiles of density, salinity, temperature and dissolved oxygen at station 8, Long Island Sound summer 2010. Density and salinity are given in the units kg m^{-3} and psu, respectively.

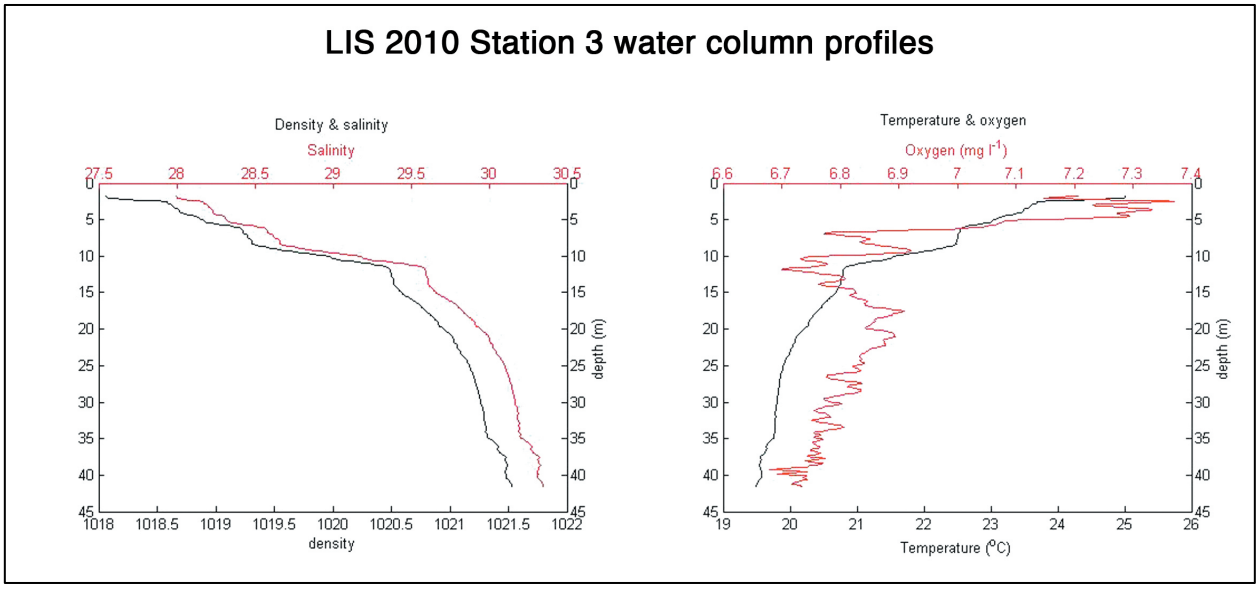

Figure A7. Water column profiles of density, salinity, temperature and dissolved oxygen at station 3, Long Island Sound summer 2010. Density and salinity are given in the units kg m^{-3} and psu, respectively.

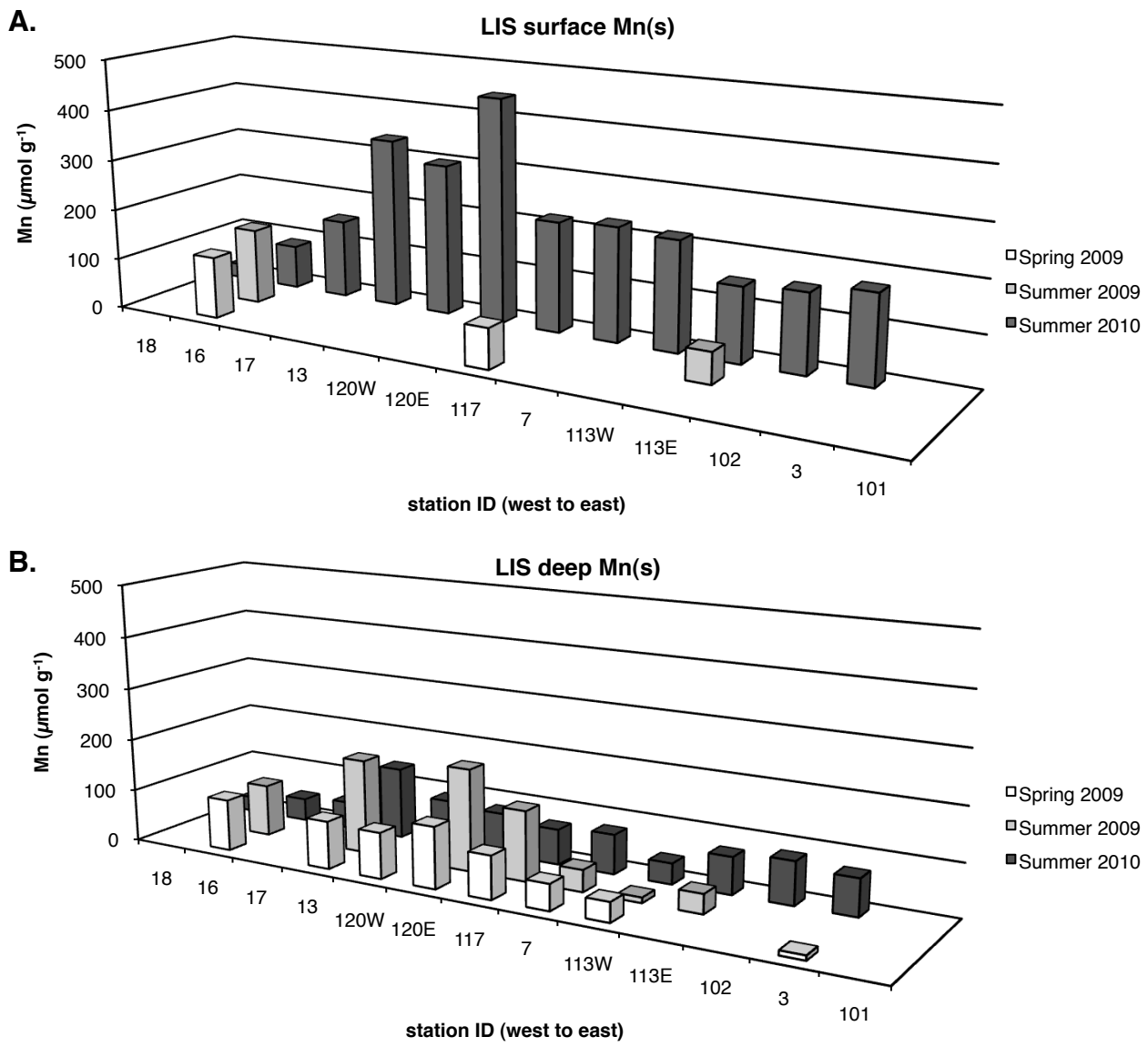

Figure A8. **A**. Long Island Sound (LIS) **surface Mn(s) concentrations** along the axial transect, from the Narrows to the Race; **B**. LIS **deep Mn(s) concentrations** along the axial transect.

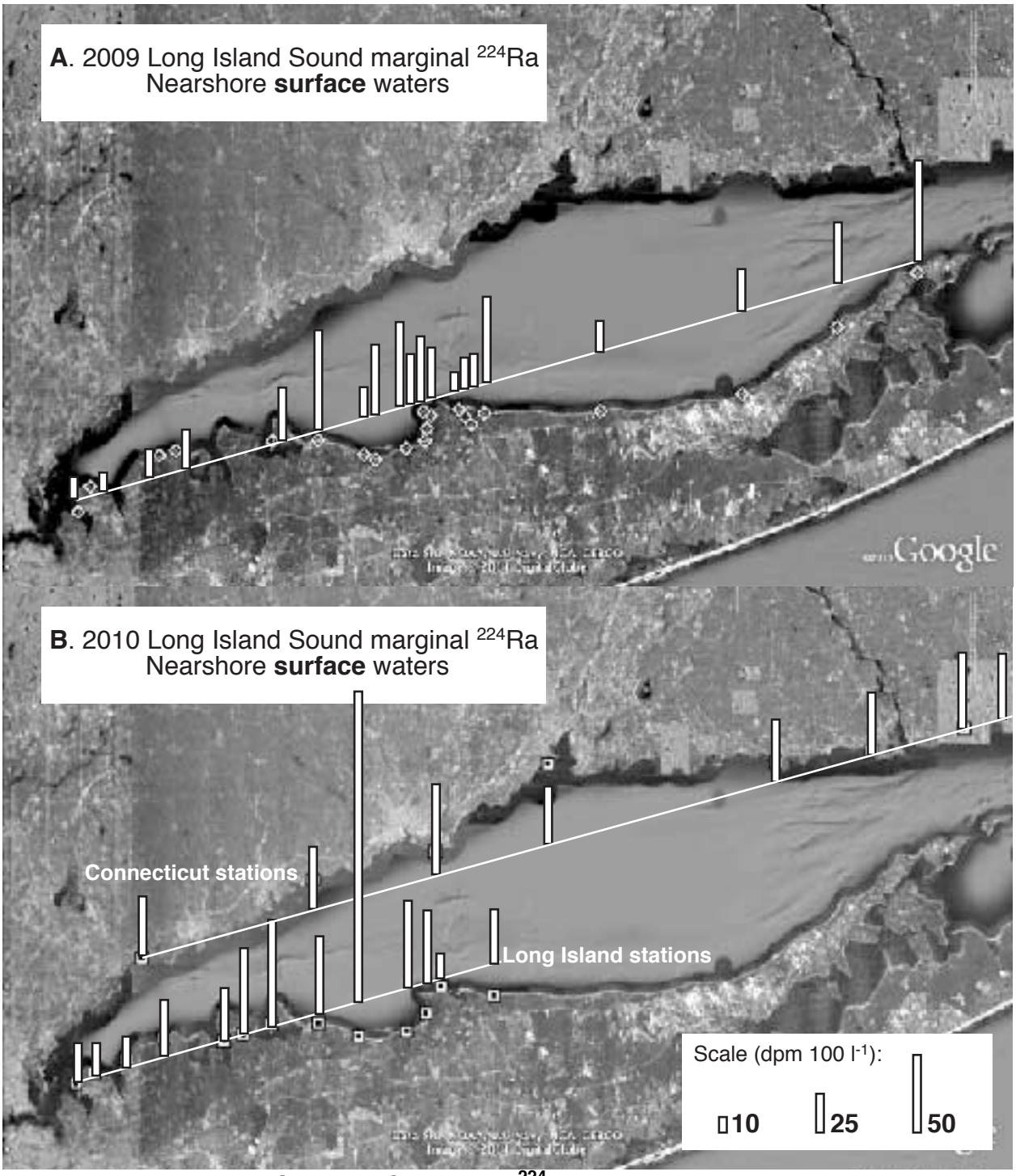

Figure A9. Long Island Sound (LIS) **surface ^{224}Ra concentrations** along the Connecticut and New York Shores: **A**. 2009; **B**. 2010.

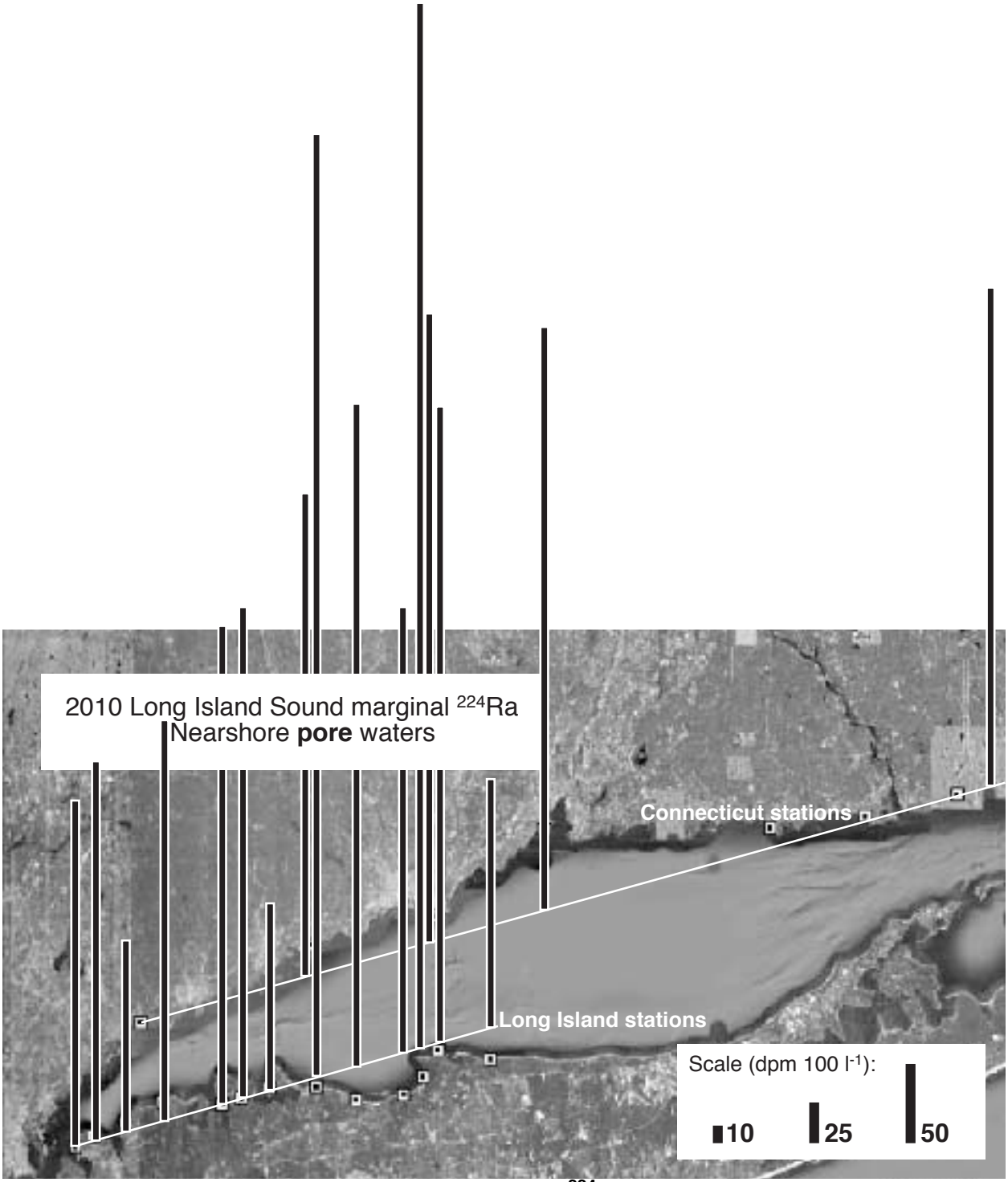

Figure A10. Long Island Sound (LIS) **pore water ^{224}Ra concentrations** along the Connecticut and New York Shores.

Figure A11. X-radiograph of station 8 subcore, Long Island Sound, summer 2010.

Figure A12. X-radiograph of station 16 subcore, Long Island Sound, summer 2010.

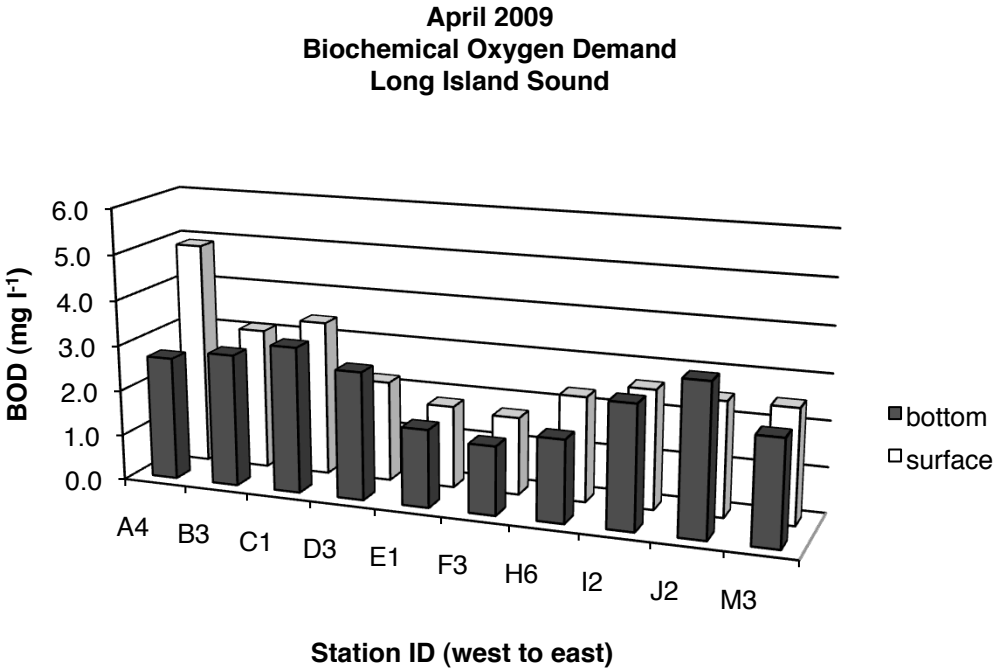

Figure A13. Biochemical oxygen demand (BOD) acquired from the Connecticut Department of Environmental Protection. The stations presented in this figure are analogous to stations along the axial transect in this study.

Tables

Table A1. Long Island Sound shore station IDs and corresponding locations 2009 and 2010. Stations are in ascending order from west to east.

Station ID	Location	Latitude (N)	Longitude (W)
2009 NEW YORK			
SBA	Sands Beach Association	40° 50.185'	73° 43.773'
SDP	Sands Point Preserve	40° 52.097'	73° 42.556'
STL	Stehli Beach, Oyster Bay	40° 54.527'	73° 35.574'
BAY	Bayville	40° 54.916'	73° 33.905'
HBT	Hobart Beach	40° 55.713'	73° 24.204'
CRM	Crab Meadow Beach	40° 55.781'	73° 19.621'
SKN	Sunken Meadow State Park	40° 54.689'	73° 15.005'
SMT	Smithtown Inlet	40° 54.307'	73° 13.853'
SLB	Smithtown (Long Beach)	40° 55.178'	73° 10.771'
STB	Stony Brook Inlet	40° 55.761'	73° 8.866'
WMB	West Meadow Beach	40° 56.686'	73° 8.685'
FLX	Flax Pond Lab, Old Field	40° 57.665'	73° 8.313'
OLD	Old Field	40° 57.975'	73° 9.043'
PJ1	Port Jefferson	40° 58.124'	73° 5.454'
PJ2	Port Jefferson	40° 57.555'	73° 4.820'
PJ3	Port Jefferson	40° 56.992'	73° 4.205'
BTR	Belle Terre, Port Jefferson	40° 57.845'	73° 2.936'
SHH	Shoreham	40° 58.019'	72° 51.225'
NTH	Northville	40° 59.265'	72° 37.011'
STH	Southold	41° 4.285'	72° 27.378'
ORI	Orient	41° 8.386'	72° 19.242'
2010 NEW YORK			
SBA	Sands Beach Association	40º 51.059'	073º 43.952'
SDP	Sands Point Preserve	40º 51.896'	073º 42.056'
NAV	Webb Institute of Naval Architecture	40º 52.999'	073º 38.868'
STL	Stehli Beach, Oyster Bay	40º 54.546'	073º 35.068'
WNR	West Neck Rd, Huntington	40º 54.401'	073º 29.015'

LYD	Lloyd Harbor, Huntington	40º 54.916'	073º 27.070'
HBT	Hobart Beach	40º 55.710'	073º 24.203'
CRM	Crab Meadow Beach	40º 55.796'	073º 19.494'
SKN	Sunken Meadow State Park	40º 54.809'	073º 15.473'
SLB	Smithtown (Long Beach)	40º 55.229'	073º 10.625'
WMB	West Meadow Beach	40º 56.590'	073º 08.701'
OFP	Old Field Point	40º 58.626'	073º 07.174'
CDB	Cedar Beach	40º 57.923'	073º 01.867'
2010 CONNECTICUT			
GRN	Greenwich (near Bruce Museum)	41º 00.658'	073º 37.339'
SIP	Sherwood Isl. State Park	41º 06.676'	073º 20.062'
LRD	Lordship Beach	41º 08.851'	073º 07.763'
PCK	Peck Ave., West Haven	41º 15.509'	072º 56.412'
HSP	Hammonasset State Park	41º 15.571'	072º 33.439'
HVY	Harvey's Beach	41º 16.420	072º 23.709'
RCK	Rocky Neck State Park	41º 18.034'	072º 14.275'
HRK	Harkness State Park	41º 18.023'	072º 06.972'

Table A2. Ra concentrations in Long Island Sound (LIS) 2009 and 2010.

		^{224}Ra						^{223}Ra					
		SPRING 2009		SUMMER 2009		SUMMER 2010		SPRING 2009		SUMMER 2009		SUMMER 2010	
Axial transect (west to east)		dpm 100 l^{-1}	error	dpm 100 l^{-1}	error	dpm 100 l^{-1}	error	dpm 100 l^{-1}	error	dpm 100 l^{-1}	error	dpm 100 l^{-1}	error
18	surf					23.56	1.24					1.93	0.21
	deep					24.10	1.17					2.04	0.21
16	surf	6.27	0.36	20.77	1.12	19.02	1.19	0.54	0.13	1.61	0.38	1.40	0.14
	mid					21.11	1.27					1.48	0.19
	deep	9.10	0.44	20.62	1.19	17.40	1.01	0.83	0.16	1.51	0.37	2.11	0.23
17	surf					14.88	1.03					1.97	0.22
	deep					21.33	1.34					1.57	0.19
13	surf	1.82	0.20	11.43	0.73	5.96	0.39	0.27	0.06	1.75	0.38	1.13	0.15
	5m					10.41	0.71					1.06	0.12
	8m					12.28	0.99					1.10	0.15
	deep	7.58	0.33	16.21	0.91	17.07	0.84	0.56	0.16	1.73	0.36	1.68	0.19
120W	surf	2.38	0.34	9.92	0.54	9.70	0.64	0.53	0.12	1.21	0.26	1.01	0.15
	deep	5.39	0.38	12.24	0.61	13.77	0.79	0.25	0.11	1.17	0.24	1.44	0.18
120E	surf	2.22	0.24	8.49	0.57	5.29	0.39	0.27	0.07	1.41	0.32	0.71	0.11
	deep	4.86	0.28	12.97	0.72	12.50	0.80	0.42	0.13	0.90	0.23	1.22	0.16
117	surf	4.68	0.23	11.07	0.71	10.76	0.51	0.40	0.09	0.99	0.28	1.15	0.16
	deep	4.78	0.21	12.70	0.76	16.40	1.01	0.43	0.08	1.26	0.31	0.91	0.11
7	surf	5.02	0.36	4.10	0.38	2.83	0.24	0.63	0.18	1.12	0.27	0.72	0.12
	5m	3.06	0.42					0.31	0.08				
	7m	2.03	0.22					0.37	0.11				
	15m	4.41	0.27					0.32	0.11				
	deep	3.95	0.25	12.99	0.77	12.23	0.91	0.28	0.09	1.11	0.27	0.98	0.14
113W	surf	2.11	0.23	4.17	0.30	3.85	0.25	0.22	0.07	0.76	0.17	0.95	0.13
	deep	6.29	0.33	17.11	0.76	17.78	1.05	0.56	0.13	1.50	0.27	1.29	0.17
113E	surf			8.63	0.53	4.21	0.26			1.24	0.27	0.76	0.10
	deep			7.80	0.49	7.30	0.62			0.83	0.19	0.75	0.13
102	surf	5.29	0.37	6.24	0.46	3.99	0.24	0.43	0.11	0.77	0.20	0.86	0.11
	deep	5.58	0.30	7.51	0.51	7.69	0.45	0.59	0.12	0.68	0.18	0.97	0.15
3	surf	5.28	0.36	5.70	0.39	3.65	0.29	0.41	0.13	0.87	0.21	0.58	0.08
	deep	5.54	0.37	7.73	0.47	6.83	0.45	0.68	0.16	0.82	0.19	0.89	0.13
101	surf	2.03	0.22					0.47	0.10				
	deep	3.60	0.23					0.35	0.11				
Western transect (north to south)													
15	surf	4.13	0.24			11.53	0.62	0.47	0.10			1.37	0.20
	deep	6.54	0.30			14.16	0.85	0.52	0.11			1.93	0.21
14	surf	2.03	0.24			5.94	0.52	0.26	0.08			0.89	0.16
	deep	7.40	0.38			15.41	1.29	0.40	0.14			1.60	0.20
13	surf	1.82	0.20	11.43	0.73	5.96	0.39	0.27	0.06	1.75	0.38	1.13	0.15
	5m					10.41	0.71					1.06	0.12
	8m					12.28	0.99					1.10	0.15
	deep	7.58	0.33	16.21	0.91	17.07	0.84	0.56	0.16	1.73	0.36	1.68	0.19
12	surf	3.72	0.29			10.60	0.73	0.60	0.17			0.89	0.11

	deep	7.70	0.98			20.76	1.40	0.84	0.18			1.44	0.15
11	surf	4.63	0.30			12.61	0.75	0.79	0.19			1.45	0.18
	deep	6.97	0.87			25.49	1.48	0.71	0.14			2.24	0.24
10	surf	7.23	0.40			11.94	0.77	0.56	0.14			1.36	0.17
	deep	6.78	0.36			27.98	1.73	0.53	0.12			2.79	0.40
Central transect (north to south)													
9	surf	6.20	0.34			20.44	1.89	0.70	0.15			1.70	0.21
	deep	10.55	0.47			27.62	2.64	0.80	0.16			1.91	0.23
8	surf	5.52	0.39			5.19	0.35	0.77	0.20			0.82	0.13
	deep	4.79	0.63			15.38	1.01	0.25	0.09			1.39	0.17
7	surf	5.02	0.36	4.10	0.38	2.83	0.24	0.63	0.18	1.12	0.27	0.72	0.12
	5m	3.06	0.42					0.31	0.08				
	7m	2.03	0.22					0.37	0.11				
	15m	4.41	0.27					0.32	0.11				
	deep	3.95	0.25	12.99	0.77	12.23	0.91	0.28	0.09	1.11	0.27	0.98	0.14
6	surf	2.35	0.19			3.97	0.30	0.20	0.08			0.76	0.10
	deep	5.08	0.23			12.60	0.97	0.25	0.08			1.29	0.18
5	surf	5.75	0.34			5.44	0.36	0.51	0.13			1.52	0.18
	deep	4.42	0.55			16.11	0.86	0.29	0.08			1.51	0.21
Eastern transect (north to south)													
1	surf	8.41	0.59	8.80	0.54	13.33	0.85	0.57	0.21	1.32	0.29	1.33	0.17
	deep	7.29	0.96	5.96	0.35	13.90	0.82	0.49	0.17	0.91	0.18	0.77	0.11
2	surf	5.06	0.42			4.54	0.29	0.66	0.18			0.53	0.07
	deep	4.09	0.33			6.79	0.60	0.39	0.13			0.71	0.12
3	surf	5.28	0.36	5.70	0.39	3.65	0.29	0.41	0.13	0.87	0.21	0.58	0.08
	deep	5.54	0.37	7.73	0.47	6.83	0.45	0.68	0.16	0.82	0.19	0.89	0.13
4	surf	6.37	0.42			7.13	0.32	0.54	0.16			0.54	0.14
	deep	4.48	0.58			6.80	0.47	0.53	0.12			0.90	0.14

Table A3. Chlorophyll *a* and nutrient concentrations in Long Island Sound (LIS) 2009 and 2010.

		Chlorophyll *a* ($\mu g\ l^{-1}$)			NO_3+NO_2 (mg l^{-1} N)	NH_4 (mg l^{-1} N)	PO_X (mg l^{-1} P)
Axial transect (west to east)		SPRING 2009	SUMMER 2009	SUMMER 2010	SUMMER 2010	SUMMER 2010	SUMMER 2010
18	surf			1.30	0.696	0.146	
	deep			1.26	0.631	0.075	
16	surf	3.13	13.77	4.68	0.382	0.000	0.056
	mid			1.63	0.415	0.000	0.053
	deep	1.25	0.77	1.04	0.308	0.016	0.052
17	surf			4.28	0.160	0.000	
	deep			0.74	0.586	0.000	
13	surf	1.24	2.42	3.09	0.503	0.000	0.051
	5m			2.74	0.267	0.001	0.051
	8m			1.19	0.677	0.010	0.052
	deep	0.72	0.26	0.35	0.338	0.003	0.055
120W	surf	0.60	4.56	1.82	0.627	0.000	0.049
	deep	0.50	0.16	0.34	0.603	0.000	0.051
120E	surf	0.29	0.62	1.61	0.357	0.000	0.053
	deep	0.34	0.14	0.21	0.767	0.000	0.053
117	surf	0.35	0.44	1.97	0.141	0.000	0.045
	deep	0.21	0.31	0.18	0.073	0.042	0.052
7	surf	0.16	0.56	0.77	0.146	0.000	0.054
	5m	0.18					
	7m	0.19					
	15m	0.19					
	deep	0.15	0.40	0.12	0.102	0.070	0.056
113W	surf	0.16	0.49	0.92	0.166	0.000	0.058
	deep	0.21	0.89	0.21	0.043	0.090	0.057
113E	surf		0.91	0.53	0.448	0.000	0.060
	deep		0.39	0.42	0.152	0.041	0.058
102	surf	0.17	0.96	0.75	0.722	0.000	0.000
	deep	0.20	0.79	0.54	0.657	0.021	0.000
3	surf	0.08	1.28	0.71	0.286	0.000	0.054
	deep	0.29	0.74	0.37	0.528	0.023	0.000
101	surf	0.26					
	deep	0.08					
Western transect (north to south							
15	surf	0.72		1.74			
	deep	0.65		0.39			
14	surf	0.58		2.64			
	deep	0.64		0.33			
13	surf	1.24	2.42	3.09	0.503	0.000	0.051
	5m			2.74	0.267	0.001	0.051
	8m			1.19	0.677	0.010	0.052
	deep	0.72	0.26	0.35	0.338	0.003	0.055

12	surf	1.26		3.50			
	deep	0.86		0.46			
11	surf	1.37		4.00			
	deep	1.12		1.58			
10	surf	0.59		1.27			
	deep	0.89		0.47			
Central transect (north to south)							
9	surf	0.96		2.19			
	deep	0.53		0.51			
8	surf	0.32		1.06			
	deep	0.31		0.18			
7	surf	0.16	0.56	0.77	0.146	0.000	0.054
	5m	0.18					
	7m	0.19					
	15m	0.19					
	deep	0.15	0.40	0.12	0.102	0.070	0.056
6	surf	0.32		0.67			
	deep	0.14		0.08			
5	surf	0.56		1.07			
	deep	0.58		1.00			
Eastern transect (north to south)							
1	surf	0.26		1.13			
	deep	0.41		0.28			
2	surf	0.08		0.71			
	deep	0.29		0.37			
3	surf	0.17	1.28	1.55	0.286	0.000	0.054
	deep	0.20	0.74	0.58	0.528	0.023	0.000
4	surf	0.09		1.40			
	deep	1.07		0.28			

Table A4. Particulate concentrations (plus dissolved Mn) in Long Island Sound (LIS) 2009 and 2010.

		SPM ($mg\ l^{-1}$)			POC ($mg\ l^{-1}$)	Mn(s) ($\mu mol\ g^{-1}$)	Al(s) ($\mu mol\ g^{-1}$)	Mn(s)/Al(s)	Mn(aq) ($\mu mol\ l^{-1}$)		
Axial transect (west to east)		SPRING 2009	SUMMER 2009	SUMMER 2010	SUMMER 2010	SUMMER 2010	SUMMER 2010	SUMMER 2010	SPRING 2009	SUMMER 2009	SUMMER 2010
18	surf			5.49	0.350	28.1	395.59	0.07			1.75
	deep			6.43	0.484	28.6	378.22	0.08			1.87
16	surf	1.53	2.64	3.50	0.371	85.9	262.01	0.33	0.66	1.19	1.76
	mid			3.34	0.369	89.0	328.41	0.27			1.70
	deep	2.00	3.68	13.51	0.643	43.2	400.36	0.11	0.61	0.91	1.58
17	surf			2.75	0.669	154.4	206.97	0.75			1.67
	deep			7.08	0.333	51.6	416.92	0.12			1.75
13	surf	0.93	1.42	2.31	0.871	334.7	156.06	2.14	0.59	0.07	1.26
	5m			1.12	0.581	359.9	274.68	1.31			1.40
	8m			2.22	0.309	259.9	335.65	0.77			1.21
	deep	2.32	4.22	5.03	0.331	136.2	384.68	0.35	0.44	0.90	1.43
120W	surf	0.72	2.00	2.15	0.436	298.2	285.91	1.04	0.52	0.17	0.85
	deep	1.82	3.42	5.94	0.290	88.4	424.09	0.21	0.40	0.59	0.88
120E	surf	0.66	0.84	1.65	0.387	442.2	155.14	2.85	0.41	0.00	0.45
	deep	1.21	3.04	6.05	0.222	80.7	462.56	0.17	0.32	0.57	0.62
117	surf	1.06	0.76	2.31	0.554	217.3	263.14	0.83	0.47	0.16	0.45
	deep	1.04	3.84	3.79	0.166	67.6	461.43	0.15	0.30	0.28	0.74
7	surf	0.84	1.24	1.05	0.368	224.4	144.99	1.55	0.27	0.02	0.00
	5m										
	7m										
	15m										
	deep	1.10	5.58	3.36	0.191	75.7	475.21	0.16	0.28	0.33	0.35
113W	surf	0.49	1.04	1.10	0.418	216.3	106.02	2.04	0.37	0.02	0.07
	deep	2.30	6.80	6.75	0.316	39.9	416.75	0.10	0.45	0.24	0.43
113E	surf		2.22	1.25	0.283	147.0	142.56	1.03		0.01	0.02
	deep		2.22	2.32	0.188	70.7	382.44	0.18		0.00	0.03
102	surf	0.51	1.10	1.00	0.376	154.8	122.50	1.26	0.04	0.04	0.02
	deep	0.40	1.14	1.51	0.336	82.0	306.23	0.27	0.02	0.00	0.00
3	surf	0.33	1.36	1.23	0.193	173.1	123.41	1.40	0.05	0.00	0.03
	deep	2.55	1.10	1.30	0.178	70.4	350.40	0.20	0.05	0.00	0.00
101	surf	0.98									
	deep	1.56									
Western transect (north to south)											
15	surf	0.96		1.80	0.558	330.2	253.45	1.30			1.08
	deep	1.23		5.26	0.222	127.8	387.36	0.33			1.11
14	surf	1.33		2.08	0.484	333.3	179.95	1.85			1.14
	deep	1.68		5.23	0.187	111.6	423.89	0.26			1.23
13	surf	0.93	1.42	2.31	0.871	334.7	156.06	2.14	0.59	0.07	1.26
	5m			1.12	0.581	359.9	274.68	1.31			1.40
	8m			2.22	0.309	259.9	335.65	0.77			1.21
	deep	2.32	4.22	5.03	0.331	136.2	384.68	0.35	0.44	0.90	1.43
12	surf	1.02		2.53	0.678	264.6	196.13	1.35			1.56
	deep	2.22		4.97	0.257	102.3	389.10	0.26			1.60

11	surf	1.09		2.24	0.629	284.5	214.53	1.33			1.72
	deep	3.15		3.26	0.387	133.9	346.29	0.39			2.14
10	surf	0.88		1.05	0.339	563.8	305.68	1.84			0.51
	deep	1.73		5.48	0.250	88.3	479.35	0.18			1.54
Central transect (north to south)											
9	surf	0.88		3.10	0.581	136.5	275.75	0.50			0.71
	deep	1.56		7.01	0.389	46.6	416.75	0.11			1.28
8	surf	0.68		1.50	0.385	199.3	138.07	1.44			0.04
	deep	1.58		3.64	0.184	65.0	404.05	0.16			0.56
7	surf	0.84	1.24	1.05	0.368	224.4	144.99	1.55	0.27	0.02	0.00
	5m	0.66									
	7m	0.82									
	15m	0.97									
	deep	1.10	5.58	3.36	0.191	75.7	475.21	0.16	0.28	0.33	0.35
6	surf	0.78		1.19	0.359	254.6	113.13	2.25			0.13
	deep	1.51		2.63	0.251	97.2	392.55	0.25			0.66
5	surf	1.03		1.53	0.572	285.9	156.53	1.83			0.04
	deep	1.11		3.64	0.459	164.3	324.45	0.51			0.56
Eastern transect (north to south)											
1	surf	4.73	1.42	2.99	0.516	131.4	367.05	0.36			0.31
	deep	8.50	0.80	4.49	0.242	47.1	373.23	0.13			0.04
2	surf	0.76		1.27	0.369	113.0	198.11	0.57			0.00
	deep	0.87		2.28	0.265	50.7	339.97	0.15			0.00
3	surf	0.33	1.36	1.23	0.193	173.1	123.41	1.40	0.05	0.00	0.03
	deep	2.55	1.10	1.30	0.178	70.4	350.40	0.20	0.05	0.00	0.00
4	surf	1.09		1.05	0.267	194.6	177.38	1.10			0.03
	deep	2.13		2.54	0.276	74.5	359.80	0.21			0.04

Table A5. Ra shore station physical data. Stations are in ascending order from west to east.

ID	TEMPERATURE (ºC) surface H_2O	TEMPERATURE (ºC) pore H_2O	SALINITY surface H_2O	SALINITY pore H_2O	DO (mg l^{-1}) surface H_2O	DO (mg l^{-1}) pore H_2O	DO (%) surface H_2O	DO (%) pore H_2O
New York								
SBA	21.82	22.13	25.53	25.12				
SDP	20.42	21.97	25.00	15.53				
NAV	20.41	20.54	24.63	22.94				
STL	21.87	21.65	25.17	23.71				
WNR	25.63	26.00	25.95	25.54				
LYD	26.50	28.20	25.81	21.41				
HBT	20.02	21.53	25.72	25.95				
CRM	19.45	21.39	23.61	25.65				
SKN	18.77	18.58	25.29	25.46				
SLB	18.93	18.63	25.39	25.11				
WMB	21.78	21.56	24.29	24.97				
OFP	20.00	19.98	25.36	24.86				
CDB	18.57	18.78	25.73	25.76				
Connecticut								
GRN	22.32		27.61		5.47		73.9	
SIP	20.82	21.93	28.15	28.13	7.29	4.41	97.1	59.3
LRD	19.20	21.77	27.76	27.86	5.94	3.22	75.4	42.9
PCK	18.89	23.20	27.48	27.42	6.51	4.29	81.6	58.6
HSP	20.01		28.54		6.15		79.7	
HVY	19.70		28.81		6.59		85.5	
RCK	19.21		30.29		6.39			
HRK	19.17	18.72	30.37	30.38	6.22	5.88	79.9	75.3

Table A6. Ra shore station activities. Stations are in ascending order from west to east.

ID	Ra activity (dpm 100 l^{-1}) surface H_2O	pore H_2O
NEW YORK		
SBA	24.50 ± 2.76	223.76 ± 35.28
SDP	21.04 ± 2.28	245.88 ± 47.94
NAV	20.37 ± 2.28	124.21 ± 24.65
STL	35.96 ± 4.04	259.95 ± 51.89
WNR	33.89 ± 3.44	309.97 ± 48.41
LYD	54.86 ± 5.40	317.64 ± 55.60
HBT	69.16 ± 6.99	120.69 ± 23.62
CRM	50.07 ± 5.55	610.87 ± 120.02
SKN	200.51 ± 21.33	430.36 ± 87.18
SLB	55.86 ± 5.91	289.33 ± 59.49
WMB	47.43 ± 5.08	677.77 ± 150.79
OFP	15.54 ± 1.77	412.26 ± 65.64
CDB	34.54 ± 3.53	160.60 ± 31.23
CONNECTICUT		
GRN	38.49 ± 3.62	
SIP	40.29 ± 2.51	312.99 ± 44.31
LRD	57.74 ± 3.43	408.13 ± 56.56
PCK	37.14 ± 3.72	378.00 ± 43.30
HSP	40.22 ± 4.07	
HVY	40.13 ± 2.72	
RCK	49.12 ± 3.18	
HRK	41.84 ± 4.21	323.26 ± 38.76

Table A7. Nutrient concentrations at stations along the Long Island Sound (LIS) Shore, summer 2010. Station locations are arranged in order from west to east. A value of "0" was substituted for all samples below the detectable limit (<0.001 mg l^{-1}).

		NO_3+NO_2 (mg l^{-1} N)		NH_4 (mg l^{-1} N)	
	location	surface water	pore water	surface water	pore water
CT	GRN	0.159	-	0	0
	SIP	0.040	0.360	0	0
	LRD	0.009	0.486	0	0
	PCK	0	0.044	0	0
	HSP	0.014	-	0	0
	HVY	0	-	0	0
	RCK	0	-	0	0
	HRK	0.001	0.036	0	0
LI	SBA	0	0.071	0	0
	SDP	0.022	1.355	0	0
	NAV	0	0.019	0	0
	STL	0.033	0.236	0	0
	WNR	0	0.405	0	0.334
	LYD	0	0.453	0	0
	HBT	0.134	0.380	0	0
	CRM	0.093	0	0	0.121
	SKN	0	0.017	0	0
	SLB	0	0.151	0	0
	WMB	0	0	0	0
	OFP	1.010	0.119	0	0
	CDB	0.049	0.112	0	0

Table A8. Sediment core data from stations 8 and 16 Long Island Sound (LIS) 2010.

station	core depth (cm)	% water	loss on ignition % dry weight	Mn (s) (μmol g^{-1})
8	0.5	77.36	6.01	27.1
	1.0	68.41	6.08	8.5
	1.5	68.27	6.26	10.1
	2.0	66.48	6.12	9.1
	2.5	65.71	6.11	7.9
	3.0	64.58	5.55	7.5
	4.0	63.64	5.73	6.5
	5.0	63.97	5.99	5.9
	6.0	65.12	5.91	5.4
16	0.5	83.39	8.26	10.3
	1.0	68.61	6.81	7.4
	1.5	65.80	6.40	8.2
	2.0	66.55	7.13	7.9
	2.5	66.42	6.88	8.8
	3.0	66.49	7.88	8.2
	4.0	64.65	7.85	8.2
	5.0	62.71	7.56	9.8
	6.0	62.34	7.69	10.5

Appendix B: Long Island Sound laboratory data

Figures

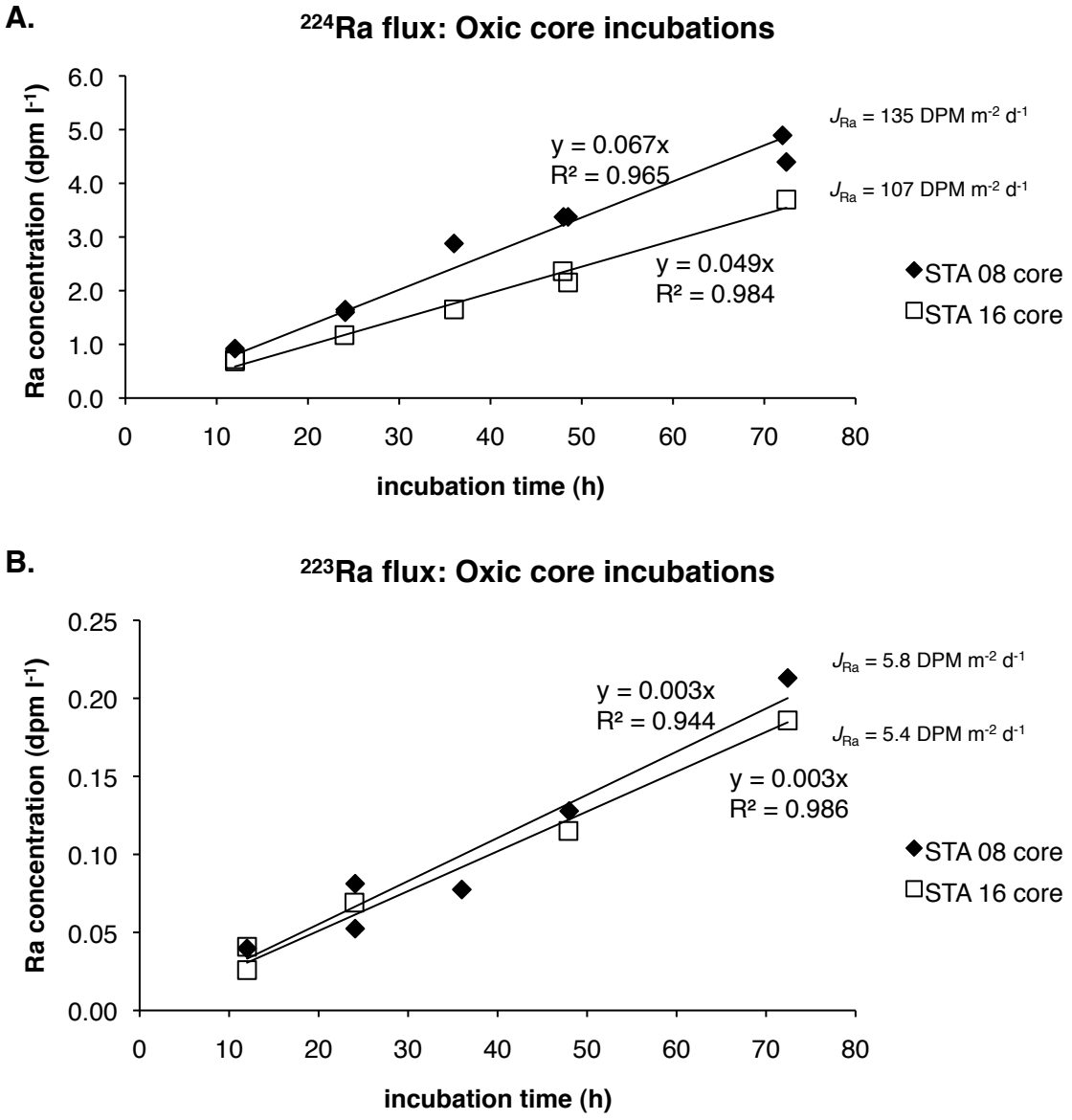

Figure B1. **A**. ^{224}Ra concentrations over time for stations 8 and 16. Fluxes (J_{Ra}) were estimated using the slope of the best-fit trendline for each respective station's Ra concentration values; **B**. ^{223}Ra concentrations over time for stations 8 and 16. Fluxes (J_{Ra}) were estimated using the slope of the best-fit trendline for each respective station's Ra concentration values.

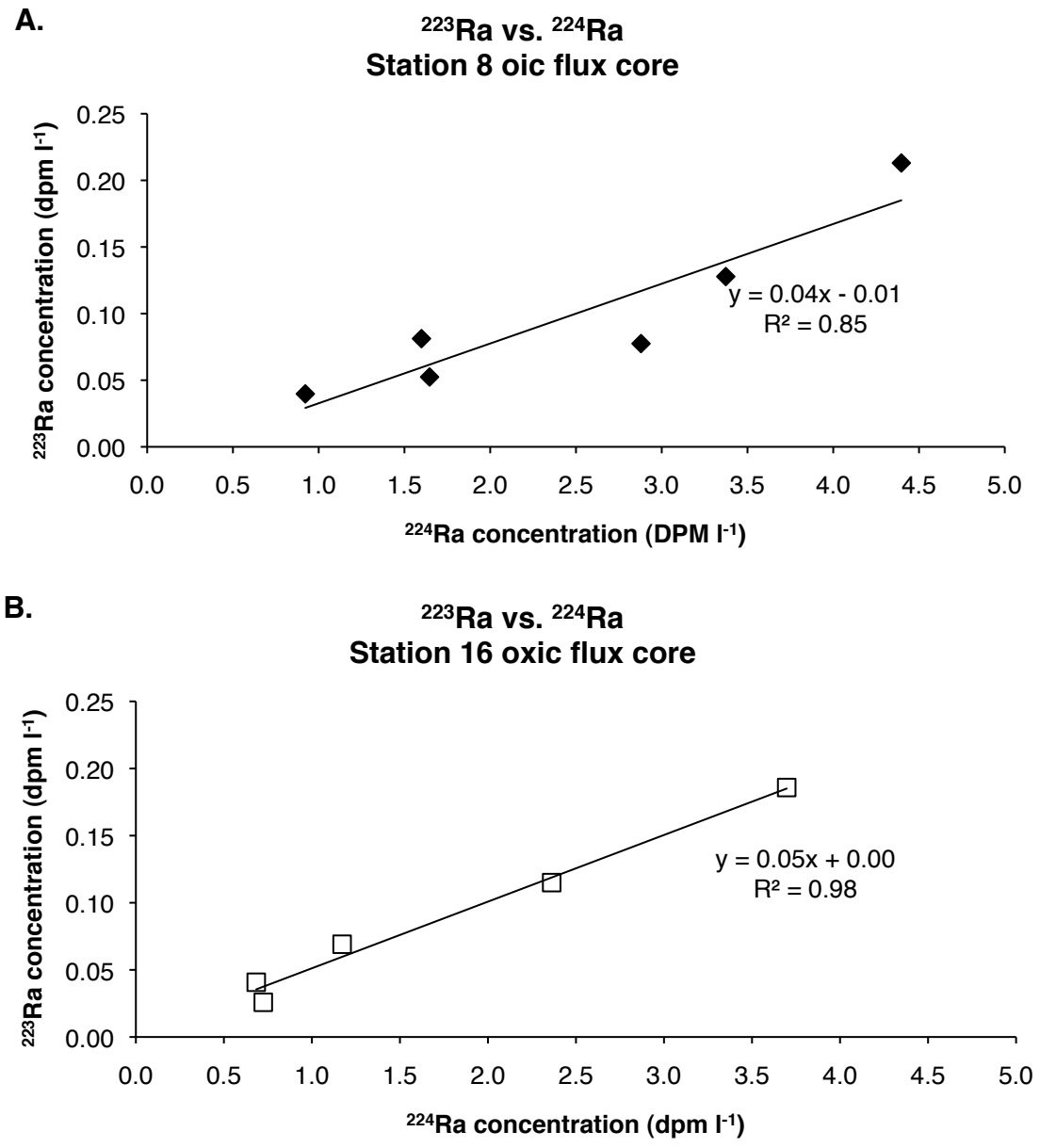

Figure B2. Correlation between ^{223}Ra and ^{224}Ra concentrations for the oxic Ra flux cores: **A**. Station 8; **B**. station 16.

Tables

Table B1. Laboratory flux core incubation data including Ra concentrations and corresponding calculated fluxes for 2009 and 2010. Dissolved oxygen (DO) for all summer oxic incubations was at saturation. DO in hypoxic core incubations ranged from 0.59 – 1.05 mg l^{-1}.

time (h)	Incubation time (h)	^{224}Ra (dpm l^{-1})	error	^{224}Ra flux (dpm m^{-2} d^{-1})	error	^{223}Ra (dpm l^{-1})	error	^{223}Ra flux (dpm m^{-2} d^{-1})	error
Station 13 (2009)		**Summer oxic**							
-	-	-	-	312	-	-	-	-	-
Station 120E (2009)									
-	-	-	-	170	-	-	-	-	-
Station 8 (2010)									
0 – 24	24	1.599	0.556	132	46	0.081	0.038	6.7	3.1
0 – 24*	24	1.647	0.571	136	47	0.052	0.024	4.3	2.0
24 – 60	36	2.879	1.000	159	55	0.077	0.043	4.3	2.4
60 – 72	12	0.922	0.321	153	53	0.040	0.021	6.6	3.5
72 – 144	72	4.397	1.539	121	42	0.213	0.079	5.9	2.2
144 – 192	48	3.373	1.181	140	49	0.128	0.067	5.3	2.8
192 – 264	72	4.893	1.675	136	46	0.088	0.037	2.4	1.0
264 – 313	49	3.374	1.181	139	49	0.134	0.067	5.5	2.8
		Summer hypoxic							
385 – 457	72	1.343	0.527	38	15	0.050	0.024	1.4	0.7
457 – 481	24	1.513	0.591	126	49	0.083	0.036	6.9	3.0
481 – 529	48	1.430	0.561	59	23	0.080	0.041	3.3	1.7
Station 16 (2010)		**Summer oxic**							
0 – 72	72	3.697	1.166	111	35	0.186	0.065	5.6	2.0
72 – 120	48	2.362	0.751	107	34	0.115	0.054	5.2	2.5
120 – 144	24	1.172	0.379	106	34	0.069	0.031	6.3	2.8
144 – 180	36	1.651	0.522	100	32	0.040	0.020	2.4	1.2
180 – 192	12	0.724	0.234	131	43	0.026	0.014	4.7	2.5
180 – 192*	12	0.684	0.221	124	40	0.041	0.016	7.4	3.0
192 – 241	49	2.153	0.697	97	31	0.049	0.035	2.2	1.6
		Summer hypoxic							
313 – 385	72	3.283	1.161	100	35	0.155	0.061	4.7	1.9
385 – 409	24	2.149	0.759	195	69	0.106	0.041	9.6	3.8
409 – 457	48	3.109	1.100	140	50	0.140	0.053	6.3	2.4

***** Denotes duplicate measurement of the same sample.

Table B2. Laboratory flux core incubation data including dissolved Mn values, calculated Mn(aq) fluxes, and respective dissolved oxygen (DO) concentrations.

		Station 8			**Station 16**		
time (h)		Mn (μM)	Mn(aq) flux (mmol m^{-2} d^{-1})	DO (mg l^{-1})	Mn (μM)	Mn(aq) flux (mmol m^{-2} d^{-1})	DO (mg l^{-1})
		Summer oxic					
	0	2.52		8.23	5.05		8.12
	6	6.05	1.59	8.28	4.02	-0.44	8.46
	12	7.63	0.53	8.49	3.39	-0.26	8.37
	18	8.39	0.31	8.33	6.06	1.00	8.62
	24	8.76	0.14	8.59	4.78	-0.62	8.40
	36				4.98	0.04	8.21
	42	10.91	0.28	8.25			
	48	11.48	0.21	8.50			
	78	6.41	-0.41	8.16			
	90	6.01	-0.08	8.20			
	102	5.01	-0.20	8.29			
		Summer hypoxic					
	0	2.52		7.11	7.33		6.56
	6	6.05	-0.42	5.88	14.38	2.91	2.18
	12	7.63	-0.04	5.11	18.65	1.71	1.69
	18	8.39	-0.50	4.54	21.40	0.99	1.39
	24	8.76	-0.19	4.50	23.86	1.14	1.74
	36				25.44	0.33	1.02
	42	10.91	0.36	3.61			
	48	11.48	1.14	2.56			
	78	6.41	2.75	2.38			
	90	6.01	1.60	1.42			
	102	5.01	2.07	1.71			
sta16 (h)	sta8 (h)	Winter oxic					
60	125	176.32		1.17	65.87		0.92
63	129	181.56	3.22	4.21	65.12	-0.48	5.45
70	135	171.61	-8.87	7.85	62.27	-2.66	8.81
79	144	161.06	-9.11	9.05	60.83	-1.29	9.89
103	168	117.96	-6.61	10.10	49.90	-1.75	10.97
130	196	107.47	-7.44	10.33	47.82	-1.54	10.66

Table B3. ^{224}Ra parent (^{232}Th) activities in the Ra flux cores post-incubations.

	^{232}Th	
Depth interval (cm)	Station 8 583 dpm g^{-1}	Station16 583 dpm g^{-1}
0 – 1.5	2.127 ± 0.061	2.126 ± 0.010
1.5 – 3	2.175 ± 0.070	1.730 ± 0.021
3 – 5	2.037 ± 0.051	2.179 ± 0.012
5 – 7	1.886 ± 0.059	2.246 ± 0.013
7 – 9	1.811 ± 0.060	2.108 ± 0.015
9 – 11	1.798 ± 0.061	2.142 ± 0.010
11.5 – 13.5	1.832 ± 0.062	2.146 ± 0.013
15 – 17	1.970 ± 0.068	2.398 ± 0.013